

Search for photonic signatures of gauge-mediated supersymmetry in 8 TeV pp collisions with the ATLAS detector

G. Aad *et al.**

(ATLAS Collaboration)

(Received 21 July 2015; published 6 October 2015)

A search is presented for photonic signatures motivated by generalized models of gauge-mediated supersymmetry breaking. This search makes use of 20.3 fb^{-1} of proton-proton collision data at $\sqrt{s} = 8 \text{ TeV}$ recorded by the ATLAS detector at the LHC, and explores models dominated by both strong and electroweak production of supersymmetric partner states. Four experimental signatures incorporating an isolated photon and significant missing transverse momentum are explored. These signatures include events with an additional photon, lepton, b -quark jet, or jet activity not associated with any specific underlying quark flavor. No significant excess of events is observed above the Standard Model prediction and model-dependent 95% confidence-level exclusion limits are set.

DOI: [10.1103/PhysRevD.92.072001](https://doi.org/10.1103/PhysRevD.92.072001)

PACS numbers: 12.60.Jv, 13.85.Rm

I. INTRODUCTION

This paper reports on a search for four classes of events containing energetic isolated photons and large missing transverse momentum (with magnitude denoted E_T^{miss}) in 20.3 fb^{-1} of proton-proton (pp) collision data at $\sqrt{s} = 8 \text{ TeV}$ recorded with the ATLAS detector at the Large Hadron Collider (LHC) in 2012. For the first of the four classes, two isolated energetic photons are required (“diphoton” events), while for the remaining classes only a single isolated photon is required. For the second and third classes, the isolated photon is required to appear in combination with a “ b -jet” identified as having arisen from the production of a bottom (b) quark (“photon + b ” events) or an isolated electron or muon (“photon + ℓ ” events), respectively. For the fourth class of events the isolated photon is required to appear in combination with multiple jets selected without regard to the flavor of the underlying parton (“photon + j ” events).

The results are interpreted in the context of a broad range of general models of gauge-mediated supersymmetry breaking (GGM) [1–3] that include the production of supersymmetric partners of strongly coupled Standard Model (SM) particles as well as SM partners possessing only electroweak charge. In all models of GGM, the lightest supersymmetric particle (LSP) is the gravitino \tilde{G} (the partner of the hypothetical quantum of the gravitational field), with a mass significantly less than 1 GeV. In the GGM models considered here, the decay of the supersymmetric states produced in LHC collisions would

proceed through the next-to-lightest supersymmetric particle (NLSP), which would then decay to the \tilde{G} LSP and one or more SM particles, with a high probability of decay into $\gamma + \tilde{G}$. In this study, several different possibilities for the nature of the NLSP are considered, providing separate motivation for the four different and complementary experimental signatures that are explored. In all models considered, all supersymmetric states with the exception of the \tilde{G} are short lived, leading to prompt production of SM particles that are observed in the ATLAS detector.

The results based on the diphoton and photon + b signatures extend and supplant studies (Refs. [4] and [5], respectively) that made use of 4.8 fb^{-1} of pp collision data at $\sqrt{s} = 7 \text{ TeV}$; the analyses based on the photon + j and photon + ℓ signatures are new and have only been performed with the 8 TeV data. Making use of 19.7 fb^{-1} of pp collision data at $\sqrt{s} = 8 \text{ TeV}$, a search [6] for events similar in nature to those of the diphoton and photon + j signatures mentioned above has been performed by the CMS Collaboration, and used to set limits on the masses of strongly coupled supersymmetric particles in several GGM scenarios.

II. GAUGE-MEDIATED SUPERSYMMETRY PHENOMENOLOGY

Supersymmetry (SUSY) [7–15] introduces a symmetry between fermions and bosons, resulting in a SUSY partner (sparticle) with identical quantum numbers except a difference by half a unit of spin for each SM particle. As none of these sparticles have been observed, SUSY must be a broken symmetry if realized in nature. Assuming R -parity conservation [16–20], sparticles are produced in pairs. These would then decay through cascades involving other sparticles until the stable, weakly interacting LSP is produced, leading to a final state with significant E_T^{miss} .

*Full author list given at the end of the article.

Published by the American Physical Society under the terms of the [Creative Commons Attribution 3.0 License](https://creativecommons.org/licenses/by/3.0/). Further distribution of this work must maintain attribution to the author(s) and the published article’s title, journal citation, and DOI.

Experimental signatures of gauge-mediated SUSY breaking models [21–26] are largely determined by the nature of the NLSP. For GGM, the NLSP is often formed from an admixture of any of the SUSY partners of the electroweak gauge and Higgs boson states. In this study, three cases are assumed for the composition of the NLSP. For the first case, the NLSP is assumed to be purely binolike [the SUSY partner of the SM U(1) gauge boson]. For the second case, the NLSP is assumed to be an admixture of bino and neutral higgsino states. For the final case, the NLSP is assumed to be a degenerate triplet of wino states [the SUSY partners of the SM SU(2) gauge bosons]. In this paper, the neutral NLSP is denoted $\tilde{\chi}_1^0$ irrespective of its composition. For the case that the NLSP is a degenerate triplet, the charged NLSP states are denoted $\tilde{\chi}_1^\pm$. The properties of the GGM models used to represent these possibilities are discussed below and summarized in Table I.

For the case that the NLSP is a bino, the final decay in each of the two cascades in a GGM event would be predominantly $\tilde{\chi}_1^0 \rightarrow \gamma + \tilde{G}$, leading to final states with $\gamma\gamma + E_T^{\text{miss}}$. For the case that the NLSP is a mixture of the bino and higgsino, both the possibilities that the higgsino mass parameter μ is less than or greater than zero are explored. For the $\mu < 0$ possibility, the final decay in the cascade would include a significant contribution from $\tilde{\chi}_1^0 \rightarrow h + \tilde{G}$ with the subsequent decay $h \rightarrow b\bar{b}$, leading to final states with a photon, multiple b -jets, and E_T^{miss} . The latter ($\mu > 0$) possibility can produce scenarios for which the final decay in the cascade can be relatively evenly split between $\tilde{\chi}_1^0 \rightarrow \gamma + \tilde{G}$ and $\tilde{\chi}_1^0 \rightarrow Z + \tilde{G}$, leading to final states with a photon, multiple jets (including two from the hadronic decay of the Z boson) that most often do not arise from b -quarks, and E_T^{miss} . For the case that the NLSP is a degenerate set of three wino states, the final step in the cascade includes charged as well as neutral wino decays. Charged wino decays tend to produce isolated leptons, while neutral wino decays produce photons with a wino-to-photon branching fraction that is no less than $\sin^2\theta_W$ for any value of the wino mass. Overall, these two wino-NLSP contributions lead to a significant number of events with an isolated photon accompanied by an isolated lepton. Of the five GGM models considered here, two (the “gluino-bino” and “wino-bino” models, where the gluino is the SUSY

partner of the gluon) incorporate a purely binolike NLSP, two (the “higgsino-bino” models) incorporate a NLSP that is a higgsino-bino admixture, and one (the “wino-NLSP” model) incorporates a winolike set of NLSPs; in all cases the mass of the NLSP state is considered to be a free parameter of the model.

The two GGM models incorporating a binolike NLSP are the focus of the diphoton analysis. For these models, one other set of SUSY partner states is taken to be potentially accessible in 8 TeV pp collisions, while all other SUSY masses are decoupled (set to inaccessibly large values). For both of these binolike NLSP cases, production proceeds solely through this set of SUSY partners, with the NLSP appearing in the subsequent decays of the produced SUSY partner states. For the gluino-bino model, the set of partners is composed of a degenerate octet of gluinos. For the wino-bino model, the set of partners is composed of a degenerate triplet of wino states $\tilde{\chi}_2^0, \tilde{\chi}_1^\pm$, and is dominated by the production of $\tilde{\chi}_1^+ \tilde{\chi}_1^-$ and $\tilde{\chi}_2^0 \tilde{\chi}_1^\pm$. For both of these models, the masses of these produced states are considered to be free parameters along with that of the chosen $\tilde{\chi}_1^0$ state, the latter of which is constrained to be less than those of the produced states. This results in a SUSY production process that proceeds through the creation of pairs of the higher-mass states, which subsequently decay through short cascades to the NLSP $\tilde{\chi}_1^0$ states. Other SM objects (jets, leptons, photons) may be produced in these cascades. The $\tilde{\chi}_1^0$ branching fraction to $\gamma + \tilde{G}$ is 100% for $m_{\tilde{\chi}_1^0} \rightarrow 0$ and approaches $\cos^2\theta_W$ for $m_{\tilde{\chi}_1^0} \gg m_Z$, with the remainder of the $\tilde{\chi}_1^0$ sample decaying to $Z + \tilde{G}$. For all $\tilde{\chi}_1^0$ masses, then, the branching fraction is dominated by the photonic decay, leading to the diphoton-plus- E_T^{miss} signature. For these models with a binolike NLSP, typical production and decay channels for strong (gluino) and electroweak (wino) production are exhibited in Fig. 1.

The higgsino-bino GGM models incorporate a NLSP composed of a higgsino-bino admixture, as well as a degenerate octet of gluinos identical in nature to those of the gluino-bino model. For the first of these models, which is the focus of the photon + b analysis, the higgsino mass parameter μ is required to be negative, and the composition of the NLSP is set by adjusting μ and the GGM U(1) mass parameter M_1 so that a constant ratio of

TABLE I. Summary of the five GGM models considered in this study. For the two higgsino-bino models, the functions $f_\pm(M_1, \mu)$ are chosen to establish NLSP decay properties commensurate with the target experimental signature, as described in the text.

| GGM Model | Experimental Signature | Produced State(s) | Composition of NLSP | Free Parameters |
|-----------------------------|------------------------|-------------------|---------------------|---------------------------------------|
| Gluino-bino | diphoton | gluino | bino | $M_{\tilde{g}}, M_{\tilde{\chi}_1^0}$ |
| Wino-bino | diphoton | wino | bino | $M_{\tilde{w}}, M_{\tilde{\chi}_1^0}$ |
| Higgsino-bino ($\mu < 0$) | photon + b | gluino, higgsino | higgsino/bino | $M_{\tilde{g}}, f_-(M_1, \mu)$ |
| Higgsino-bino ($\mu > 0$) | photon + j | gluino, higgsino | higgsino/bino | $M_{\tilde{g}}, f_+(M_1, \mu)$ |
| Wino NLSP | photon + ℓ | wino | wino | $M_{\tilde{w}}$ |

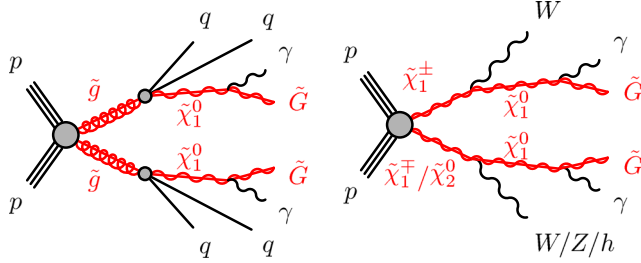


FIG. 1 (color online). Typical production and decay-chain processes for the gluino-production (left) and electroweak-production (right) instances of the GGM model for which the NLSP is a binolike neutralino, referred to in the text as the gluino-bino and wino-bino models, respectively.

the branching fraction of $\tilde{\chi}_1^0 \rightarrow h + \tilde{G}$ to that of $\tilde{\chi}_1^0 \rightarrow \gamma + \tilde{G}$ is maintained at approximately 1.7:1 over the full range of NLSP masses. The photon + b analysis was found to provide the greatest advantage relative to the diphoton analysis for this ratio of branching fractions. In the limit that $m_{\tilde{\chi}_1^0} \gg m_Z$, the NLSP branching fractions to $h + \tilde{G}$, $\gamma + \tilde{G}$, and $Z + \tilde{G}$ approach 56%, 33%, and 11%, respectively. The GGM SU(3) mass parameter M_3 bears a direct relation to the gluino mass, and is taken to be a free parameter in this $\mu < 0$ higgsino-bino model, with all squark states decoupled. The GGM SU(2) mass parameter M_2 is set to a value of 2.5 TeV. Four other electroweak gaugino states typically lie within 25 GeV of the $\tilde{\chi}_1^0$ NLSP: the two lightest charginos $\tilde{\chi}_{1,2}^\pm$, and two additional neutralinos $\tilde{\chi}_2^0$ and $\tilde{\chi}_3^0$. The pair production of gluinos or any of these four additional gaugino states leads to decays to the $\tilde{\chi}_1^0$ via cascades involving SM particles.

For the second of the higgsino-bino models, which is the focus of the photon + j analysis, the μ parameter is chosen to be positive, which suppresses the $h + \tilde{G}$ decay mode of the higgsino. As in the models described above, the NLSP mass is taken to be a free parameter. The M_1 and μ parameters are adjusted so that the branching fractions of the $\tilde{\chi}_1^0$ to $\gamma + \tilde{G}$, $Z + \tilde{G}$ and $h + \tilde{G}$ are maintained close to 50%, 49% and 1% for most values of the $\tilde{\chi}_1^0$ and gluino masses. In this model, the production of gluino pairs can be followed by decays to both a single photon and a hadronically decaying Z boson, producing events with a single isolated high-energy photon accompanied by two jets. In the case that the gluino mass is substantially larger than the $\tilde{\chi}_1^0$ mass, additional jets can be produced in the cascade. Three additional electroweak gaugino states lie close in mass to the $\tilde{\chi}_1^0$, allowing for the possibility of SUSY production through pairs of these states. Such events tend to produce fewer jets than those that proceed through gluino production, but in certain regions of the model space can provide a significant contribution to data samples selected to isolate the photon-plus-jets signature. As in the $\mu < 0$ higgsino-bino model, the value of M_3 , which is

directly related to the gluino mass, is taken to be a free parameter, M_2 is set to a value of 2.5 TeV, and all squark states are decoupled. Typical production and decay-chain processes for the two models for which the NLSP is a higgsino-bino admixture are shown in Fig. 2.

Finally, the wino-NLSP model, which is the focus of the photon + ℓ analysis, incorporates a set of three degenerate winolike NLSPs. This set includes the neutral \tilde{W}^0 , which as the lightest neutral gaugino is also referred to as the $\tilde{\chi}_1^0$, as well as the two charged wino states, which form the $\tilde{\chi}_1^\pm$ states. Production proceeds through the direct production of pairs of NLSP states; such events usually contain at least one \tilde{W}^0 NLSP. Although the \tilde{W}^0 couples preferentially to the Z boson relative to the photon, the \tilde{W}^0 decays into a photon + gravitino final state with unit branching fraction for wino mass below that of the Z boson. The \tilde{W}^0 branching fraction to photon + gravitino approaches $\sin^2 \theta_W$ for wino masses far above that of the Z boson. Leptons can be produced either through the decays of charged wino states, or through the decays of Z bosons that arise from \tilde{W}^0 decay, leading to a significant probability that the overall final state would contain both a photon and a lepton. In this model, a common wino mass scale is taken as a free parameter, with all other GGM mass parameters set to a value of 2.5 TeV, except the squark masses, which are set to infinity. A production and decay diagram typical for this model is shown in Fig. 3.

For all five models considered here, the mass of the gravitino is chosen so that the NLSP decay length is never greater than 1 mm. This ensures that all particles arising from the decay of the NLSP are prompt, and in particular that the relationship between the point and direction of impact of photons from NLSP decay upon the face of the

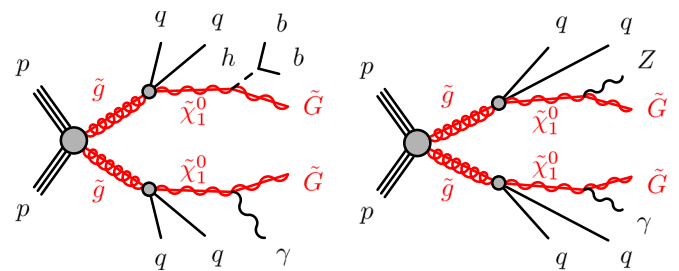


FIG. 2 (color online). Typical production and decay-chain processes for the gluino-production instance of the GGM model for which the NLSP is a higgsino-bino neutralino admixture, referred to in the text as the higgsino-bino model. For the model with $\mu < 0$ (left), the final step of the cascade (the $\tilde{\chi}_1^0$ decay) would have a probability of order 50% of producing a Higgs boson rather than a photon or Z boson; for the model with $\mu > 0$ (right), the $\tilde{\chi}_1^0$ decay would have a probability of order 50% of producing a Z boson rather than a photon. For both of these models, production can also proceed through gaugino and neutralino states, which can dominate the production cross section for high values of gluino mass.

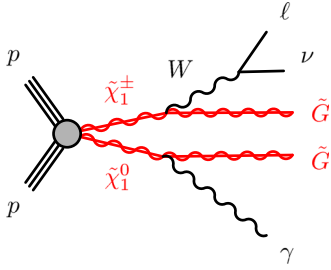


FIG. 3 (color online). Typical production and decay-chain processes for the wino-NLSP model. In this model, the $\tilde{\chi}_1^0$ is a pure \tilde{W}^0 state, while the $\tilde{\chi}_1^\pm$ are the two charged wino states.

detector is consistent with that of a prompt photon (a separate analysis [27] searches for GGM models with a longer-lived binolike NLSP, leading to signatures with nonprompt photons). In addition, the ratio $\tan\beta$ of the two SUSY Higgs-doublet vacuum-expectation values is set to a value of 1.5; for all five models, the phenomenology relevant to this search is only weakly dependent on the value of $\tan\beta$.

III. SAMPLES OF SIMULATED PROCESSES

For the GGM models under study, the SUSY mass spectra and branching ratios are calculated using SUSPECT 2.41 [28] and SDECAY 1.3b [29], respectively, inside the package SUSY-HIT 1.3 [30]. The Monte Carlo (MC) SUSY signal samples are produced using HERWIG++ 2.5.2 [31] with CTEQ6L1 parton distribution functions (PDFs) [32]. Signal cross sections are calculated to next-to-leading order (NLO) in the strong coupling constant, including, for the case of strong production, the resummation of soft gluon emission at next-to-leading-logarithmic accuracy (NLO + NLL) [33–37]. The nominal cross section and its uncertainty are taken from an envelope of cross-section predictions using different PDF sets and factorization and renormalization scales [38]. At fixed center-of-mass energy, SUSY production cross sections decrease rapidly with increasing SUSY partner mass. At $\sqrt{s} = 8$ TeV, the gluino-production cross section is approximately 24 fb for a gluino mass of 1000 GeV and falls to below 1 fb for a gluino mass of 1400 GeV. The wino production cross section is approximately 15 fb for a wino mass of 500 GeV, and falls to approximately 1 fb for a wino mass of 750 GeV.

While most of the backgrounds to the GGM models under examination are estimated through the use of control samples selected from data, as described below, the extrapolation from control regions (CRs) to signal regions (SRs) depends on simulated samples, as do the optimization studies. The simulation of W and Z boson production, including events with up to five accompanying partons, is calculated by two different generators. The ALPGEN 2.14 [39] Monte Carlo generator is interfaced to HERWIG 6.520 for showering and fragmentation and to JIMMY [40] for simulation of the underlying event. Parton distributions are

provided by the CTEQ6L1 functions. Similar samples are produced with the SHERPA 1.4.1 generator [41] with CT10 [42] PDFs, for up to four accompanying partons.

$W\gamma$ production is also simulated via ALPGEN interfaced to HERWIG and JIMMY, but makes use of the CT10 PDFs. Other $W\gamma$ samples are generated, as is the $Z\gamma$ process, by using SHERPA with the CT10 PDFs. The $t\bar{t}\gamma$ process is simulated at leading order (LO) using MADGRAPH 5.1.5.11 [43] and CTEQ6L1, interfaced to the PYTHIA 6.427 parton shower generator [44]. The $t\bar{t}$ process is simulated not only with the POWHEG generator interfaced to PYTHIA and the CTEQ6L1 PDFs, but also with the MC@NLO 4.06 generator [45,46] and the CT10 PDFs, including full NLO QCD corrections. This contribution is rescaled to match the $t\bar{t}$ cross section at NNLO with NNLL soft gluon terms, as calculated with top++ 2.0 [47–52]. The $t\gamma$ and $\bar{t}\gamma$ processes are simulated with the WHIZARD 2.1.1 [53,54] generator, with four-flavor/five-flavor matching provided using HOPPET [55]. Additional photon radiation is added with PHOTOS [56], with parton showering and fragmentation again simulated with PYTHIA. Other t and \bar{t} samples are generated with POWHEG.

The $\gamma + \text{jet}(s)$ process is simulated in a similar manner to the W^\pm or Z samples using ALPGEN interfaced to HERWIG and JIMMY and the CTEQ6L1 PDFs. A generator-level requirement of 35 GeV is applied to the photon transverse momentum p_T^γ , and the sample is generated in exclusive bins of p_T^γ to produce a more statistically significant sample at higher values of p_T^γ . Additional $\gamma + \text{jet}(s)$ samples are used, simulated with SHERPA and the CT10 PDFs. The prompt diphoton sample is generated with PYTHIA 6.423, which includes the subprocesses $gg \rightarrow \gamma\gamma$ and $q\bar{q} \rightarrow \gamma\gamma$, with the requirement that there be at least two prompt photons with generated transverse momentum greater than 20 GeV. Parton densities are modeled according to the MRST 2007 LO* [57] functions.

The background from $Z(\rightarrow \nu\bar{\nu}) + \gamma\gamma$ production is simulated using the SHERPA MC generator, normalized to a cross section calculated at LO using MADGRAPH 5 and the CTEQ6L1 PDF, and then corrected by a K -factor of 2.0 ± 1.0 [58]. The background from $W(\rightarrow \ell\nu) + \gamma\gamma$ production is simulated using the ALPGEN MC generator, although the overall normalization is set via a study making use of data events containing two photons and a charged lepton (to be discussed below). Diboson production, for the case that each boson is a W or Z , is simulated with POWHEG.

All MC samples are processed with the GEANT4-based simulation [59] of the ATLAS detector [60], or, where appropriate, a simulation of the ATLAS detector based on parametrized shower shapes in the calorimeter, and GEANT4 elsewhere. Corrections are applied to the simulated samples to account for differences between data and simulation for the lepton and photon trigger, identification, and reconstruction efficiencies, as well as for the efficiency and misidentification rate of the algorithm used to identify

jets containing b -hadrons (b -tagging). The variation of the number of pp interactions per bunch crossing (“pileup”) as a function of the instantaneous luminosity is taken into account by overlaying simulated minimum-bias events according to the observed distribution of the number of pileup interactions in data, with an average of 21 interactions per event.

IV. ATLAS DETECTOR

The ATLAS experiment makes use of a multipurpose detector [61] with a forward-backward symmetric cylindrical geometry and nearly 4π solid angle coverage.¹ Closest to the beam line are solid-state tracking devices comprising layers of silicon-based pixel and strip detectors covering $|\eta| < 2.5$ and straw-tube detectors covering $|\eta| < 2.0$, located inside a thin superconducting solenoid that provides a 2 T magnetic field. Outside the solenoid, fine-grained lead/liquid-argon electromagnetic (EM) calorimeters provide coverage over $|\eta| < 3.2$ for the measurement of the energy and position of electrons and photons. A presampler, covering $|\eta| < 1.8$, is used to correct for energy lost upstream of the EM calorimeter. An iron/scintillator-tile hadronic calorimeter covers the region $|\eta| < 1.7$, while a copper/liquid-argon medium is used for hadronic calorimeters in the end cap region $1.5 < |\eta| < 3.2$. In the forward region $3.2 < |\eta| < 4.9$ liquid-argon calorimeters with copper and tungsten absorbers measure the electromagnetic and hadronic energy. A muon spectrometer consisting of three superconducting toroidal magnet systems, each comprising eight toroidal coils, tracking chambers, and detectors for triggering, surrounds the calorimeter system. The muon system reconstructs penetrating tracks over a range $|\eta| < 2.7$ and provides input to the trigger system over a range $|\eta| < 2.4$. A three-level trigger system is used to select events. The first-level trigger is implemented in hardware and uses a subset of the detector information to reduce the accepted rate to at most 75 kHz. This is followed by two software-based trigger levels that together reduce the accepted event rate to 400 Hz on average depending on the data-taking conditions during 2012.

V. RECONSTRUCTION OF CANDIDATES AND OBSERVABLES

Primary vertices are formed from sets of two or more tracks, each with transverse momentum $p_T^{\text{track}} > 400$ MeV,

¹ATLAS uses a right-handed coordinate system with its origin at the nominal interaction point (IP) in the center of the detector and the z axis along the beam pipe. The x axis points from the IP to the center of the LHC ring, and the y axis points upwards. Cylindrical coordinates (r, ϕ) are used in the transverse plane, ϕ being the azimuthal angle around the beam pipe. The pseudorapidity is defined in terms of the polar angle θ as $\eta = -\ln[\tan(\theta/2)]$. Angular distance is measured in units of $\Delta R \equiv \sqrt{(\Delta\eta)^2 + (\Delta\phi)^2}$.

that are mutually consistent with having originated at the same three-dimensional space point within the luminous region of the colliding proton beams. When more than one such primary vertex is found, the vertex with the largest scalar sum of the squared transverse momenta of the associated tracks is chosen. To further ensure the event resulted from a beam collision, the primary vertex of the event is required to have at least five associated tracks.

Electron candidates are reconstructed from EM calorimeter energy clusters consistent with having arisen from the impact of an electromagnetic particle (electron or photon) upon the face of the calorimeter. For the object to be considered an electron, it is required to match a track identified by a reconstruction algorithm optimized for recognizing charged particles with a high probability of bremsstrahlung. In addition, the matched track is required to include information from at least seven layers of the solid-state tracking system; a track within the acceptance of the tracking system typically traverses eleven layers of the solid-state tracking system. The energy of the electron candidate is determined from the EM cluster, while its pseudorapidity is determined from the associated reconstructed track. Further details of the reconstruction of electrons can be found in Refs. [62] and [63]. Electron candidates used by these analyses are further required to have $p_T > 20$ GeV and $|\eta| < 2.47$. For the photon + ℓ analysis, signal electrons are not allowed to be within the transition region $1.37 < |\eta| < 1.52$ between the barrel and end cap calorimeters. A track-based isolation requirement is imposed, with the scalar sum of the transverse momenta of tracks within a cone of size $\Delta R = 0.3$ required to be less than 16% of the electron p_T . Finally, the electron track is required to be consistent with coming from the primary vertex in the r - z plane.

Electromagnetic clusters are classified as photon candidates provided that they either have no matched track or have one or more matched tracks consistent with coming from a photon conversion vertex. Based on the characteristics of the longitudinal and transverse shower development in the EM calorimeter, photons are classified as “loose” or “tight.” Further details of the reconstruction of photons can be found in Ref. [64]. In the case that an EM calorimeter deposition is identified as both a photon and an electron, the photon candidate is discarded and the electron candidate retained. Photon candidates used by these analyses are required to be within $|\eta| < 2.37$, and to be outside the transition region $1.37 < |\eta| < 1.52$. Finally, an isolation requirement is imposed. After correcting for contributions from pileup and the deposition ascribed to the photon itself, loose and tight isolation criteria are defined, with the tight criterion requiring less than 4 GeV of transverse “isolation energy” in a cone of size $\Delta R = 0.4$ surrounding the energy deposition in the calorimeter associated with the photon. For the loose isolation criterion, no more than 5 GeV of isolation energy is allowed within a cone of size $\Delta R = 0.2$.

The tight criterion is used for the diphoton analysis, while the loose criterion is used for the remaining three signatures (photon + b , photon + j , photon + ℓ).

Muon candidates make use of reconstructed tracks from the tracking system as well as information from the muon system [65]. Muons are required to be either “combined,” for which the muon is reconstructed independently in both the muon spectrometer and the tracking system and then combined, or “segment tagged,” for which the muon spectrometer is used to tag tracks as muons, without requiring a fully reconstructed candidate in the muon spectrometer. Signal muons are required to have $p_T > 20$ GeV and $|\eta| < 2.4$. Track-based as well as calorimeter-based isolation requirements are imposed, with the scalar sum of the transverse momenta of tracks within a cone of size $\Delta R = 0.3$ required to be less than 12% of the muon p_T , and the energy in the calorimeter projected in the transverse plane within a cone of size $\Delta R = 0.3$, corrected for pileup, also required to be less than 12% of the muon p_T . Finally, the muon track is required to be consistent with coming from the primary vertex in both the r - z and r - ϕ planes.

Jets are reconstructed from three-dimensional calorimeter energy clusters using the anti- k_r algorithm [66] with a radius parameter $R = 0.4$. Jets arising from detector noise, cosmic rays or other noncollision sources are rejected, as described in Ref. [67]. Each cluster is classified, prior to the jet reconstruction, as coming from an electromagnetic or hadronic shower on the basis of its shape [68]. Each cluster energy is then corrected by weighting electromagnetic and hadronic energy deposits with correction factors derived from Monte Carlo simulation. A correction is applied to subtract the expected contamination from pileup, calculated as the product of the jet area in η - ϕ space and the average energy density of the event [69]. A further calibration, relating the response of the calorimeter to *in situ* jet-energy measurements [69] is then applied. Once calibrated, jets are required to have $p_T > 20$ GeV and $|\eta| < 2.8$. Jets containing b -hadrons are identified using the MV1c b -tagging algorithm [70]. This neural network algorithm combines the information from various algorithms based on track impact-parameter significance or explicit reconstruction of b - and c -hadron decay vertices. The analyses presented in this paper use an operating point corresponding to 70% efficiency for jets originating from the fragmentation of a b -quark in simulated $t\bar{t}$ events, selecting approximately 0.7% of light-quark and gluon-induced jets and 20% of c -quark-induced jets.

In the case that two reconstructed objects are in close enough proximity to one another to raise a concern that they are a single detector object reconstructed as more than one particle or jet candidate, an overlap-removal procedure is followed. To reduce the rate of electrons misidentified as photons, if the angular distance ΔR between a reconstructed electron and photon is less than 0.01, the object is classified as an electron.

To avoid ambiguity that arises when an electron or photon is also reconstructed as a jet, if a jet and an electron or photon are reconstructed within an angular distance $\Delta R = 0.2$ of one another, the electron or photon is retained and the jet is discarded; if $0.2 < \Delta R < 0.4$ then the jet is retained and the electron or photon is discarded. Finally, in order to suppress the reconstruction of muons arising from showers induced by jets, if a jet and a muon are found with $\Delta R < 0.4$ the jet is retained and the muon is discarded.

The vector momentum imbalance in the transverse plane is obtained from the negative vector sum of the reconstructed and calibrated physics objects and is referred to as missing transverse momentum E_T^{miss} [71]. Calorimeter energy deposits are associated with a reconstructed and identified high- p_T object in a specific order: electrons with $p_T > 10$ GeV, photons with $p_T > 10$ GeV, and jets with $p_T > 20$ GeV. Deposits not associated with any such objects are also taken into account in the E_T^{miss} determination, as are muons with $p_T > 10$ GeV.

The transverse mass M_T of a system of two massless particles with four-vectors p_1 and p_2 is given by

$$M_T = \sqrt{2p_{T,1}p_{T,2}(1 - \cos \Delta\phi_{1,2})},$$

where $\Delta\phi_{1,2}$ is the angular separation between the two vectors projected into the transverse plane. The analyses presented here make use of the transverse mass of both the photon- E_T^{miss} ($M_T^{\gamma, E_T^{\text{miss}}}$) and lepton- E_T^{miss} ($M_T^{\ell, E_T^{\text{miss}}}$) systems, where the lepton is taken to be massless in the transverse-mass determination.

Several additional observables are defined to help in the discrimination of SM backgrounds from potential GGM signals. The total visible transverse energy H_T is calculated as the scalar sum of the transverse momenta of the selected photons and any additional leptons and jets in the event; a similar observable based only on the momenta of jets in the events is referred to as H_T^{jets} . The “effective mass” m_{eff} is defined as the scalar sum of H_T and E_T^{miss} . The photon- E_T^{miss} separation $\Delta\phi(\gamma, E_T^{\text{miss}})$ is defined as the azimuthal angle between the missing transverse momentum vector and the selected photon. In the case of the diphoton analysis, $\Delta\phi_{\text{min}}(\gamma, E_T^{\text{miss}})$ is defined to be the minimum value of $\Delta\phi(\gamma, E_T^{\text{miss}})$ of the two selected photons. The minimum jet- E_T^{miss} separation $\Delta\phi_{\text{min}}(\text{jet}, E_T^{\text{miss}})$ is defined as the minimum azimuthal angle between the missing transverse momentum vector and the leading (highest- p_T) jets in the event. The number of leading jets used differs depending on the signature under study and is shown in Tables II and III. For the diphoton analysis, leading jets are required to have $p_T > 75$ GeV, and if no such jet is found, no requirement is placed on the observable. The quantity $\Delta\phi_{\text{min}}(\text{jet}, \gamma)$ is defined as the minimum separation between the selected photon and each of the two leading jets in the event. The quantity $\Delta R(\ell, \gamma)$ is defined as the distance in

TABLE II. Enumeration of the requirements defining the four SRs developed for the diphoton signature search.

| Signal Region | $\text{SR}_{\text{S-L}}^{\gamma\gamma}$ | $\text{SR}_{\text{S-H}}^{\gamma\gamma}$ | $\text{SR}_{\text{W-L}}^{\gamma\gamma}$ | $\text{SR}_{\text{W-H}}^{\gamma\gamma}$ |
|--|---|---|---|---|
| Number of photons (E_{T} [GeV]) | > 1 (> 75) | > 1 (> 75) | > 1 (> 75) | > 1 (> 75) |
| $E_{\text{T}}^{\text{miss}}$ [GeV] | > 150 | > 250 | > 150 | > 200 |
| H_{T} [GeV] | ... | ... | > 600 | > 400 |
| m_{eff} [GeV] | > 1800 | > 1500 | ... | ... |
| $\Delta\phi_{\text{min}}(\text{jet}, E_{\text{T}}^{\text{miss}})$ (number of leading jets) | > 0.5 (2) | > 0.5 (2) | > 0.5 (2) | > 0.5 (2) |
| $\Delta\phi_{\text{min}}(\gamma, E_{\text{T}}^{\text{miss}})$ | ... | > 0.5 | ... | > 0.5 |

TABLE III. Enumeration of the requirements defining the four SRs developed for the photon + b and photon + j signature searches.

| Signal Region | $\text{SR}_{\text{L}}^{\gamma b}$ | $\text{SR}_{\text{H}}^{\gamma b}$ | $\text{SR}_{\text{L}}^{\gamma j}$ | $\text{SR}_{\text{H}}^{\gamma j}$ |
|--|-----------------------------------|-----------------------------------|-----------------------------------|-----------------------------------|
| Number of photons (E_{T} [GeV]) | > 0 (> 125) | > 0 (> 150) | 1 (> 125) | 1 (> 300) |
| $E_{\text{T}}^{\text{miss}}$ [GeV] | > 100 | > 200 | > 200 | > 300 |
| H_{T} [GeV] | ... | > 1000 | ... | > 800 |
| Number of jets (number of b -jets) | 2–4 (> 1) | > 3 (> 0) | $> 3^{\text{a}}$ | $> 1^{\text{a}}$ |
| Number of leptons | 0 | ... | 0 | 0 |
| M_{bb} [GeV] | 75–150 | ... | ... | ... |
| $M_{\text{T}}^{\gamma, E_{\text{T}}^{\text{miss}}}$ [GeV] | > 90 | > 90 | ... | ... |
| $\Delta\phi_{\text{min}}(\text{jet}, E_{\text{T}}^{\text{miss}})$ (number of leading jets) | > 0.3 (2) | > 0.3 (4) | > 0.4 (2) | > 0.4 (2) |
| R_{T}^4 | ... | ... | < 0.85 | ... |
| $\Delta\phi_{\text{min}}(\text{jet}, \gamma)$ | ... | ... | ... | < 2.0 |

^aFor $\text{SR}_{\text{L}}^{\gamma j}$ and $\text{SR}_{\text{H}}^{\gamma j}$, the two leading jets are required to have $p_{\text{T}} > 100$ and $p_{\text{T}} > 40$ GeV, respectively.

η - ϕ space between the leading photon and lepton. Finally, the quantity R_{T}^4 is defined as the scalar sum of the transverse momentum of the four highest- p_{T} jets in the event divided by the sum of the transverse momentum of all jets in the event.

VI. EVENT SELECTION

The data sample is selected by a trigger requiring the presence of one loose photon with energy projected into the plane transverse to the beam pipe (E_{T}) of greater than 120 GeV for the photon + b , photon + j and photon + ℓ analyses, or two loose photons with $E_{\text{T}} > 40$ GeV for the diphoton analysis. Events are removed from the data sample if they contain jets likely to be produced by beam backgrounds, cosmic rays or detector noise, as described in Ref. [67]. After applying data-quality requirements related to the beam and detector conditions, the total available integrated luminosity is 20.3 fb^{-1} . The uncertainty on the integrated luminosity is $\pm 2.8\%$, estimated via the methodology of Ref. [72].

For the diphoton analysis, geared towards the exploration of the gluino-bino and wino-bino GGM models incorporating a purely binolike $\tilde{\chi}_1^0$, two separate SR selection strategies were developed: a “ $\text{SR}_{\text{S}}^{\gamma\gamma}$ ” selection geared towards the production of higher-mass strongly coupled SUSY states (gluinos and squarks) and a “ $\text{SR}_{\text{W}}^{\gamma\gamma}$ ” selection geared towards the production of lower-mass

weakly coupled SUSY states (winos). For each of these approaches, two SRs are defined: the first ($\text{SR}_{\text{S-L}}^{\gamma\gamma}$, $\text{SR}_{\text{W-L}}^{\gamma\gamma}$) optimized for the case of a lower-mass $\tilde{\chi}_1^0$ and the second ($\text{SR}_{\text{S-H}}^{\gamma\gamma}$, $\text{SR}_{\text{W-H}}^{\gamma\gamma}$) for a higher-mass $\tilde{\chi}_1^0$.

For the photon + b analysis, geared towards the higgsino-bino GGM model with a negative value of the μ parameter, two SRs ($\text{SR}_{\text{L}}^{\gamma b}$, $\text{SR}_{\text{H}}^{\gamma b}$) are defined. The SRs are again distinguished by their optimization for low- and high- $\tilde{\chi}_1^0$ mass, respectively. In particular, the $\text{SR}_{\text{L}}^{\gamma b}$ selection is designed to have a high acceptance for events that arise through the production of pairs of weakly coupled SUSY partners, which can have a significant cross section for the low- $\tilde{\chi}_1^0$ -mass reaches of the higgsino-bino GGM model explored here. For the photon + j analysis, geared towards the higgsino-bino GGM model with a positive value of the μ parameter, a further set of two SRs are defined ($\text{SR}_{\text{L}}^{\gamma j}$, $\text{SR}_{\text{H}}^{\gamma j}$). These two SRs are once again distinguished by their optimization for low and high $\tilde{\chi}_1^0$ mass, respectively.

A final “ $\text{SR}_{e/\mu}^{\gamma\ell}$ ” signal region was developed to search for photon + ℓ events arising from the GGM model with a winolike set of NLSPs. This SR is divided into two subsets— $\text{SR}_e^{\gamma\ell}$ and $\text{SR}_{\mu}^{\gamma\ell}$ —depending on the flavor of the leading lepton (electron or muon).

All four diphoton SRs require two tight, isolated photons with $E_{\text{T}} > 75$ GeV, while the $\text{SR}_{\text{L}}^{\gamma b}$ and $\text{SR}_{\text{H}}^{\gamma b}$ signal regions require a single tight, isolated photon with $E_{\text{T}} > 125$ GeV

and $E_T > 150$ GeV, respectively, and the $\text{SR}_L^{\gamma j}$ and $\text{SR}_H^{\gamma j}$ signal regions require a single tight, isolated photon with $E_T > 125$ GeV and $E_T > 300$ GeV, respectively. The $\text{SR}_{e/\mu}^{\ell}$ signal region requires a single tight, isolated photon with $E_T > 125$ GeV. Along with E_T^{miss} , leptonic, and (b -) jet activity, requirements are made on a number of additional observables, with values chosen to optimize the sensitivity to the GGM signal of interest for each SR. To ensure that the E_T^{miss} observable is accurately measured, minimum requirements on $\Delta\phi_{\min}(\gamma, E_T^{\text{miss}})$ and $\Delta\phi_{\min}(\text{jet}, E_T^{\text{miss}})$ are considered for each SR. For the $\text{SR}_H^{\gamma j}$ signal region of the photon + j analysis, rejecting events with jets misidentified as photons by placing a requirement on $\Delta\phi_{\min}(\text{jet}, \gamma)$ is found to improve the sensitivity of the analysis.

To exploit the high-energy scale associated with SUSY production at masses close to the expected limit of sensitivity of the various SRs, several SRs include minimum requirements on one of the two total-transverse-energy observables H_T or m_{eff} . As an illustration, Fig. 4 (left) shows the m_{eff} distribution of selected diphoton events as well as that expected from several SM sources and from characteristic strong-production points of the binolike NLSP GGM model. For electrons from W boson decay that are misreconstructed as photons, the transverse

mass $M_T^{\gamma, E_T^{\text{miss}}}$ of the photon- E_T^{miss} system tends to be less than that of the W boson; because of this, the photon + b analysis is found to benefit from a minimum requirement on $M_T^{\gamma, E_T^{\text{miss}}}$. The $\text{SR}_L^{\gamma b}$ analysis also benefits from a requirement that the invariant mass M_{bb} of the system formed by the two most energetic b -jets be close to the Higgs boson mass. A minimum requirement on the transverse mass $M_T^{\ell, E_T^{\text{miss}}}$ of the lepton- E_T^{miss} system is similarly found to be effective in rejecting backgrounds from W boson and semileptonic $t\bar{t}$ decay for the photon + ℓ analysis. A further requirement that the electron-photon system invariant mass not be close to the Z boson mass helps to reject Z boson backgrounds to the photon + ℓ analysis. A requirement that $\text{SR}_L^{\gamma b}$ signal events have no identified charged leptons helps to reduce the background from semileptonic $t\bar{t}$ events, while a requirement that $\text{SR}_H^{\gamma j}$ signal events have $R_T^4 < 0.85$ helps reduce the background from SM events, which tend to have fewer and softer jets than do signal events; as an illustration, see Fig. 4 (right). Finally, a requirement that the total transverse energy from jets with $p_T > 40$ GeV (H_T^{jets}) be less than 100 GeV helps reduce the backgrounds to $\text{SR}_{e/\mu}^{\ell}$ due to top quark production.

A summary of the selection requirements specific to each of the diphoton SRs is presented in Table II, to $\text{SR}_L^{\gamma b}$, $\text{SR}_H^{\gamma b}$,

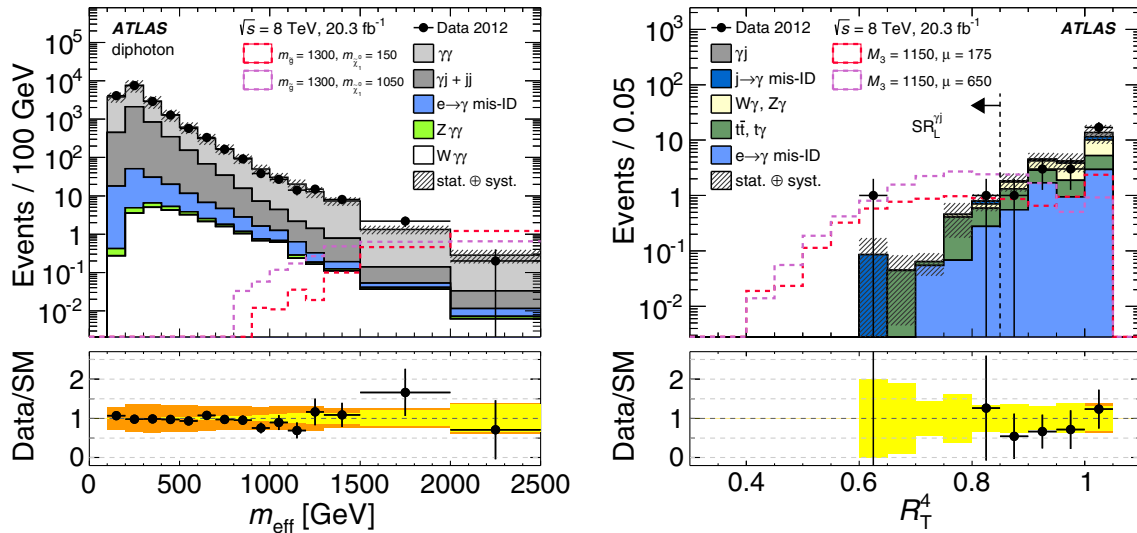


FIG. 4 (color online). (Left) Distribution of m_{eff} , the sum of the total visible transverse energy and E_T^{miss} , for selected diphoton events, after requiring $\Delta\phi_{\min}(\text{jet}, E_T^{\text{miss}}) > 0.5$ but before application of a requirement on E_T^{miss} and $\Delta\phi_{\min}(\gamma, E_T^{\text{miss}})$. Also shown are the expected contributions of SM processes, estimated as described in Sec. VII, as well as the expected m_{eff} distributions for the $(m_{\tilde{g}}, m_{\tilde{\chi}_1^0}) = (1300, 150)$ GeV and $(m_{\tilde{g}}, m_{\tilde{\chi}_1^0}) = (1300, 1050)$ GeV gluino-bino GGM models. (Right) Distribution of R_T^4 , the scalar sum of the transverse momentum of the four highest- p_T jets in the event divided by the sum of the transverse momentum of all jets in the event, for the sample surviving all $\text{SR}_L^{\gamma j}$ selection criteria except the R_T^4 requirement itself. Also shown are the expected contributions of SM processes, estimated as described in Sec. VII, as well as the signal expectation for the two points in the M_3 - μ parameter space characteristic of the $\mu > 0$ GGM model relevant to the photon + j analysis. For both figures, the lower plot shows the ratio of observed data to the combined SM expectation, with the inner band representing the range of statistical uncertainty and the outer band (visible only in the highest R_T^4 bin in the right-hand figure) the combined statistical and systematic uncertainty. Events outside the range of the displayed region are included in the highest-valued bin.

TABLE IV. Enumeration of the requirements defining the two SRs developed for the photon + ℓ signature search.

| Signal Region | $\text{SR}_e^{\gamma\ell}$ | $\text{SR}_\mu^{\gamma\ell}$ |
|---------------------------------------|----------------------------|------------------------------|
| Number of photons (E_T [GeV]) | > 0 (> 125) | > 0 (> 125) |
| E_T^{miss} [GeV] | > 120 | > 120 |
| H_T^{jets} [GeV] | < 100 | < 100 |
| Number of leptons | > 0 (e) | > 0 (μ) |
| $ M_{e\gamma} - M_Z $ [GeV] | (> 15) | ... |
| $M_T^{\ell, E_T^{\text{miss}}}$ [GeV] | > 120 | > 120 |
| $\Delta R(\ell, \gamma)$ | > 0.7 | > 0.7 |

$\text{SR}_L^{\gamma j}$ and $\text{SR}_H^{\gamma j}$ in Table III, and to the two photon + ℓ SRs in Table IV. After all selection requirements, the numbers of events remaining in the various signal regions are 0 ($\text{SR}_{S-L}^{\gamma\gamma}$, $\text{SR}_{S-H}^{\gamma\gamma}$), 5 ($\text{SR}_{W-L}^{\gamma\gamma}$), 1 ($\text{SR}_{W-H}^{\gamma\gamma}$), 12 ($\text{SR}_L^{\gamma b}$), 2 ($\text{SR}_H^{\gamma b}$, $\text{SR}_L^{\gamma j}$, $\text{SR}_H^{\gamma j}$), 16 ($\text{SR}_e^{\gamma\ell}$) and 10 ($\text{SR}_\mu^{\gamma\ell}$).

VII. BACKGROUND ESTIMATION

Backgrounds to the various SRs arise from a number of sources, including processes such as radiative vector boson production that generate real photons in combination with energetic neutrinos, as well as events in which one or more energetic jets or electrons are misidentified as a photon. While these sources contribute generically to all four signatures explored in this study, the differing definitions of each of the associated SRs lead to, in many cases, significant differences in the manner in which the contributions of these various background sources are estimated. In the following, the methodology of the background estimation for each of the four experimental signatures is discussed, and the resulting background estimates, broken down by source, are tabulated. For the estimation of background contributions that rely upon MC simulation, either directly or through the estimation of “transfer factors” relating the background content of control regions to that of corresponding SRs, the effect of MC modeling uncertainties have been considered; in general, these uncertainties are found not to be dominant contributions to the overall uncertainty in the background estimates. Background models are confirmed in validation regions (VRs) with selection criteria closely related to those of the corresponding SR, but with one or more selection criteria modified to suppress the contribution of possible GGM signal to the VR.

A. Backgrounds to the diphoton analysis

Backgrounds from SM contributions to the four diphoton SRs are grouped into three primary components. The first of these, referred to as “QCD background,” arises from a mixture of processes that include $\gamma\gamma$ production as well as γ + jet and multijet events with at least one jet misreconstructed as a photon. The second background component,

referred to as “EW background,” is due to $W + X$ (here “ X ” can be any number of jets, accompanied by no more than one photon; the two-photon case is treated separately) and $t\bar{t}$ events, with a smaller contribution arising from $Z + X$ events. These events tend to include final-state neutrinos that produce significant E_T^{miss} . In both cases, EW background events entering the signal regions generally have at least one electron misreconstructed as a photon. The QCD and EW backgrounds are estimated through the use of dedicated control samples of data events.

The third background component, referred to as “irreducible,” consists of W and Z bosons produced in association with two real photons, with a subsequent decay into one or more neutrinos. For this background, the $W(\rightarrow \ell\nu) + \gamma\gamma$ component dominates, and requires corrections to its LO contribution that are both large and rapidly varying across the phase space of the $W(\rightarrow \ell\nu) + \gamma\gamma$ (plus possible additional jets) process [73]. Thus a data-driven approach was developed to constrain the $W(\rightarrow \ell\nu) + \gamma\gamma$ contribution to the four SRs. The $Z(\rightarrow \nu\bar{\nu}) + \gamma\gamma$ contribution is estimated directly from the MC simulation.

The QCD background to $\text{SR}_{S-L}^{\gamma\gamma}$, $\text{SR}_{S-H}^{\gamma\gamma}$, $\text{SR}_{W-L}^{\gamma\gamma}$ and $\text{SR}_{W-H}^{\gamma\gamma}$ is expected to arise from events with two real, isolated photons (diphoton QCD events) unaccompanied by any additional electroweak bosons, and from events with a single real, isolated photon and a jet whose fragmentation fluctuates in such a manner as to cause it to be misidentified as a second isolated photon (“photon + jet” QCD events). A contribution from dijet QCD events is found to be small and largely incorporated into the photon + jet background estimate. To estimate the photon + jet contribution a “QCD control sample” is identified within the diphoton-trigger data sample by selecting events for which one photon candidate satisfies the tight selection criterion, while the other satisfies the loose but not the tight photon criterion. QCD control sample events containing electrons are vetoed to reduce contamination from $W \rightarrow e\nu$ decays. Studies with MC simulated samples as well as E_T^{miss} and H_T sideband data suggest that the E_T^{miss} distribution of this control sample adequately reproduces the E_T^{miss} distribution of the QCD background in the high- E_T^{miss} region used for the signal selection. A diphoton MC sample is used for the estimation of the diphoton contribution to the QCD background.

The H_T , m_{eff} , $\Delta\phi_{\text{min}}(\text{jet}, E_T^{\text{miss}})$ and $\Delta\phi_{\text{min}}(\gamma, E_T^{\text{miss}})$ requirements associated with each of the four SRs are applied to the QCD control and diphoton MC samples, and the resulting samples are scaled so that the combination of the two samples exactly reproduces the number of observed diphoton events (for the given SR) in the region $0 < E_T^{\text{miss}} < 60$ GeV, and with the diphoton MC sample providing a specified fraction of the total event count in this region. As suggested by the independent ATLAS $H \rightarrow \gamma\gamma$ [74] and isolated photon pair cross-section [75] analyses, this fraction is set to 75%, although in this analysis a range

between 50% and 100% is adopted to reflect the degree of uncertainty in this fraction. The resulting QCD-background estimate, for each of the four binlike SRs, is then obtained by summing the scaled number of combined QCD control and diphoton MC events with E_T^{miss} above the minimum requirement for the given SR. Additional sources of systematic uncertainty on the QCD-background estimate include its dependence on the low- E_T^{miss} region used to scale the diphoton MC and QCD control samples, and the effect of possible mismodeling of the $\Delta\phi_{\text{min}}(\text{jet}, E_T^{\text{miss}})$ and $\Delta\phi_{\text{min}}(\gamma, E_T^{\text{miss}})$ distributions of the QCD background by the QCD control sample. Including both systematic uncertainty and the statistical uncertainty associated with the limited number of events in the QCD control and diphoton MC samples, the result for the QCD background and its overall uncertainty is shown in Table V.

The QCD-background model is validated by comparing the observed numbers of events to the total expected SM background in bins of 300 GeV in H_T for the sideband region $100 < E_T^{\text{miss}} < 150$ GeV, for which event rates are expected to be dominated by the QCD background. The observed event rate tends to be somewhat lower than that predicted by the overall background model, although it is within 1 standard deviation of the overall background model uncertainty for all H_T bins.

The EW background, arising predominantly from $W + X$ and $t\bar{t}$ events, is estimated via an “electron-photon” control sample composed of events with at least one isolated tight photon and one isolated electron, each with $E_T > 75$ GeV, and scaled by the probability for such an electron to be misreconstructed as a tight photon, as estimated from a “tag-and-probe” study of the Z boson in the ee and $e\gamma$ sample. The electron-to-photon scale factor varies between 1.9% ($0 < |\eta| < 0.6$) and 3.7% ($1.52 < |\eta| < 1.81$), since it depends on the amount of material in front of the calorimeter. Events with two or more tight photons are vetoed from the control sample to preserve its orthogonality to the signal sample. In the case of more than one electron, the one with the highest p_T is used. Including systematic uncertainties of $\pm 25\%$ each, associated with a possible p_T dependence of the scale factor and a possible overlap between the QCD and EW background estimates, leads to the estimates

for the EW background to the four diphoton SRs shown in Table V.

The irreducible background is composed of two distinct components: diphoton production in association with either a W or Z boson. The latter contribution is relatively small and is sufficiently well understood to allow the use of the MC simulation, with a total cross section scaled to that of Ref. [58], to directly estimate the $Z(\rightarrow \nu\bar{\nu}) + \gamma\gamma$ contribution to the four SRs. The value of this estimate is shown in Table V; the uncertainty is dominated by a $\pm 50\%$ uncertainty on the $Z(\rightarrow \nu\bar{\nu}) + \gamma\gamma$ cross section of Ref. [58] that arises from the variation of the factorization and renormalization scales used to quantify the uncertainty due to missing higher-order processes.

The $W(\rightarrow \ell\nu) + \gamma\gamma$ background to the four SRs is estimated using a lepton-diphoton ($\ell\gamma\gamma$) CR. To enhance the contribution of $W(\rightarrow \ell\nu) + \gamma\gamma$ and ensure that the $\ell\gamma\gamma$ CR is exclusive of the four SRs, the photon p_T requirement is lowered to 50 GeV and a requirement of $50 < E_T^{\text{miss}} < 150$ GeV is imposed. To ensure that the CR sample arises from the same region of the $W(\rightarrow \ell\nu) + \gamma\gamma$ process phase space as the expected background, a further requirement that the transverse momentum of the $\ell\gamma\gamma$ system be greater than 100 GeV is imposed. A total of seven events is observed in the CR, for which MC simulation suggests that 2.2 are expected to arise from SM sources other than $W(\rightarrow \ell\nu) + \gamma\gamma$. When setting limits on contributions from new physics in the four SRs, a simultaneous fit to the CR and the signal region under study is performed, allowing both the signal and $W(\rightarrow \ell\nu) + \gamma\gamma$ contributions to float to their best-fit values. When setting model-dependent limits, the fit also takes into account a possible signal contribution to the $\ell\gamma\gamma$ CR, which can be significant for the electroweak-production models in the case that the $\tilde{\chi}_1^0$ mass is light. In the limit that no GGM signal contributes to the $\ell\gamma\gamma$ control region, an enhancement factor of 2.3 must be applied to the $W(\rightarrow \ell\nu) + \gamma\gamma$ MC sample to achieve agreement between the MC simulation and data in the $\ell\gamma\gamma$ control region. The resulting $W(\rightarrow \ell\nu) + \gamma\gamma$ -background estimate in each of the four SRs, under the assumption that there is no signal contribution to the $\ell\gamma\gamma$ CR, is shown in Table V; the uncertainty is dominated by that of the limited number of events in the $\ell\gamma\gamma$ CR. Also shown is the combined

TABLE V. The expected and observed numbers of events for the four diphoton signal regions. The quoted errors are the combined statistical and systematic uncertainties.

| Signal Regions | SR $^{\gamma\gamma}_{S-L}$ | SR $^{\gamma\gamma}_{S-H}$ | SR $^{\gamma\gamma}_{W-L}$ | SR $^{\gamma\gamma}_{W-H}$ |
|--|----------------------------|----------------------------|----------------------------|----------------------------|
| Expected background events | $0.06^{+0.24}_{-0.03}$ | $0.06^{+0.24}_{-0.04}$ | $2.04^{+0.82}_{-0.75}$ | $1.01^{+0.48}_{-0.42}$ |
| QCD | $0.00^{+0.24}_{-0.00}$ | $0.00^{+0.24}_{-0.00}$ | $0.32^{+0.45}_{-0.32}$ | $0.22^{+0.33}_{-0.22}$ |
| EW | 0.02 ± 0.02 | 0.0 ± 0.0 | 0.64 ± 0.27 | 0.13 ± 0.08 |
| $(W \rightarrow \ell\nu)\gamma\gamma$ | 0.04 ± 0.02 | 0.05 ± 0.04 | 1.01 ± 0.62 | 0.53 ± 0.34 |
| $(Z \rightarrow \nu\bar{\nu})\gamma\gamma$ | 0.00 ± 0.00 | 0.01 ± 0.01 | 0.07 ± 0.04 | 0.13 ± 0.07 |
| Observed events | 0 | 0 | 5 | 1 |

background estimate, including uncertainty, from all four sources.

B. Backgrounds to the photon + b analysis

For both $\text{SR}_L^{\gamma b}$ and $\text{SR}_H^{\gamma b}$, which include a requirement of at least one b -jet, backgrounds arise from two predominant sources: from leptonic decays of real or virtual W bosons accompanied by the production of b -quark pairs, including those arising in $t\bar{t}$ events [“ $W(\rightarrow \ell\nu)$ ” backgrounds]; and from events containing no electroweak bosons or top quarks (QCD backgrounds). $W(\rightarrow \ell\nu)$ background events are further classified according to the origin of the high-energy isolated photon. Contributions from $W(\rightarrow \ell\nu)$ backgrounds for which the photon arises from the misidentification of an electron are estimated via a control sample for which the photon requirement is replaced by an electron requirement, scaled by an electron-to-photon misidentification probability; this approach is similar in nature to that of the diphoton analysis. Estimates of this component of the background to $\text{SR}_L^{\gamma b}$ and $\text{SR}_H^{\gamma b}$ are shown in Table VI; the quoted uncertainty arises from the limited number of events in the control sample, as well as systematic uncertainty associated with the possible p_T dependence of the electron-to-photon misidentification-rate scale factor.

Contributions from $W(\rightarrow \ell\nu)$ backgrounds for which the photon is real, or for which the photon arises from a misidentified jet or τ lepton, are estimated via lepton-enriched CRs that constrain the normalization of MC samples used to simulate contributions from these two sources. Separate control regions CR_L^{lep} and CR_H^{lep} are defined for the low- and high-neutralino-mass SRs by requiring a lepton in addition to the requirements already imposed to define the SRs. In addition, in order to increase the number of events in the CR, the E_T^{miss} requirement is reduced, the M_{bb} requirement is removed (for the $\text{SR}_L^{\gamma b}$ analysis), and the H_T requirement is relaxed (for the $\text{SR}_H^{\gamma b}$ analysis). Events in these two CRs are expected to be dominated by $t\bar{t}$, $t\bar{t}\gamma$ and $W\gamma$ production, as is expected for the corresponding background contributions to the SRs, and any overlapping phase space is subtracted as part of the

TABLE VI. The expected and observed numbers of events for the two photon + b signal regions. The quoted errors are the combined statistical and systematic uncertainties.

| Signal Regions | $\text{SR}_L^{\gamma b}$ | $\text{SR}_H^{\gamma b}$ |
|----------------------------|--------------------------|--------------------------|
| Expected background events | 18.8 ± 5.3 | 3.82 ± 1.25 |
| $e \rightarrow \gamma$ | 3.2 ± 0.4 | 0.18 ± 0.08 |
| $W(\rightarrow \ell\nu)$ | 12.6 ± 4.9 | 3.35 ± 1.05 |
| QCD | 2.3 ± 2.1 | 0.00 ± 0.65 |
| $Z \rightarrow \nu\nu$ | 0.8 ± 0.4 | 0.29 ± 0.15 |
| Observed events | 12 | 2 |

background estimation. Including all SM sources, a total of 14.5 (58.0) events are expected in the CR_L^{lep} (CR_H^{lep}) control regions, to be compared to an observation of 18 (61) events. Scaling the combined SM MC samples by these ratios of data to expectation, after having subtracted the contributions estimated by other techniques, yields the SR background estimates shown in Table VI. It is found that the data-to-expectation scale factor is somewhat dependent upon the requirements used to define the lepton-enriched CRs; these variations are included in the systematic error on the resulting SR background prediction.

The QCD background is estimated via the definition of a two-dimensional signal- and control-sample grid (the “ABCD” method). For the $\text{SR}_L^{\gamma b}$ analysis, three control samples are defined by requiring only a single tagged b -jet, by requiring that $E_T^{\text{miss}} < 75$ GeV, or by requiring both of these SR modifications. For the $\text{SR}_H^{\gamma b}$ analysis, three similar control samples are defined by requiring that no jet be identified as a b -jet, by requiring that $E_T^{\text{miss}} < 150$ GeV, or by requiring both of these SR modifications. A transfer factor is calculated by taking the ratio of the number of events with only the E_T^{miss} requirement changed to the number of events with both the E_T^{miss} and b -jet requirements changed. Assuming that the relaxation of the b -jet requirement is uncorrelated with the relaxation of the E_T^{miss} requirement, the number of QCD-background events in the SR can then be estimated by scaling, by this transfer factor, the number of events with only the b -tag requirement changed. This scaling is done only after subtracting the number of events expected to come from sources other than those that produce QCD-background events from each of the control samples. To avoid the biasing effects of possible correlations between the relaxation of the b -jet requirement and the E_T^{miss} requirement, for the $\text{SR}_L^{\gamma b}$ ($\text{SR}_H^{\gamma b}$) analysis events are binned in E_T^{miss} and weighted bin by bin in the ratio of the number of events in the 2-tag (1-tag) region to the number of events in the 1-tag (0-tag) region in the γ + jet MC sample. The resulting estimate of the small expected QCD background in the two SRs is shown in Table VI, with the systematic uncertainty dominated by the limited number of events to which the scale factor is applied.

An additional background due to the production of a Z boson that decays into two neutrinos, in association with a photon and a b -jet, is estimated directly from the MC simulation, and is tabulated in Table VI. For this final contribution, a 50% scale error is assumed for the overall rate of production for this process. The combined background from all expected sources is also shown in Table VI.

For both photon + b SRs, the background model is validated in four VRs, defined for $\text{SR}_L^{\gamma b}$ by requiring $75 < E_T^{\text{miss}} < 100$ GeV, by reversing the M_{bb} requirement, by requiring $M_T^{\gamma, E_T^{\text{miss}}} < 90$ GeV, or by requiring

$\Delta\phi_{\min}(\text{jet}, E_{\text{T}}^{\text{miss}}) < 0.3$, respectively. Since no M_{bb} requirement is made for $\text{SR}_{\text{H}}^{\text{b}}$, the second validation region is instead defined by changing the H_{T} requirement to $500 < H_{\text{T}} < 1000$ GeV. The observed numbers of events in the VRs are consistent with the predictions of the overall background model.

C. Backgrounds to the photon + j analysis

Backgrounds to the photon + j analysis are expected to arise both from events with real photons as well as events for which an electron or a jet is misidentified as a photon. The former source is expected to receive contributions from events for which a W/Z boson, a single-top quark, or a $t\bar{t}$ pair is produced in association with a real photon, with neutrinos in the subsequent weak decays of these produced states providing significant $E_{\text{T}}^{\text{miss}}$ ($W\gamma$, $Z\gamma$ and $t\bar{t}\gamma$ background). Events with real photons can also contribute to the background to the photon + j analysis when significant $E_{\text{T}}^{\text{miss}}$ arises from instrumental sources (QCD background). The $W\gamma$, $t\bar{t}\gamma$ and QCD backgrounds are estimated by scaling a corresponding MC sample to match the observed event count in a corresponding CR enriched in the given background process but otherwise kinematically similar to the corresponding SR. The MC simulation is then used to provide an estimate of the expected background in the $\text{SR}_{\text{L}}^{\text{ij}}$ and $\text{SR}_{\text{H}}^{\text{ij}}$ SRs. Smaller contributions from single-top + γ and $Z\gamma$ are estimated directly from the MC simulation.

The QCD-background CR is defined by changing the $\text{SR}_{\text{L}}^{\text{ij}}$ and $\text{SR}_{\text{H}}^{\text{ij}}$ $E_{\text{T}}^{\text{miss}}$ requirements to instead select events with $E_{\text{T}}^{\text{miss}} < 50$ GeV, but leaving all other selection requirements unchanged, providing a region dominated by real photons arising from radiative QCD processes. The $W\gamma$ -background CR is defined by requiring, in addition to the other $\text{SR}_{\text{L}}^{\text{ij}}$ and $\text{SR}_{\text{H}}^{\text{ij}}$ requirements, that there be a single identified isolated lepton (electron or muon) and no b -jet in the event. The $t\bar{t}\gamma$ -background CR is defined similarly, but requires instead at least one b -jet. In both cases, in order to increase the number of events in the CR the $E_{\text{T}}^{\text{miss}}$ requirement is changed to $100 < E_{\text{T}}^{\text{miss}} < 200$ GeV. The event counts in the resulting QCD, $W\gamma$ and $t\bar{t}\gamma$ CRs are used to scale the γ + jet, $W\gamma$ and $t\bar{t}\gamma$ MC samples, respectively, after applying a selection identical to that of the corresponding CR. The scale factors are determined in a simultaneous fit to all CRs, taking into account mutual cross contamination between the different backgrounds. Estimates for the contributions of all three of the real-photon backgrounds are shown in Table VII. Systematic uncertainty on the scale factor is dominated by the theoretical uncertainties on the relevant MC samples, related in turn to the PDF choice and the renormalization and factorization scales.

As in the other analyses, backgrounds from events for which electrons are misidentified as photons are estimated

TABLE VII. The expected and observed numbers of events for the two photon + j signal regions. The quoted errors are the combined statistical and systematic uncertainties.

| Signal Regions | $\text{SR}_{\text{L}}^{\text{ij}}$ | $\text{SR}_{\text{H}}^{\text{ij}}$ |
|---------------------------------|------------------------------------|------------------------------------|
| Expected background events | 1.27 ± 0.43 | 0.84 ± 0.38 |
| $W + \gamma$ | 0.13 ± 0.12 | 0.54 ± 0.28 |
| $Z + \gamma$ | $0.03^{+0.05}_{-0.03}$ | $0.21^{+0.23}_{-0.21}$ |
| $t\bar{t} + \gamma$ | 0.64 ± 0.40 | 0.05 ± 0.05 |
| Single- $t + \gamma$ | 0.06 ± 0.02 | 0.03 ± 0.01 |
| γ + jet (QCD background) | $0.00^{+0.06}_{-0.00}$ | 0.00 ± 0.00 |
| $e \rightarrow \gamma$ | 0.38 ± 0.10 | 0.00 ± 0.00 |
| $j \rightarrow \gamma$ | $0.02^{+0.08}_{-0.02}$ | $0.00^{+0.08}_{-0.00}$ |
| Observed events | 2 | 2 |

by identifying a control sample of events through the application of a set of selection requirements that are identical to those of the given SR, but with a requirement that the event have an electron that replaces the required photon. The estimate of the background in the SR ($\text{SR}_{\text{L}}^{\text{ij}}$ or $\text{SR}_{\text{H}}^{\text{ij}}$) is then, as in the other analyses, derived by scaling each event in the control sample by an η -dependent electron-to-photon misidentification factor. The resulting background estimates are displayed in Table VII.

Finally, the contribution of a background due to events for which the selected photon arises from the misidentification of a jet is estimated by determining the jet-to-photon misidentification rate from the observed isolation-energy distribution of energy in a cone of size $\Delta R = 0.2$ surrounding the energy deposition in the calorimeter associated with the photon. The isolation-energy distribution for real photons is modeled with electrons from Z boson decays, while that of misidentified jets is modeled with a sample of events for which there is a ‘‘pseudophoton.’’ A pseudophoton is defined to be an object that passed all loose photon selection requirements, as well as all tight photon selection requirements except one or more from a set of four that relate to the shape of the deposition in the finely granulated front portion of the EM calorimeter. The fraction of misidentified jets within the tight, isolated photon sample is determined with a control sample composed of events with tight, isolated photons with $p_{\text{T}} > 125$ GeV, as well as a relaxed $E_{\text{T}}^{\text{miss}}$ requirement of $50 < E_{\text{T}}^{\text{miss}} < 150$ GeV and an intermediate requirement of $H_{\text{T}} > 600$ GeV. The photon isolation-energy distribution of this control sample is fit to establish the relative amounts of these two sources (real photons and misidentified jets), with the misidentification fraction taken to be the relative integrals of the isolation-energy distributions of the misidentified and total contributions in the region for which the isolation energy is less than 5 GeV. The estimation of the jet-misidentification background in each signal region and control sample (as well as for the validation regions described below) is then obtained by scaling the observed number of events in each

region or sample by the jet-misidentification factor. The number of misidentified jets is then parametrized as a function of E_T^{miss} by fitting the E_T^{miss} dependence of the estimated misidentified-jet contribution in the range $E_T^{\text{miss}} < 200$ GeV. The estimates in the $\text{SR}_L^{\gamma j}$ and $\text{SR}_H^{\gamma j}$ signal regions are then extracted by integrating the fit function over the relevant E_T^{miss} range. The result for the contribution of the jet-misidentification backgrounds for each SR is shown in Table VII. Systematic uncertainties arise due to the uncertainties in the combined fit used to derive the misidentification factor, for which the parameters of the signal and background templates are allowed to vary within their uncertainties, and from the uncertainties of the extrapolation fit used for the estimation of the SR contamination.

The background model is validated by comparing expected and observed event rates in several VRs. For $\text{SR}_L^{\gamma j}$, this includes three VRs for which the $\Delta\phi_{\text{min}}(\text{jet}, E_T^{\text{miss}})$ is reversed, E_T^{miss} is required to be within an intermediate range of $75 < E_T^{\text{miss}} < 150$ GeV, and for which the R_T^4 requirement is reversed. For $\text{SR}_H^{\gamma j}$ two VRs are made use of, including one for which $\Delta\phi_{\text{min}}(\text{jet}, E_T^{\text{miss}})$ is reversed and another that requires that $400 < H_T < 800$ GeV. Good agreement is observed between the number of expected and observed events in all five VRs.

D. Backgrounds to the photon + ℓ analysis

Backgrounds to the photon + ℓ analysis ($\text{SR}_e^{\gamma\ell}$ and $\text{SR}_\mu^{\gamma\ell}$) are expected to arise primarily from events with hard photons produced in association with electroweak bosons ($W\gamma$ or $Z\gamma$) and top quarks ($t\bar{t}\gamma$), and events containing W bosons or semileptonically decaying top quarks for which an accompanying jet is misidentified as a photon (jet-to-photon events). Lesser contributions are expected to arise from $t\bar{t}$ events and events containing two electroweak bosons that produce two final-state leptons, one of which is an electron that is subsequently misidentified as a photon. As in the other analyses, data-driven techniques making use of CRs similar to but exclusive of the SRs, or control samples appropriate for assessing jet-to-photon and electron-to-photon misidentification rates, are used to estimate or constrain the primary backgrounds, while lesser backgrounds are estimated directly from MC simulation.

The most prevalent background in the photon + ℓ sample is expected to arise from $W\gamma$ events. A $W\gamma$ CR is defined by requiring an isolated electron or muon, and by requiring in addition that $45 < E_T^{\text{miss}} < 100$ GeV and $35 < M_T^{\ell, E_T^{\text{miss}}} < 90$ GeV, but otherwise requiring that the sample satisfy the $\text{SR}_e^{\gamma\ell}$ and $\text{SR}_\mu^{\gamma\ell}$ criteria. Transfer factors relating the number of events observed in the $W\gamma$ CR to the number of $W\gamma$ events expected in the SRs are estimated,

separately for the electron and muon contributions, from the $W\gamma$ MC simulation. Systematic uncertainties on the resulting $W\gamma$ -background estimate for the two SRs arise from the scale and PDF uncertainties associated with the transfer factors. A somewhat lesser contribution from $t\bar{t}\gamma$ events is estimated directly from the MC simulation, with uncertainties arising from imprecise knowledge of the strong-interaction scale and the rate of final-state photon production into the acceptance of the SRs. A smaller background contribution from $Z\gamma$ events is estimated directly from the MC simulation, with an uncertainty of $\pm 50\%$ assumed for the production rate into the region of the $Z\gamma$ phase space that populates the photon + ℓ SRs.

As in the other analyses, a potentially sizable contribution to the photon + ℓ sample arises from jet-to-photon misidentification. The contribution of SR events arising from jet-to-photon misidentification is estimated by exploring the isolation-energy distribution of events in an extended $W\gamma$ control sample for which the requirement on isolation energy has been removed. Isolation-energy distribution templates for true photons and for jets misidentified as photons are developed in the manner described for the photon + j analysis. A fit is then performed on the isolation-energy distribution of the extended $W\gamma$ control sample to estimate the number of events in the isolated (isolation energy less than 5 GeV) $W\gamma$ CR that arise from jets misidentified as photons. A scale factor is defined as the ratio of the estimated number of events in the isolated $W\gamma$ CR arising from misidentified jets to that expected from the W + jets and semileptonic $t\bar{t}$ MC simulations. A data-driven estimate of the number of events arising from misidentified jets in $\text{SR}_e^{\gamma\ell}$ and $\text{SR}_\mu^{\gamma\ell}$ is then derived by multiplying the number of such events expected from the combination of the W + jets and semileptonic $t\bar{t}$ MC simulations by this scale factor. Because the MC simulation is relied upon to propagate the background estimate from the control sample into the SR, uncertainties on the jet-to-photon misidentification background arise due to imprecise knowledge of the proton PDFs and strong-interaction scale. An additional uncertainty is assigned based on the difference between the scale factors determined for the separate electron and muon samples.

A final significant source of background is expected to arise from $t\bar{t}$ events, single-top events, and events containing two electroweak bosons that produce two final-state leptons, one of which is an electron that is subsequently misidentified as a photon. The contribution from these backgrounds is estimated from MC simulation, applying a correction based on the relative electron-to-photon misidentification rate between data and MC simulation. This correction is determined from $Z \rightarrow e^+e^-$ events as described above for other analyses. In addition to the uncertainty in the measurement of the misidentification rate, uncertainties in the estimate arise from PDF and scale uncertainty in the $t\bar{t}$ production process as well as an

TABLE VIII. The expected and observed numbers of events for the two photon + ℓ signal regions. The quoted errors are the combined statistical and systematic uncertainties. The contribution from the $Z\gamma$ process arises from events for which one of the leptons from the $Z \rightarrow \ell^+\ell^-$ decay is either missed or badly mismeasured. The likelihood of this occurring is significantly greater for muons than electrons.

| Signal Regions | $\text{SR}_e^{\gamma\ell}$ | $\text{SR}_\mu^{\gamma\ell}$ |
|----------------------------|----------------------------|------------------------------|
| Expected background events | 10.5 ± 1.4 | 14.1 ± 1.5 |
| $W\gamma$ | 6.7 ± 1.2 | 8.8 ± 1.3 |
| $i\bar{t}\gamma$ | 1.4 ± 0.6 | 1.7 ± 0.7 |
| $Z\gamma$ | 0.0 ± 0.0 | 1.2 ± 0.6 |
| Jet $\rightarrow \gamma$ | 1.5 ± 1.0 | 1.2 ± 0.7 |
| $e \rightarrow \gamma$ | 0.7 ± 0.2 | 0.8 ± 0.3 |
| Other sources | 0.3 ± 0.1 | 0.4 ± 0.2 |
| Observed events | 16 | 10 |

assumption of a $\pm 50\%$ uncertainty in the rate of single-top and diboson production.

All other sources of background, including those from $Z + \text{jet}$, $\gamma + \text{jet}$ and $\gamma\gamma$ production, are expected to contribute only minimally to the total SR backgrounds. In particular, a potential background from $\gamma + \text{jet}$ events arising from jet-to-lepton misidentification is estimated using a matrix method (as described in Ref. [76]) making use of a control region incorporating nonisolated lepton candidates, and is found to contribute 0.1 events to the overall background estimate for each of the $\text{SR}_e^{\gamma\ell}$ and $\text{SR}_\mu^{\gamma\ell}$ samples. A summary of the resulting background estimates for the $\text{SR}_e^{\gamma\ell}$ and $\text{SR}_\mu^{\gamma\ell}$ SRs is shown in Table VIII, broken down by source.

The background model is validated for each SR by comparing expected and observed event rates in two VRs. An M_T VR is defined by relaxing the $M_T^{\ell, E_T^{\text{miss}}}$ requirement to $35 < M_T^{\ell, E_T^{\text{miss}}} < 90$ GeV; to increase the number of events in this VR, the E_T^{miss} requirement is also relaxed to $E_T^{\text{miss}} > 100$ GeV. A E_T^{miss} VR is defined by relaxing the E_T^{miss} requirement to $45 < E_T^{\text{miss}} < 100$ GeV while leaving the $M_T^{\ell, E_T^{\text{miss}}}$ requirement unchanged. For the electron and muon channels combined, the number of events in the E_T^{miss} VR is observed to be somewhat less than that expected for the background model, although still within 2 standard deviations of the combined statistical and systematic uncertainty. Good agreement is found for the M_T VR.

VIII. SIGNAL EFFICIENCY AND SYSTEMATIC UNCERTAINTY

GGM signal acceptances and efficiencies are estimated using MC simulation for each simulated point in the gluino-bino, wino-bino, higgsino-bino, and wino-NLSP parameter spaces, and vary widely across the regions of these spaces relevant to establishing the limit contours presented below.

The product of acceptance times efficiency tends to be greatest (10%–25%) when the masses of both the produced and the NLSP states are largest, leading to large amounts of both visible energy and missing transverse momentum that would clearly distinguish signal from background events. However, for the lower accessible mass scales associated with electroweak production, and particularly for the case of a low-mass NLSP, the product of acceptance times efficiency can be significantly smaller. For example, for the region relevant to establishing limits at low values of μ , the efficiency of the $\text{SR}_L^{\gamma\ell}$ analysis is less than 0.1%, leading to a relatively modest lower limit on the mass of produced SUSY states.

Making use of a bootstrap method [77], the efficiencies of both the single photon and diphoton triggers are determined to be greater than 99%, with an uncertainty of less than 1%.

The reconstruction efficiency for tight, isolated photons is estimated with complementary data-driven methods [78]. Photons identified kinematically as having come from radiative decays of a Z boson ($Z \rightarrow \ell^+\ell^-\gamma$ events) are used to study the photon reconstruction efficiency as a function of p_T and η . Independent measurements making use of a tag-and-probe approach with $Z \rightarrow ee$ events, with one of the electrons used to probe the calorimeter response to electromagnetic depositions, also provide information about the photon reconstruction efficiency. For photons with $E_T > 75$ GeV, the identification efficiency in the range $0 < |\eta| < 1.81$ is greater than 95%; for the range $1.81 < |\eta| < 2.37$ the efficiency is approximately 90%. The uncertainty in the efficiency also varies with $|\eta|$, and lies between $\pm(1-2)\%$.

The isolated electron efficiency is also estimated using tag-and-probe methods, making use of samples of $Z \rightarrow ee$ and $J/\psi \rightarrow ee$ events as described in Refs. [62,63]. The efficiency and its uncertainty are estimated as a function of electron p_T and η , leading to an overall uncertainty of $\pm 1.0\%$ on the efficiency of the photon + ℓ analysis, the only analysis that explicitly requires an electron. The muon identification uncertainty, estimated as described in Ref. [65], is found to contribute an uncertainty of only 0.4% on the efficiency of the photon + ℓ analysis.

In portions of the GGM parameter space, uncertainties that vary across the parameter space dominate the systematic uncertainty on the signal acceptance times efficiency. These model-dependent uncertainties include those due to uncertainties in the photon, electron and jet-energy scales, the b -jet tagging efficiency, and the ‘‘pileup’’ uncertainty arising from the modeling of additional interactions in the same or nearby bunch crossings.

The electron and photon energy scale is determined using samples of $Z \rightarrow ee$ and $J/\psi \rightarrow ee$ events [79], both of whose masses are known precisely and thus provide an accurate calibration signal for determination of the electromagnetic calorimeter response. Uncertainties arise from

imprecise knowledge of the material burden between the IP and the face of the EM calorimeter. The muon energy scale and uncertainty are similarly estimated with calibration samples of $Z \rightarrow \mu\mu$, $\Upsilon \rightarrow \mu\mu$ and $J/\psi \rightarrow \mu\mu$ events [65].

The jet-energy scale is established via the propagation of single-particle test-beam measurements of the calorimeter response through simulations of jets arising from pp collisions [67,80]. The jet-energy scale uncertainty is constrained by the study of momentum imbalance in dijet events [81], as well as from an assessment of the effect of uncertainties in the modeling of jet properties with MC simulations, and from uncertainties in the modeling of the varying response to differing jet flavor composition.

Uncertainties in the values of whole-event observables, such as E_T^{miss} and H_T , arise from uncertainties on the energy of the underlying objects from which they are constructed. In addition, the E_T^{miss} observable receives a contribution from calorimetric energy deposits not associated with any of the reconstructed objects in the event. Uncertainties on the energy scale of these unassigned contributions are found to contribute negligibly to the overall uncertainty on the value of the E_T^{miss} observable.

The uncertainty due to pileup is estimated by varying the distribution of the number of interactions per bunch crossing overlaid in the simulation by $\pm 10\%$. The uncertainty on the b -tagging efficiency in the MC simulation is estimated from measurements of dedicated heavy-flavor calibration data samples.

In the regions of GGM parameter space relevant for establishing the exclusion limits discussed below, and excepting MC statistical uncertainty, the quadrature sum of the individual sources of systematic uncertainty on the signal reconstruction efficiency for the diphoton, photon + b and photon + ℓ analyses is of order 10%. For the photon + j analysis the systematic uncertainty is somewhat larger—approximately 20%—due to an increased sensitivity to the jet-energy scale and resolution associated with the multiple-jet requirement.

IX. RESULTS

An accounting of events observed in each SR is shown in Table IX, along with the size of the expected SM background. Comparisons of the E_T^{miss} distribution between signal and expected background is shown for several different SRs in Figs. 5–7. No evidence for physics beyond the SM is observed in any of the SRs. The largest excess relative to the expected background is observed for the $\text{SR}_{\text{W-L}}^{\gamma\gamma}$ analysis; considering both statistical and systematic uncertainty, and assuming that all observed events are from SM sources, an observation of five or more events over an expected background of $2.04^{+0.82}_{-0.75}$ represents an upward fluctuation with a probability of occurrence of approximately 6%.

TABLE IX. Summary of the number of events expected from SM sources ($N_{\text{exp}}^{\text{SM}}$), and the observed number of events (N_{obs}), for each of the ten SRs. Also shown is the derived model-independent 95% CL limit (S_{obs}^{95}) on the number of possible events from new physics, as well as both the observed ($\langle\epsilon\sigma\rangle_{\text{obs}}^{95}$) and expected ($\langle\epsilon\sigma\rangle_{\text{exp}}^{95}$) 95% CL limit on the visible cross section from new physics. Due to the discrete nature of the number-of-observed-events likelihood distribution in background-only pseudoexperiments, when both the expected number of background events and its uncertainty are close to zero the expected limit is dominated by the case of zero observed events. This leads to a very narrow one-standard-deviation range for the expected limit for $\text{SR}_{\text{S-L}}^{\gamma\gamma}$ and $\text{SR}_{\text{S-H}}^{\gamma\gamma}$.

| Signal Region | N_{obs} | $N_{\text{exp}}^{\text{SM}}$ | S_{obs}^{95} | $\langle\epsilon\sigma\rangle_{\text{obs}}^{95}$ [fb] | $\langle\epsilon\sigma\rangle_{\text{exp}}^{95}$ [fb] |
|---|------------------|------------------------------|-----------------------|---|---|
| $\text{SR}_{\text{S-L}}^{\gamma\gamma}$ | 0 | $0.06^{+0.24}_{-0.03}$ | 3.0 | 0.15 | 0.15 ± 0.01 |
| $\text{SR}_{\text{S-H}}^{\gamma\gamma}$ | 0 | $0.06^{+0.24}_{-0.04}$ | 3.0 | 0.15 | 0.15 ± 0.01 |
| $\text{SR}_{\text{W-L}}^{\gamma\gamma}$ | 5 | $2.04^{+0.82}_{-0.75}$ | 8.2 | 0.41 | $0.25^{+0.09}_{-0.06}$ |
| $\text{SR}_{\text{W-H}}^{\gamma\gamma}$ | 1 | $1.01^{+0.48}_{-0.42}$ | 3.7 | 0.18 | $0.18^{+0.07}_{-0.02}$ |
| $\text{SR}_{\text{L}}^{\gamma b}$ | 12 | 18.8 ± 5.4 | 8.1 | 0.40 | $0.57^{+0.24}_{-0.16}$ |
| $\text{SR}_{\text{H}}^{\gamma b}$ | 2 | 3.82 ± 1.25 | 4.0 | 0.20 | $0.27^{+0.09}_{-0.07}$ |
| $\text{SR}_{\text{L}}^{\gamma j}$ | 2 | 1.27 ± 0.43 | 5.5 | 0.27 | $0.19^{+0.10}_{-0.06}$ |
| $\text{SR}_{\text{H}}^{\gamma j}$ | 2 | 0.84 ± 0.38 | 5.6 | 0.28 | $0.20^{+0.11}_{-0.05}$ |
| $\text{SR}_{\text{e}}^{\gamma\ell}$ | 16 | 10.5 ± 1.4 | 14.2 | 0.70 | $0.41^{+0.20}_{-0.12}$ |
| $\text{SR}_{\mu}^{\gamma\ell}$ | 10 | 14.1 ± 1.5 | 6.0 | 0.30 | $0.45^{+0.21}_{-0.14}$ |

Based on the numbers of observed events in the ten SRs and the background expectation shown in Table IX, 95% confidence-level (CL) upper limits are set for each SR on the number of events from any scenario of physics beyond the SM, using the profile likelihood and CL_s prescriptions [82]. Uncertainties on the background expectations are treated as Gaussian-distributed nuisance parameters in the maximum-likelihood fit. Assuming that no events due to physical processes beyond those of the SM populate the various CRs used to estimate SR backgrounds, observed 95% CL limits on the number of such events vary between 3.0 (for the $\text{SR}_{\text{S-L}}^{\gamma\gamma}$ and $\text{SR}_{\text{S-H}}^{\gamma\gamma}$ SRs) and 14.2 (for the $\text{SR}_{\text{e}}^{\gamma\ell}$ SR). Taking into account the integrated luminosity of $20.3 \pm 0.6 \text{ fb}^{-1}$ these number-of-event limits translate into 95% CL upper limits on the visible cross section for new physics, defined by the product of cross section, branching fraction, acceptance and efficiency for the different SR definitions. Correspondingly, the observed visible cross-section limits vary between 0.15 and 0.70 fb.

By considering, in addition, the value and uncertainty of the acceptance times efficiency of the selection requirements associated with the various SRs, as well as the NLO (+NLL) GGM cross sections [33–37], which vary steeply with gluino and gaugino mass, 95% CL lower limits may be set on the masses of these states in the context of the various GGM scenarios explored in this study. For the diphoton, photon + b and photon + j analysis, the SR with

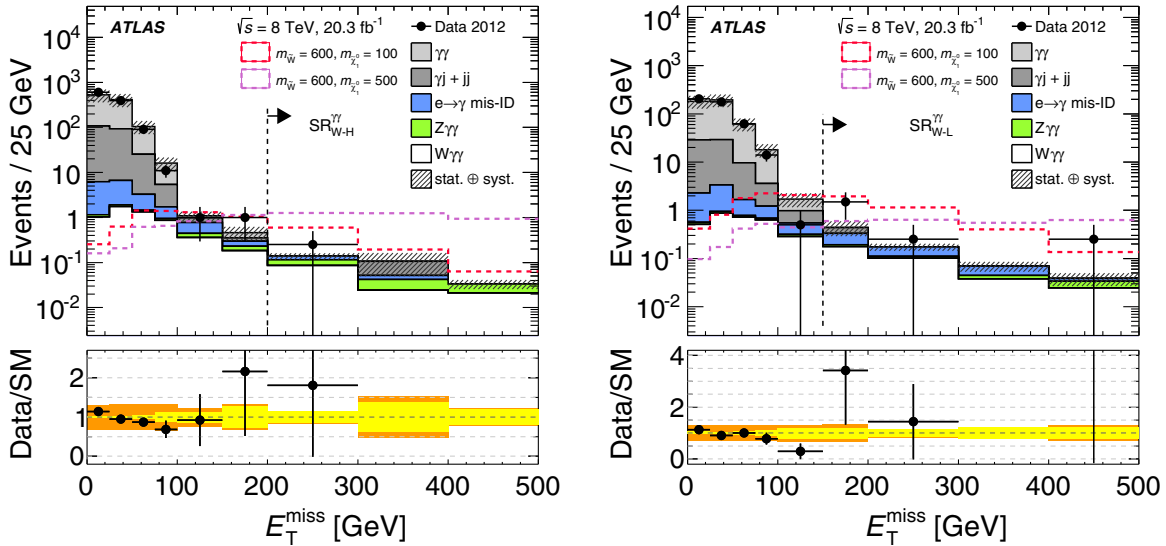


FIG. 5 (color online). Distribution of the missing transverse momentum E_T^{miss} for the sample surviving all requirements of the $\text{SR}_{\text{W-H}}^{\gamma\gamma}$ (left) and $\text{SR}_{\text{W-L}}^{\gamma\gamma}$ (right) selection except the E_T^{miss} requirement itself. Overlain are the expected SM backgrounds as a function of E_T^{miss} , separated into the various contributing sources. Also shown are the signal expectations for the $(m_{\tilde{W}}, m_{\tilde{\chi}_1^0}) = (600, 100)$ GeV and $(m_{\tilde{W}}, m_{\tilde{\chi}_1^0}) = (600, 500)$ GeV models. The lower plots show the ratio of observed data to the combined SM expectation. For these plots, the inner band represents the range of statistical uncertainty while the outer band represents the combined statistical and systematic uncertainty. Events outside the range of the displayed region are included in the highest-valued bin.

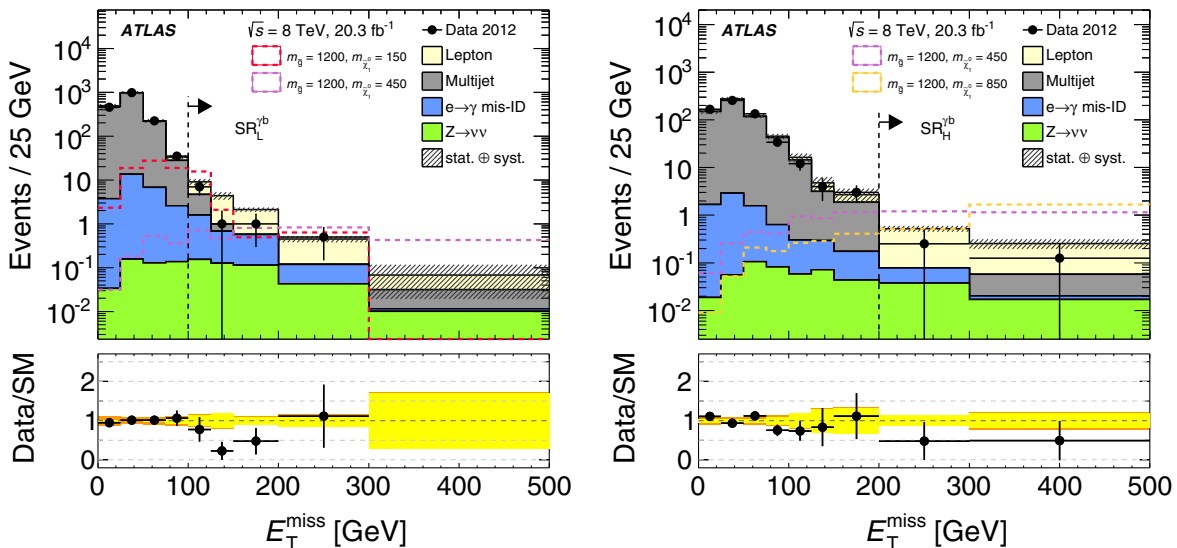


FIG. 6 (color online). E_T^{miss} distribution for the sample surviving all requirements of the $\text{SR}_{\text{L}}^{\gamma b}$ (left) and $\text{SR}_{\text{H}}^{\gamma b}$ (right) selection except the E_T^{miss} requirement itself. Overlain are the expected SM backgrounds as a function of E_T^{miss} , separated into the various contributing sources. Also shown are the signal expectations for the $(m_{\tilde{g}}, m_{\tilde{\chi}_1^0}) = (1200, 150)$, $(1200, 450)$, and $(1200, 850)$ GeV models. The lower plots show the ratio of observed data to the combined SM expectation. For these plots, the inner band represents the range of statistical uncertainty while the outer band represents the combined statistical and systematic uncertainty. Events outside the range of the displayed region are included in the highest-valued bin.

the best expected sensitivity at each simulated point in the parameter space of the corresponding GGM model(s) is used to determine the degree of exclusion of that model point. For the photon + ℓ analysis, the 95% CL exclusion limits are derived from the combined likelihood of the

electron and muon channels, taking into account the correlation between the systematic uncertainty estimates in the two channels.

For the diphoton analysis, $\text{SR}_{\text{S-H}}^{\gamma\gamma}$ is expected to provide the greatest sensitivity to the gluino-bino model for bino

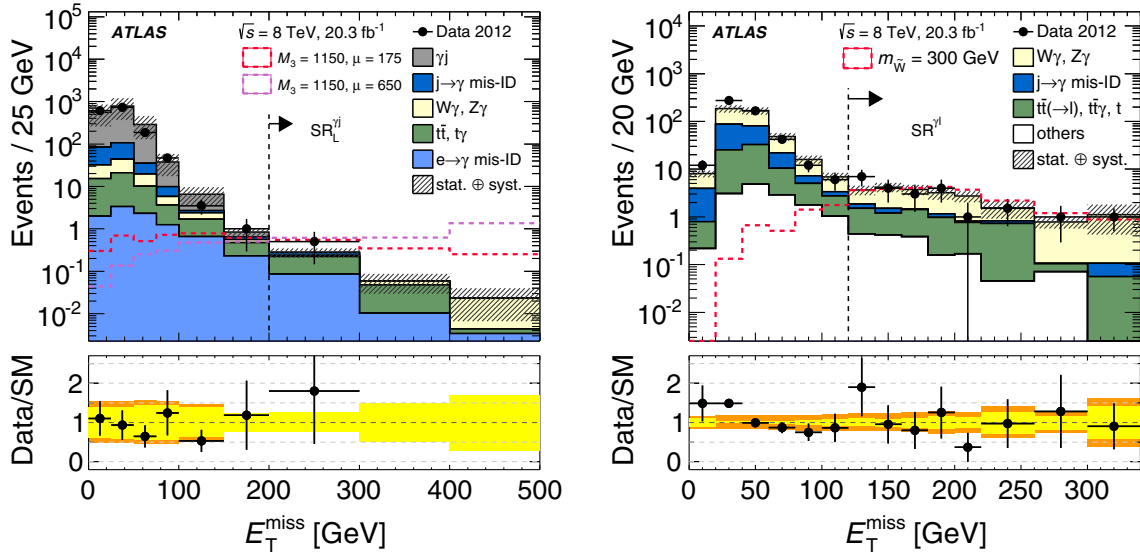


FIG. 7 (color online). (Left) E_T^{miss} distribution for the sample surviving all $\text{SR}_L^{j\ell}$ requirements except the E_T^{miss} requirement itself. Overlain are the expected SM backgrounds as a function of E_T^{miss} , separated into the various contributing sources. Also shown are the signal expectations for the two points in the $M_3 - \mu$ parameter space of the GGM model relevant to the photon + j analysis. (Right) E_T^{miss} distribution for the combined sample of events surviving all $\text{SR}_e^{\ell\ell}$ and $\text{SR}_\mu^{\ell\ell}$ requirements except the E_T^{miss} requirement itself. Overlain are the expected SM backgrounds as a function of E_T^{miss} , separated into the various contributing sources. Also shown is the signal expectation for the $m_{\tilde{W}} = 300$ GeV GGM model relevant to the photon + ℓ analysis. For both figures, the lower plot shows the ratio of observed data to the combined SM expectation, with the inner band representing the range of statistical uncertainty and the outer band the combined statistical and systematic uncertainty. Events outside the range of the displayed region are included in the highest-valued bin.

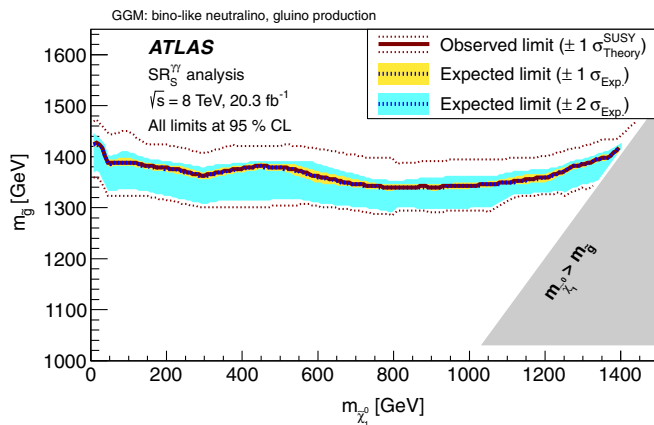


FIG. 8 (color online). Exclusion limits in the gluino-bino mass plane, using the $\text{SR}_{S-H}^{\gamma\gamma}$ analysis for $m_{\tilde{\chi}_1^0} \geq 800$ GeV and the $\text{SR}_{S-L}^{\gamma\gamma}$ analysis for $m_{\tilde{\chi}_1^0} < 800$ GeV. Combinations of gluino and bino mass are excluded at 95% CL in the area below the unbroken curve. The observed limits are exhibited for the nominal SUSY model cross-section expectation, as well as for a SUSY cross section increased and decreased by 1 standard deviation of the cross-section systematic uncertainty. Also shown is the expected limit, as well as the ± 1 and ± 2 standard-deviation ranges of the expected limit.

masses above 800 GeV and $\text{SR}_{S-L}^{\gamma\gamma}$ for bino masses below this. For the wino-bino model, the similar transition point between the use of $\text{SR}_{W-L}^{\gamma\gamma}$ and $\text{SR}_{W-H}^{\gamma\gamma}$ is found to be at 350 GeV. The resulting observed limits on the gluino and wino masses are exhibited, as a function of bino mass, for the diphoton analysis gluino and wino production models in Figs. 8 and 9, respectively. For the purpose of establishing these model-dependent limits, for all four diphoton SRs both the normalization of the $W(\rightarrow \ell\nu) + \gamma\gamma$ -background estimate and the limit on the possible number of events from new physics are extracted from a simultaneous fit to the SR and $W(\rightarrow \ell\nu) + \gamma\gamma$ control region, although the signal contamination in the $W(\rightarrow \ell\nu) + \gamma\gamma$ control sample is appreciable only for the low-bino-mass region of the wino-bino parameter space. Also shown for these two figures, as well as for the following two figures (Figs. 10 and 11), are the expected limits, including their statistical and background uncertainty ranges, as well as observed limits for SUSY model cross sections ± 1 standard deviation of theoretical uncertainty from their central value. Conservatively choosing the -1 standard-deviation observed contour, 95% CL lower limits of 1290 and 590 GeV are set by the diphoton analysis on the value of the gluino or wino mass, respectively, for

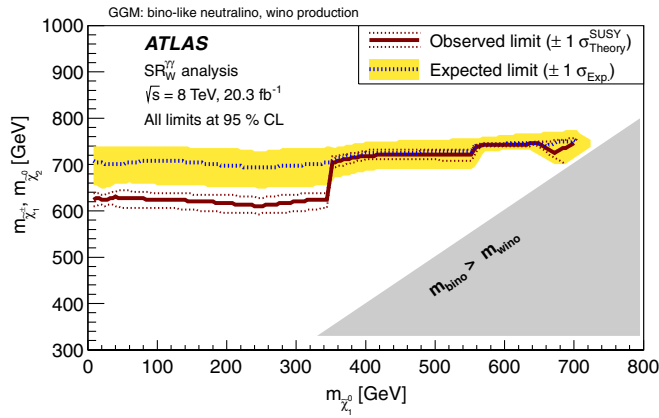


FIG. 9 (color online). Exclusion limits in the wino-bino mass plane, using the $SR_{W-H}^{\gamma\gamma}$ analysis for $m_{\tilde{\chi}_1^0} \geq 350$ GeV and the $SR_{W-L}^{\gamma\gamma}$ analysis for $m_{\tilde{\chi}_1^0} < 350$ GeV. The vertical axis represents wino mass while the horizontal axis represents bino mass. The observed limits are exhibited for the nominal SUSY model cross-section expectation, as well as for a SUSY cross section increased and decreased by 1 standard deviation of the cross-section systematic uncertainty. Also shown is the expected limit, along with its ± 1 standard-deviation range. The discontinuity at $m_{\tilde{\chi}_1^0} = 350$ GeV is due to the switch between the use of the $SR_{W-L}^{\gamma\gamma}$ and $SR_{W-H}^{\gamma\gamma}$ analyses, the former of which exhibits a small excess of observed events relative to the expected SM background.

any value of the NLSP bino mass less than that of the gluino (wino) mass.

Due to the discrete nature of the number-of-observed-events likelihood distribution in background-only pseudoexperiments, when both the expected number of observed events and its uncertainty are close to zero the expected limit is dominated by the case of zero observed events. This leads to a very narrow one-standard-deviation range for the expected limit, as observed for the expected-limit contour displayed in Fig. 8. In addition, because the observed number of events is very close to the expected number of events for $SR_{S-H}^{\gamma\gamma}$ and $SR_{S-L}^{\gamma\gamma}$, the expected and observed limits are nearly identical in Fig. 8.

For the photon + b analysis, limits are set in the two-dimensional plane of gluino and $\tilde{\chi}_1^0$ mass for the higgsino-bino GGM model with a negative value of the μ parameter. For NLSP masses near the 95% CL exclusion contour, $SR_L^{\gamma b}$ is expected to provide greater sensitivity for NLSP masses below approximately 600 GeV, and so is made use of in this region; above that, $SR_H^{\gamma b}$ is used to establish the degree of exclusion of points in the GGM model space. The resulting observed exclusion contour is shown in Fig. 10. Again choosing the -1 standard-deviation observed contour, in the context of this GGM model a conservative lower limit of 1300 GeV is established for the gluino mass over much of the range of the higgsino-bino NLSP mass. For NLSP masses above 1000 GeV the sensitivity lessens due to the restriction of the phase space for producing an energetic b -jet, while for NLSP masses below 600 GeV,

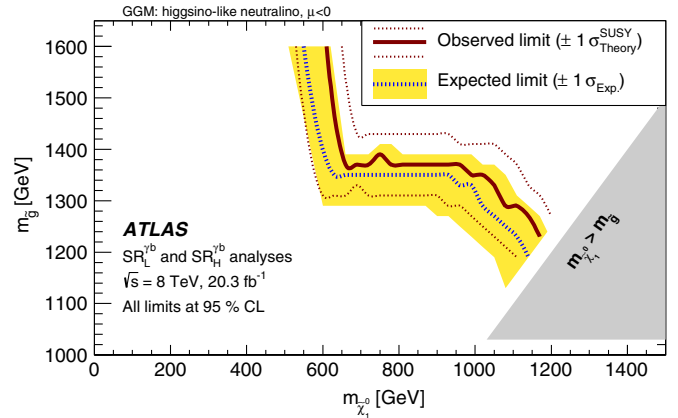


FIG. 10 (color online). Exclusion limits in the gluino-neutralino mass plane, for the higgsino-bino GGM model with $\mu < 0$, using the merged (see text) $SR_L^{\gamma b}$ and $SR_H^{\gamma b}$ analyses. The observed limits are shown for the nominal SUSY model cross-section expectation, as well as for a SUSY cross section increased and decreased by 1 standard deviation of the cross-section systematic uncertainty. The expected limit is also shown, along with its $\pm 1\sigma$ range. For NLSP masses below approximately 450 GeV, the onset of the direct production of gaugino states makes the analysis insensitive to the value of the gluino mass.

the onset of the direct production of gaugino states begins to make the analysis insensitive to the value of the gluino mass.

For the photon + j analysis, limits are set in the two-dimensional plane of the GGM parameters μ and M_3 for the higgsino-bino GGM model with a positive value of the μ parameter. For values of μ near the 95% CL exclusion contour, $SR_L^{\gamma j}$ is expected to provide a greater sensitivity for NLSP masses below approximately 900 GeV, and so is made use of in this region; above that, $SR_H^{\gamma j}$ is used to establish the degree of exclusion of GGM model-space points. The resulting observed exclusion contour is shown in Fig. 11. Again choosing the -1 standard-deviation observed contour, in the context of this GGM model a conservative lower limit of 1140 GeV is established for the gluino mass parameter M_3 over much of the range of the μ parameter. For values of M_3 close to the value of μ for which the gluino mass approaches that of the higgsino-bino NLSP, the sensitivity of the analysis lessens due to the restriction of phase space for producing multiple high- p_T jets.

For the photon + ℓ analysis, a limit is set on the wino mass, the single free parameter of the wino-NLSP model. Figure 12 shows the observed limit on the cross section for wino production in this model, as well as the corresponding expected limit with ± 1 and ± 2 standard-deviation uncertainty bands. Also shown is the cross section as a function of wino mass, with its ± 1 standard-deviation range. In the context of this wino-NLSP model, conservatively choosing the -1 standard-deviation cross-section contour leads to an

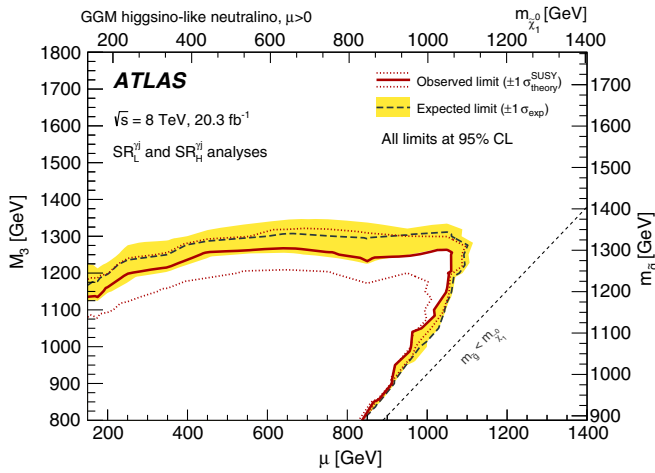


FIG. 11 (color online). Exclusion limits imposed by the photon + j analysis in the two-dimensional plane of the GGM parameters M_3 and μ , for the higgsino-bino GGM model with $\mu > 0$, using the merged (see text) $SR_L^{\gamma j}$ and $SR_H^{\gamma j}$ analyses. The observed limits are shown for the nominal SUSY model cross-section expectation, as well as for a SUSY cross section increased and decreased by 1 standard deviation of the cross-section systematic uncertainty. The expected limit is also shown, along with its ± 1 standard-deviation range. Values of M_3 below 1100 GeV are excluded for most values of the μ parameter, although a significant region corresponding to the case for which the gluino mass is close to that of the lightest neutralino masses remains unexcluded due to the requirements of one or more jets arising from the gluino decay. The top and right axes represent the corresponding values of the lightest neutralino and gluino masses, respectively.

exclusion of GGM winos in the range $124 < M_{\tilde{W}} < 361$ GeV; for $M_{\tilde{W}} < 124$ GeV the signal contamination in the $W\gamma$ CR becomes too large to permit a reliable estimate of the $W\gamma$ background. These limits are based on

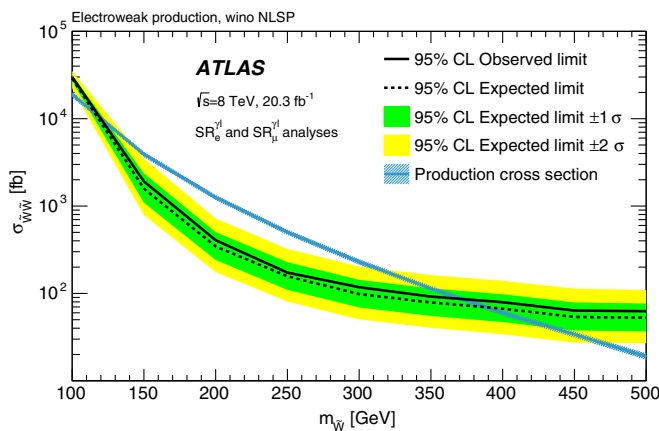


FIG. 12 (color online). Contour of exclusion in wino production cross section from the photon + ℓ analysis, as a function of the wino mass parameter $M_{\tilde{W}}$. The expected limit is shown along with its ± 1 and ± 2 standard-deviation ranges. Also shown is the total cross section for the production of \tilde{W} pairs, again as a function of $M_{\tilde{W}}$.

the direct production of the wino NLSP in the limit where squark masses are infinite, and are independent of gluino mass.

X. CONCLUSION

Making use of 20.3 fb^{-1} of pp collision data at $\sqrt{s} = 8$ TeV recorded by the ATLAS detector at the LHC, a search is performed for photonic signatures of new physics associated with significant E_T^{miss} . Four experimental signatures are explored, each involving at least one energetic isolated final-state photon in association with significant E_T^{miss} , and used to search for evidence for several GGM SUSY scenarios. No significant excess of events over the SM expectation is observed in any of the searches and so limits are set on possible contributions of new physics. Model-independent limits are set on the numbers of events from new physics and the associated visible cross section. Model-dependent limits are set on the masses of SUSY particles or on mass parameters associated with the various GGM scenario models.

A diphoton signature is used to explore both strongly and weakly produced SUSY states with a decay chain proceeding through a binolike NLSP. In the context of these models, lower limits of 1290 and 590 GeV are set on the masses of a degenerate octet of gluinos and a degenerate set of winos, respectively, for any value of the bino mass less than the mass of these produced states. A photon-plus- b -jet signature is used to search for a scenario in which the GGM NLSP is a higgsino-bino admixture with a roughly equal branching fraction to photons and to the SM Higgs boson. In the context of this model, a lower limit of 1260 GeV is established for the gluino mass over much of the range of the higgsino-bino NLSP mass; for NLSP masses below approximately 450 GeV, the onset of the direct production of gaugino states makes the analysis insensitive to the value of the gluino mass. A photon-plus-jet signature is used to search for an alternative scenario for which the GGM NLSP is a higgsino-bino admixture with a roughly equal branching fraction to photons and to the SM Z boson. In the context of this model, a lower limit of 1140 GeV is established for the gluino mass parameter M_3 over much of the range of the higgsino mass parameter μ . Finally, a photon-plus-lepton signature is used to search for a scenario for which the GGM NLSP is a degenerate set of three wino states. Based on the possible direct production of these states, in the limit of infinite squark mass GGM winos are excluded in the range $124 < M_{\tilde{W}} < 361$ GeV, independent of the gluino mass.

ACKNOWLEDGMENTS

We thank CERN for the very successful operation of the LHC, as well as the support staff from our institutions without whom ATLAS could not be operated efficiently.

We acknowledge the support of ANPCyT, Argentina; YerPhI, Armenia; ARC, Australia; BMWFW and FWF, Austria; ANAS, Azerbaijan; SSTC, Belarus; CNPq and FAPESP, Brazil; NSERC, NRC and CFI, Canada; CERN; CONICYT, Chile; CAS, MOST and NSFC, China; COLCIENCIAS, Colombia; MSMT CR, MPO CR and VSC CR, Czech Republic; DNkRF, DNSRC and Lundbeck Foundation, Denmark; EPLANET, ERC and NSRF, European Union; IN2P3-CNRS, CEA-DSM/IRFU, France; GNSF, Georgia; BMBF, DFG, Helmholtz Association, MPG and AvH Foundation, Germany; GSRT and NSRF, Greece; RGC, Hong Kong SAR, China; ISF, MINERVA, GIF, I-CORE and Benoziyo Center, Israel; INFN, Italy; MEXT and JSPS, Japan; CNRST, Morocco; FOM and NWO, Netherlands; BRF and RCN, Norway; MNiSW and NCN, Poland; GRICES

and FCT, Portugal; MNE/IFA, Romania; MES of Russia and NRC KI, Russian Federation; JINR; MSTD, Serbia; MSSR, Slovakia; ARRS and MIZŠ, Slovenia; DST/NRF, South Africa; MINECO, Spain; SRC and Wallenberg Foundation, Sweden; SER, SNSF and Cantons of Bern and Geneva, Switzerland; NSC, Taiwan; TAEK, Turkey; STFC, the Royal Society and Leverhulme Trust, U.K.; DOE and NSF, U.S. The crucial computing support from all WLCG partners is acknowledged gratefully, in particular from CERN and the ATLAS Tier-1 facilities at TRIUMF (Canada), NDGF (Denmark, Norway, Sweden), CC-IN2P3 (France), KIT/GridKA (Germany), INFN-CNAF (Italy), NL-T1 (Netherlands), PIC (Spain), ASGC (Taiwan), RAL (U.K.) and BNL (U.S.) and in the Tier-2 facilities worldwide.

-
- [1] P. Meade, N. Seiberg, and D. Shih, General gauge mediation, *Prog. Theor. Phys. Suppl.* **177**, 143 (2009).
- [2] M. Buican, P. Meade, N. Seiberg, and D. Shih, Exploring general gauge mediation, *J. High Energy Phys.* **03** (2009) 016.
- [3] J. T. Ruderman and D. Shih, General neutralino NLSPs at the early LHC, *J. High Energy Phys.* **08** (2012) 159.
- [4] G. Aad *et al.* (ATLAS Collaboration), Search for diphoton events with large missing transverse momentum in 7 TeV proton-proton collision data with the ATLAS detector, *Phys. Lett. B* **718**, 411 (2012).
- [5] G. Aad *et al.* (ATLAS Collaboration), Search for supersymmetry in events with photons, bottom quarks, and missing transverse momentum in proton-proton collisions at a centre-of-mass energy of 7 TeV with the ATLAS detector, *Phys. Lett. B* **719**, 261 (2013).
- [6] CMS Collaboration, Search for supersymmetry with photons in pp collisions at $\sqrt{s} = 8$ TeV, [arXiv:1507.02898](https://arxiv.org/abs/1507.02898).
- [7] H. Miyazawa, Baryon number changing currents, *Prog. Theor. Phys.* **36**, 1266 (1966).
- [8] P. Ramond, Dual theory for free fermions, *Phys. Rev. D* **3**, 2415 (1971).
- [9] Y. A. Gol'fand and E. P. Likhtman, Extension of the algebra of Poincare group generators and violation of p invariance, *Pis'ma Zh. Eksp. Teor. Fiz.* **13**, 452 (1971) [*JETP Lett.* **13**, 323 (1971)].
- [10] A. Neveu and J. H. Schwarz, Factorizable dual model of pions, *Nucl. Phys.* **B31**, 86 (1971).
- [11] A. Neveu and J. H. Schwarz, Quark model of dual pions, *Phys. Rev. D* **4**, 1109 (1971).
- [12] J. Gervais and B. Sakita, Field theory interpretation of supergauge in dual models, *Nucl. Phys.* **B34**, 632 (1971).
- [13] D. V. Volkov and V. P. Akulov, Is the neutrino a Goldstone particle?, *Phys. Lett.* **46B**, 109 (1973).
- [14] J. Wess and B. Zumino, A Lagrangian model invariant under supergauge transformations, *Phys. Lett.* **49B**, 52 (1974).
- [15] J. Wess and B. Zumino, Supergauge transformations in four-dimensions, *Nucl. Phys.* **B70**, 39 (1974).
- [16] P. Fayet, Supersymmetry and weak, electromagnetic and strong interactions, *Phys. Lett.* **64B**, 159 (1976).
- [17] P. Fayet, Spontaneously broken supersymmetric theories of weak, electromagnetic and strong interactions, *Phys. Lett.* **69B**, 489 (1977).
- [18] G. R. Farrar and P. Fayet, Phenomenology of the production, decay, and detection of new hadronic states associated with supersymmetry, *Phys. Lett.* **76B**, 575 (1978).
- [19] P. Fayet, Relations between the masses of the superpartners of leptons and quarks, the Goldstino couplings and the neutral currents, *Phys. Lett.* **84B**, 416 (1979).
- [20] S. Dimopoulos and H. Georgi, Softly broken supersymmetry and SU(5), *Nucl. Phys.* **B193**, 150 (1981).
- [21] M. Dine and W. Fischler, A phenomenological model of particle physics based on supersymmetry, *Phys. Lett.* **110B**, 227 (1982).
- [22] L. Alvarez-Gaume, M. Claudson, and M. B. Wise, Low-energy supersymmetry, *Nucl. Phys.* **B207**, 96 (1982).
- [23] C. R. Nappi and B. A. Ovrut, Supersymmetric extension of the $SU(3) \times SU(2) \times U(1)$ model, *Phys. Lett.* **113B**, 175 (1982).
- [24] M. Dine and A. E. Nelson, Dynamical supersymmetry breaking at low-energies, *Phys. Rev. D* **48**, 1277 (1993).
- [25] M. Dine, A. E. Nelson, and Y. Shirman, Low-energy dynamical supersymmetry breaking simplified, *Phys. Rev. D* **51**, 1362 (1995).
- [26] M. Dine, A. E. Nelson, Y. Nir, and Y. Shirman, New tools for low-energy dynamical supersymmetry breaking, *Phys. Rev. D* **53**, 2658 (1996).
- [27] G. Aad *et al.* (ATLAS Collaboration), Search for non-pointing and delayed photons in the diphoton and missing transverse momentum final state in 8 TeV pp collisions at the LHC using the ATLAS detector, *Phys. Rev. D* **90**, 112005 (2014).

- [28] A. Djouadi, J.-L. Kneur, and G. Moultaka, SuSpect: A Fortran code for the supersymmetric and Higgs particle spectrum in the MSSM, *Comput. Phys. Commun.* **176**, 426 (2007).
- [29] M. Mühlleitner, A. Djouadi, and Y. Mambrini, SDECAY: A Fortran code for the decays of the supersymmetric particles in the MSSM, *Comput. Phys. Commun.* **168**, 46 (2005).
- [30] A. Djouadi, M. Mühlleitner, and M. Spira, Decays of supersymmetric particles: The program SUSY-HIT (SUSpect-SdecaY-Hdecay-Interface), *Acta Phys. Pol. B* **38**, 635 (2007).
- [31] M. Bähr *et al.*, Herwig++ physics and manual, *Eur. Phys. J. C* **58**, 639 (2008).
- [32] J. Pumplin, D. R. Stump, J. Huston, H.-L. Lai, P. Nadolsky, and W.-K. Tung, New generation of parton distributions with uncertainties from global QCD analysis, *J. High Energy Phys.* **07** (2002) 012.
- [33] W. Beenakker, R. Hopker, M. Spira, and P. Zerwas, Squark and gluino production at hadron colliders, *Nucl. Phys.* **B492**, 51 (1997).
- [34] A. Kulesza and L. Motyka, Threshold Resummation for Squark-Antisquark and Gluino-Pair Production at the LHC, *Phys. Rev. Lett.* **102**, 111802 (2009).
- [35] A. Kulesza and L. Motyka, Soft gluon resummation for the production of gluino-gluino and squark-antisquark pairs at the LHC, *Phys. Rev. D* **80**, 095004 (2009).
- [36] W. Beenakker, S. Brensing, M. Krämer, A. Kulesza, E. Laenen, and I. Niessen, Soft-gluon resummation for squark and gluino hadroproduction, *J. High Energy Phys.* **12** (2009) 041.
- [37] W. Beenakker, S. Brensing, M. Krämer, A. Kulesza, E. Laenen, L. Motyka, and I. Niessen, Squark and gluino hadroproduction, *Int. J. Mod. Phys. A* **26**, 2637 (2011).
- [38] M. Krämer *et al.*, Supersymmetry production cross sections in pp collisions at $\sqrt{s} = 7$ TeV, [arXiv:1206.2892](https://arxiv.org/abs/1206.2892).
- [39] M. L. Mangano, F. Piccinini, A. D. Polosa, M. Moretti, and R. Pittau, ALPGEN, a generator for hard multiparton processes in hadronic collisions, *J. High Energy Phys.* **07** (2003) 001.
- [40] J. Butterworth, J. R. Forshaw, and M. Seymour, Multiparton interactions in photoproduction at HERA, *Z. Phys. C* **72**, 637 (1996).
- [41] T. Gleisberg, S. Höche, F. Krauss, M. Schönherr, S. Schumann, F. Siegert, and J. Winter, Event generation with SHERPA 1.1, *J. High Energy Phys.* **02** (2009) 007.
- [42] H.-L. Lai, M. Guzzi, J. Huston, Z. Li, P. M. Nadolsky, J. Pumplin, and C.-P. Yuan, New parton distributions for collider physics, *Phys. Rev. D* **82**, 074024 (2010).
- [43] J. Alwall, P. Demin, S. de Visscher, R. Frederix, M. Herquet, F. Maltoni, T. Plehn, D. L. Rainwater, and T. Stelzer, MadGraph/MadEvent v4: The new web generation, *J. High Energy Phys.* **09** (2007) 028.
- [44] T. Sjöstrand, S. Mrenna, and P. Z. Skands, PYTHIA 6.4 physics and manual, *J. High Energy Phys.* **05** (2006) 026.
- [45] S. Frixione and B. R. Webber, Matching NLO QCD computations and parton shower simulations, *J. High Energy Phys.* **06** (2002) 029.
- [46] S. Frixione, P. Nason, and B. Webber, Matching NLO QCD and parton showers in heavy flavour production, *J. High Energy Phys.* **08** (2003) 007.
- [47] M. Cacciari, M. Czakon, M. Mangano, A. Mitov, and P. Nason, Top-pair production at hadron colliders with next-to-next-to-leading logarithmic soft-gluon resummation, *Phys. Lett. B* **710**, 612 (2012).
- [48] P. Baerzreuther, M. Czakon, and A. Mitov, Percent Level Precision Physics at the Tevatron: First Genuine NNLO QCD Corrections to $q\bar{q} \rightarrow t\bar{t} + X$, *Phys. Rev. Lett.* **109**, 132001 (2012).
- [49] M. Czakon and A. Mitov, NNLO corrections to top-pair production at hadron colliders: The all-fermionic scattering channels, *J. High Energy Phys.* **12** (2012) 054.
- [50] M. Czakon and A. Mitov, NNLO corrections to top pair production at hadron colliders: The quark-gluon reaction, *J. High Energy Phys.* **01** (2013) 080.
- [51] M. Czakon, P. Fiedler, and A. Mitov, Total Top-Quark Pair-Production Cross Section at Hadron Colliders Through $\mathcal{O}(\alpha_s^4)$, *Phys. Rev. Lett.* **110**, 252004 (2013).
- [52] M. Czakon and A. Mitov, Top++: A program for the calculation of the top-pair cross-section at hadron colliders, *Comput. Phys. Commun.* **185**, 2930 (2014).
- [53] W. Kilian, T. Ohl, and J. Reuter, WHIZARD: Simulating multi-particle processes at LHC and ILC, *Eur. Phys. J. C* **71**, 1742 (2011).
- [54] M. Moretti, T. Ohl, and J. Reuter, O'Mega: An optimizing matrix element generator, [arXiv:hep-ph/0102195](https://arxiv.org/abs/hep-ph/0102195).
- [55] G. P. Salam and J. Rojo, A higher order perturbative parton evolution toolkit (HOPPET), *Comput. Phys. Commun.* **180**, 120 (2009).
- [56] P. Golonka and Z. Was, PHOTOS Monte Carlo: A Precision tool for QED corrections in Z and W decays, *Eur. Phys. J. C* **45**, 97 (2006).
- [57] A. Sherstnev and R. S. Thorne, Parton distributions for LO Generators, *Eur. Phys. J. C* **55**, 553 (2008).
- [58] G. Bozzi, F. Campanario, M. Rauch, and D. Zeppenfeld, $Z\gamma\gamma$ production with leptonic decays and triple photon production at NLO QCD, *Phys. Rev. D* **84**, 074028 (2011).
- [59] GEANT4 Collaboration, GEANT4: A Simulation toolkit, *Nucl. Instrum. Methods Phys. Res., Sect. A* **506**, 250 (2003).
- [60] G. Aad *et al.* (ATLAS Collaboration), The ATLAS simulation infrastructure, *Eur. Phys. J. C* **70**, 823 (2010).
- [61] G. Aad *et al.* (ATLAS Collaboration), The ATLAS experiment at the CERN Large Hadron Collider, *JINST* **3**, S08003 (2008).
- [62] G. Aad *et al.* (ATLAS Collaboration), Electron reconstruction and identification efficiency measurements with the ATLAS detector using the 2011 LHC proton-proton collision data, *Eur. Phys. J. C* **74**, 2941 (2014).
- [63] ATLAS Collaboration, Tech. Report No. ATLAS-CONF-2014-032, CERN, Geneva, 2014.
- [64] G. Aad *et al.* (ATLAS Collaboration), Measurement of the inclusive isolated prompt photon cross section in pp collisions at $\sqrt{s} = 7$ TeV with the ATLAS detector, *Phys. Rev. D* **83**, 052005 (2011).
- [65] G. Aad *et al.* (ATLAS Collaboration), Measurement of the muon reconstruction performance of the ATLAS detector using 2011 and 2012 LHC proton-proton collision data, *Eur. Phys. J. C* **74**, 3130 (2014).
- [66] M. Cacciari, G. Salam, and G. Soyez, The anti- k_r jet clustering algorithm, *J. High Energy Phys.* **04** (2008) 063.

- [67] G. Aad *et al.* (ATLAS Collaboration), Jet energy measurement with the ATLAS detector in proton-proton collisions at $\sqrt{s} = 7$ TeV, *Eur. Phys. J. C* **73**, 2304 (2013).
- [68] W. Lampl *et al.*, Tech. Report No. ATL-LARG-PUB-2008-002, CERN, Geneva, 2008.
- [69] G. Aad *et al.* (ATLAS Collaboration), Jet energy measurement and its systematic uncertainty in proton-proton collisions at $\sqrt{s} = 7$ TeV with the ATLAS detector, *Eur. Phys. J. C* **75**, 17 (2015).
- [70] ATLAS Collaboration, Tech. Report No. ATLAS-CONF-2014-046, CERN, Geneva, 2014.
- [71] G. Aad *et al.* (ATLAS Collaboration), Performance of missing transverse momentum reconstruction in proton-proton collisions at $\sqrt{s} = 7$ TeV with ATLAS, *Eur. Phys. J. C* **72**, 1844 (2012).
- [72] G. Aad *et al.* (ATLAS Collaboration), Improved luminosity determination in pp collisions at $\sqrt{s} = 7$ TeV using the ATLAS detector at the LHC, *Eur. Phys. J. C* **73**, 2518 (2013).
- [73] G. Bozzi, F. Campanario, M. Rauch, and D. Zeppenfeld, $W\gamma\gamma$ production with leptonic decays at NLO QCD, *Phys. Rev. D* **83**, 114035 (2011).
- [74] G. Aad *et al.* (ATLAS Collaboration), Measurements of fiducial and differential cross sections for Higgs boson production in the diphoton decay channel at $\sqrt{s} = 8$ TeV with ATLAS, *J. High Energy Phys.* **09** (2014) 112.
- [75] G. Aad *et al.* (ATLAS Collaboration), Measurement of isolated-photon pair production in pp collisions at $\sqrt{s} = 7$ TeV with the ATLAS detector, *J. High Energy Phys.* **01** (2013) 086.
- [76] G. Aad *et al.* (ATLAS Collaboration), Measurement of the top quark-pair production cross section with ATLAS in pp collisions at $\sqrt{s} = 7$ TeV, *Eur. Phys. J. C* **71**, 1577 (2011).
- [77] ATLAS Collaboration, Tech. Report No. ATLAS-CONF-2012-048, CERN, Geneva, 2012.
- [78] ATLAS Collaboration, Tech. Report No. ATLAS-CONF-2012-123, CERN, Geneva, 2012.
- [79] G. Aad *et al.* (ATLAS Collaboration), Electron performance measurements with the ATLAS detector using the 2010 LHC proton-proton collision data, *Eur. Phys. J. C* **72**, 1909 (2012).
- [80] G. Aad *et al.* (ATLAS Collaboration), Single hadron response measurement and calorimeter jet energy scale uncertainty with the ATLAS detector at the LHC, *Eur. Phys. J. C* **73**, 2305 (2013).
- [81] G. Aad *et al.* (ATLAS Collaboration), Jet energy resolution in proton-proton collisions at $\sqrt{s} = 7$ TeV recorded in 2010 with the ATLAS detector, *Eur. Phys. J. C* **73**, 2306 (2013).
- [82] A. L. Read, Presentation of search results: TheCL_s technique, *J. Phys. G* **28**, 2693 (2002).

G. Aad,⁸⁵ B. Abbott,¹¹³ J. Abdallah,¹⁵¹ O. Abdinov,¹¹ R. Aben,¹⁰⁷ M. Abolins,⁹⁰ O. S. AbouZeid,¹⁵⁸ H. Abramowicz,¹⁵³ H. Abreu,¹⁵² R. Abreu,¹¹⁶ Y. Abulaiti,^{146a,146b} B. S. Acharya,^{164a,164b} L. Adamczyk,^{38a} D. L. Adams,²⁵ J. Adelman,¹⁰⁸ S. Adomeit,¹⁰⁰ T. Adye,¹³¹ A. A. Affolder,⁷⁴ T. Agatonovic-Jovin,¹³ J. Agricola,⁵⁴ J. A. Aguilar-Saavedra,^{126a,126f} S. P. Ahlen,²² F. Ahmadov,^{65,c} G. Aielli,^{133a,133b} H. Akerstedt,^{146a,146b} T. P. A. Åkesson,⁸¹ A. V. Akimov,⁹⁶ G. L. Alberghi,^{20a,20b} J. Albert,¹⁶⁹ S. Albrand,⁵⁵ M. J. Alconada Verzini,⁷¹ M. Aleksa,³⁰ I. N. Aleksandrov,⁶⁵ C. Alexa,^{26a} G. Alexander,¹⁵³ T. Alexopoulos,¹⁰ M. Alhroob,¹¹³ G. Alimonti,^{91a} L. Alio,⁸⁵ J. Alison,³¹ S. P. Alkire,³⁵ B. M. M. Allbrooke,¹⁴⁹ P. P. Allport,⁷⁴ A. Aloisio,^{104a,104b} A. Alonso,³⁶ F. Alonso,⁷¹ C. Alpigiani,⁷⁶ A. Altheimer,³⁵ B. Alvarez Gonzalez,³⁰ D. Álvarez Piqueras,¹⁶⁷ M. G. Alviggi,^{104a,104b} B. T. Amadio,¹⁵ K. Amako,⁶⁶ Y. Amaral Coutinho,^{24a} C. Amelung,²³ D. Amidei,⁸⁹ S. P. Amor Dos Santos,^{126a,126c} A. Amorim,^{126a,126b} S. Amoroso,⁴⁸ N. Amram,¹⁵³ G. Amundsen,²³ C. Anastopoulos,¹³⁹ L. S. Ancu,⁴⁹ N. Andari,¹⁰⁸ T. Andeen,³⁵ C. F. Anders,^{58b} G. Anders,³⁰ J. K. Anders,⁷⁴ K. J. Anderson,³¹ A. Andreazza,^{91a,91b} V. Andrei,^{58a} S. Angelidakis,⁹ I. Angelozzi,¹⁰⁷ P. Anger,⁴⁴ A. Angerami,³⁵ F. Anghinolfi,³⁰ A. V. Anisenkov,^{109,d} N. Anjos,¹² A. Annovi,^{124a,124b} M. Antonelli,⁴⁷ A. Antonov,⁹⁸ J. Antos,^{144b} F. Anulli,^{132a} M. Aoki,⁶⁶ L. Aperio Bella,¹⁸ G. Arabidze,⁹⁰ Y. Arai,⁶⁶ J. P. Araque,^{126a} A. T. H. Arce,⁴⁵ F. A. Arduh,⁷¹ J-F. Arguin,⁹⁵ S. Argyropoulos,⁴² M. Arik,^{19a} A. J. Armbruster,³⁰ O. Arnaez,³⁰ V. Arnal,⁸² H. Arnold,⁴⁸ M. Arratia,²⁸ O. Arslan,²¹ A. Artamonov,⁹⁷ G. Artoni,²³ S. Asai,¹⁵⁵ N. Asbah,⁴² A. Ashkenazi,¹⁵³ B. Åsman,^{146a,146b} L. Asquith,¹⁴⁹ K. Assamagan,²⁵ R. Astalos,^{144a} M. Atkinson,¹⁶⁵ N. B. Atlay,¹⁴¹ K. Augsten,¹²⁸ M. Auresseau,^{145b} G. Avolio,³⁰ B. Axen,¹⁵ M. K. Ayoub,¹¹⁷ G. Azeleos,^{95,e} M. A. Baak,³⁰ A. E. Baas,^{58a} M. J. Baca,¹⁸ C. Bacci,^{134a,134b} H. Bachacou,¹³⁶ K. Bachas,¹⁵⁴ M. Backes,³⁰ M. Backhaus,³⁰ P. Bagiacchi,^{132a,132b} P. Bagnaia,^{132a,132b} Y. Bai,^{33a} T. Bain,³⁵ J. T. Baines,¹³¹ O. K. Baker,¹⁷⁶ E. M. Baldin,^{109,d} P. Balek,¹²⁹ T. Balestri,¹⁴⁸ F. Balli,⁸⁴ E. Banas,³⁹ Sw. Banerjee,¹⁷³ A. A. E. Bannoura,¹⁷⁵ H. S. Bansil,¹⁸ L. Barak,³⁰ E. L. Barberio,⁸⁸ D. Barberis,^{50a,50b} M. Barbero,⁸⁵ T. Barillari,¹⁰¹ M. Barisonzi,^{164a,164b} T. Barklow,¹⁴³ N. Barlow,²⁸ S. L. Barnes,⁸⁴ B. M. Barnett,¹³¹ R. M. Barnett,¹⁵ Z. Barnovska,⁵ A. Baroncelli,^{134a} G. Barone,²³ A. J. Barr,¹²⁰ F. Barreiro,⁸² J. Barreiro Guimarães da Costa,⁵⁷ R. Bartoldus,¹⁴³ A. E. Barton,⁷² P. Bartos,^{144a} A. Basalaeu,¹²³ A. Bassalat,¹¹⁷ A. Basye,¹⁶⁵ R. L. Bates,⁵³ S. J. Batista,¹⁵⁸ J. R. Batley,²⁸ M. Battaglia,¹³⁷ M. Bauce,^{132a,132b} F. Bauer,¹³⁶ H. S. Bawa,^{143,f} J. B. Beacham,¹¹¹ M. D. Beattie,⁷² T. Beau,⁸⁰ P. H. Beauchemin,¹⁶¹ R. Beccherle,^{124a,124b} P. Bechtel,²¹ H. P. Beck,^{17,g}

K. Becker,¹²⁰ M. Becker,⁸³ S. Becker,¹⁰⁰ M. Beckingham,¹⁷⁰ C. Becot,¹¹⁷ A. J. Beddall,^{19b} A. Beddall,^{19b} V. A. Bednyakov,⁶⁵ C. P. Bee,¹⁴⁸ L. J. Beemster,¹⁰⁷ T. A. Beermann,¹⁷⁵ M. Begel,²⁵ J. K. Behr,¹²⁰ C. Belanger-Champagne,⁸⁷ W. H. Bell,⁴⁹ G. Bella,¹⁵³ L. Bellagamba,^{20a} A. Bellerive,²⁹ M. Bellomo,⁸⁶ K. Belotskiy,⁹⁸ O. Beltramello,³⁰ O. Benary,¹⁵³ D. Bencheekroun,^{135a} M. Bender,¹⁰⁰ K. Bendtz,^{146a,146b} N. Benekos,¹⁰ Y. Benhamou,¹⁵³ E. Benhar Noccioli,⁴⁹ J. A. Benitez Garcia,^{159b} D. P. Benjamin,⁴⁵ J. R. Bensinger,²³ S. Bentvelsen,¹⁰⁷ L. Beresford,¹²⁰ M. Beretta,⁴⁷ D. Berge,¹⁰⁷ E. Bergeaas Kuutmann,¹⁶⁶ N. Berger,⁵ F. Berghaus,¹⁶⁹ J. Beringer,¹⁵ C. Bernard,²² N. R. Bernard,⁸⁶ C. Bernius,¹¹⁰ F. U. Bernlochner,²¹ T. Berry,⁷⁷ P. Berta,¹²⁹ C. Bertella,⁸³ G. Bertoli,^{146a,146b} F. Bertolucci,^{124a,124b} C. Bertsche,¹¹³ D. Bertsche,¹¹³ M. I. Besana,^{91a} G. J. Besjes,³⁶ O. Bessidskaia Bylund,^{146a,146b} M. Bessner,⁴² N. Besson,¹³⁶ C. Betancourt,⁴⁸ S. Bethke,¹⁰¹ A. J. Bevan,⁷⁶ W. Bhimji,¹⁵ R. M. Bianchi,¹²⁵ L. Bianchini,²³ M. Bianco,³⁰ O. Biebel,¹⁰⁰ D. Biedermann,¹⁶ S. P. Bieniek,⁷⁸ M. Biglietti,^{134a} J. Bilbao De Mendizabal,⁴⁹ H. Bilokon,⁴⁷ M. Bindi,⁵⁴ S. Binet,¹¹⁷ A. Bingul,^{19b} C. Bini,^{132a,132b} S. Biondi,^{20a,20b} C. W. Black,¹⁵⁰ J. E. Black,¹⁴³ K. M. Black,²² D. Blackburn,¹³⁸ R. E. Blair,⁶ J.-B. Blanchard,¹³⁶ J. E. Blanco,⁷⁷ T. Blazek,^{144a} I. Bloch,⁴² C. Blocker,²³ W. Blum,^{83,a} U. Blumenschein,⁵⁴ G. J. Bobbink,¹⁰⁷ V. S. Bobrovnikov,^{109,d} S. S. Bocchetta,⁸¹ A. Bocci,⁴⁵ C. Bock,¹⁰⁰ M. Boehler,⁴⁸ J. A. Bogaerts,³⁰ D. Bogavac,¹³ A. G. Bogdanchikov,¹⁰⁹ C. Bohm,^{146a} V. Boisvert,⁷⁷ T. Bold,^{38a} V. Boldea,^{26a} A. S. Boldyrev,⁹⁹ M. Bomben,⁸⁰ M. Bona,⁷⁶ M. Boonekamp,¹³⁶ A. Borisov,¹³⁰ G. Borissov,⁷² S. Borroni,⁴² J. Bortfeldt,¹⁰⁰ V. Bortolotto,^{60a,60b,60c} K. Bos,¹⁰⁷ D. Boscherini,^{20a} M. Bosman,¹² J. Boudreau,¹²⁵ J. Bouffard,² E. V. Bouhova-Thacker,⁷² D. Boumediene,³⁴ C. Bourdarios,¹¹⁷ N. Bousson,¹¹⁴ A. Boveia,³⁰ J. Boyd,³⁰ I. R. Boyko,⁶⁵ I. Bozic,¹³ J. Bracinik,¹⁸ A. Brandt,⁸ G. Brandt,⁵⁴ O. Brandt,^{58a} U. Bratzler,¹⁵⁶ B. Brau,⁸⁶ J. E. Brau,¹¹⁶ H. M. Braun,^{175,a} S. F. Brazzale,^{164a,164c} W. D. Breaden Madden,⁵³ K. Brendlinger,¹²² A. J. Brennan,⁸⁸ L. Brenner,¹⁰⁷ R. Brenner,¹⁶⁶ S. Bressler,¹⁷² K. Bristow,^{145c} T. M. Bristow,⁴⁶ D. Britton,⁵³ D. Britzger,⁴² F. M. Brochu,²⁸ I. Brock,²¹ R. Brock,⁹⁰ J. Bronner,¹⁰¹ G. Brooijmans,³⁵ T. Brooks,⁷⁷ W. K. Brooks,^{32b} J. Brosamer,¹⁵ E. Brost,¹¹⁶ J. Brown,⁵⁵ P. A. Bruckman de Renstrom,³⁹ D. Bruncko,^{144b} R. Bruneliere,⁴⁸ A. Bruni,^{20a} G. Bruni,^{20a} M. Bruschi,^{20a} N. Brusino,²¹ L. Bryngemark,⁸¹ T. Buanes,¹⁴ Q. Buat,¹⁴² P. Buchholz,¹⁴¹ A. G. Buckley,⁵³ S. I. Buda,^{26a} I. A. Budagov,⁶⁵ F. Buehrer,⁴⁸ L. Bugge,¹¹⁹ M. K. Bugge,¹¹⁹ O. Bulekov,⁹⁸ D. Bullock,⁸ H. Burckhart,³⁰ S. Burdin,⁷⁴ C. D. Burgard,⁴⁸ B. Burghgrave,¹⁰⁸ S. Burke,¹³¹ I. Burmeister,⁴³ E. Busato,³⁴ D. Büscher,⁴⁸ V. Büscher,⁸³ P. Bussey,⁵³ J. M. Butler,²² A. I. Butt,³ C. M. Buttar,⁵³ J. M. Butterworth,⁷⁸ P. Butti,¹⁰⁷ W. Buttinger,²⁵ A. Buzatu,⁵³ A. R. Buzykaev,^{109,d} S. Cabrera Urbán,¹⁶⁷ D. Caforio,¹²⁸ V. M. Cairo,^{37a,37b} O. Cakir,^{4a} N. Calace,⁴⁹ P. Calafiura,¹⁵ A. Calandri,¹³⁶ G. Calderini,⁸⁰ P. Calfayan,¹⁰⁰ L. P. Caloba,^{24a} D. Calvet,³⁴ S. Calvet,³⁴ R. Camacho Toro,³¹ S. Camarda,⁴² P. Camarri,^{133a,133b} D. Cameron,¹¹⁹ R. Caminal Armadans,¹⁶⁵ S. Campana,³⁰ M. Campanelli,⁷⁸ A. Campoverde,¹⁴⁸ V. Canale,^{104a,104b} A. Canepa,^{159a} M. Cano Bret,^{33e} J. Cantero,⁸² R. Cantrill,^{126a} T. Cao,⁴⁰ M. D. M. Capeans Garrido,³⁰ I. Caprini,^{26a} M. Caprini,^{26a} M. Capua,^{37a,37b} R. Caputo,⁸³ R. Cardarelli,^{133a} F. Cardillo,⁴⁸ T. Carli,³⁰ G. Carlino,^{104a} L. Carminati,^{91a,91b} S. Caron,¹⁰⁶ E. Carquin,^{32a} G. D. Carrillo-Montoya,³⁰ J. R. Carter,²⁸ J. Carvalho,^{126a,126c} D. Casadei,⁷⁸ M. P. Casado,¹² M. Casolino,¹² E. Castaneda-Miranda,^{145b} A. Castelli,¹⁰⁷ V. Castillo Gimenez,¹⁶⁷ N. F. Castro,^{126a,h} P. Catastini,⁵⁷ A. Catinaccio,³⁰ J. R. Catmore,¹¹⁹ A. Cattai,³⁰ J. Caudron,⁸³ V. Cavaliere,¹⁶⁵ D. Cavalli,^{91a} M. Cavalli-Sforza,¹² V. Cavasinni,^{124a,124b} F. Ceradini,^{134a,134b} B. C. Cerio,⁴⁵ K. Cerny,¹²⁹ A. S. Cerqueira,^{24b} A. Cerri,¹⁴⁹ L. Cerrito,⁷⁶ F. Cerutti,¹⁵ M. Cerv,³⁰ A. Cervelli,¹⁷ S. A. Cetin,^{19c} A. Chafaq,^{135a} D. Chakraborty,¹⁰⁸ I. Chalupkova,¹²⁹ P. Chang,¹⁶⁵ J. D. Chapman,²⁸ D. G. Charlton,¹⁸ C. C. Chau,¹⁵⁸ C. A. Chavez Barajas,¹⁴⁹ S. Cheatham,¹⁵² A. Chegwiddden,⁹⁰ S. Chekanov,⁶ S. V. Chekulaev,^{159a} G. A. Chelkov,^{65,i} M. A. Chelstowska,⁸⁹ C. Chen,⁶⁴ H. Chen,²⁵ K. Chen,¹⁴⁸ L. Chen,^{33d,j} S. Chen,^{33c} X. Chen,^{33f} Y. Chen,⁶⁷ H. C. Cheng,⁸⁹ Y. Cheng,³¹ A. Cheplakov,⁶⁵ E. Cheremushkina,¹³⁰ R. Cherkaoui El Moursli,^{135e} V. Chernyatin,^{25,a} E. Cheu,⁷ L. Chevalier,¹³⁶ V. Chiarella,⁴⁷ G. Chiarelli,^{124a,124b} G. Chiodini,^{73a} A. S. Chisholm,¹⁸ R. T. Chislett,⁷⁸ A. Chitan,^{26a} M. V. Chizhov,⁶⁵ K. Choi,⁶¹ S. Chouridou,⁹ B. K. B. Chow,¹⁰⁰ V. Christodoulou,⁷⁸ D. Chromek-Burckhart,³⁰ J. Chudoba,¹²⁷ A. J. Chuinard,⁸⁷ J. J. Chwastowski,³⁹ L. Chytka,¹¹⁵ G. Ciapetti,^{132a,132b} A. K. Ciftci,^{4a} D. Cinca,⁵³ V. Cindro,⁷⁵ I. A. Cioara,²¹ A. Ciocio,¹⁵ Z. H. Citron,¹⁷² M. Ciubancan,^{26a} A. Clark,⁴⁹ B. L. Clark,⁵⁷ P. J. Clark,⁴⁶ R. N. Clarke,¹⁵ W. Cleland,¹²⁵ C. Clement,^{146a,146b} Y. Coadou,⁸⁵ M. Cobal,^{164a,164c} A. Coccaro,⁴⁹ J. Cochran,⁶⁴ L. Coffey,²³ J. G. Cogan,¹⁴³ L. Colasurdo,¹⁰⁶ B. Cole,³⁵ S. Cole,¹⁰⁸ A. P. Colijn,¹⁰⁷ J. Collot,⁵⁵ T. Colombo,^{58c} G. Compostella,¹⁰¹ P. Conde Muiño,^{126a,126b} E. Coniavitis,⁴⁸ S. H. Connell,^{145b} I. A. Connelly,⁷⁷ S. M. Consonni,^{91a,91b} V. Consorti,⁴⁸ S. Constantinescu,^{26a} C. Conta,^{121a,121b} G. Conti,³⁰ F. Conventi,^{104a,k} M. Cooke,¹⁵ B. D. Cooper,⁷⁸ A. M. Cooper-Sarkar,¹²⁰ T. Cornelissen,¹⁷⁵ M. Corradi,^{20a} F. Corriveau,^{87,l} A. Corso-Radu,¹⁶³ A. Cortes-Gonzalez,¹² G. Cortiana,¹⁰¹ G. Costa,^{91a} M. J. Costa,¹⁶⁷ D. Costanzo,¹³⁹ D. Côté,⁸ G. Cottin,²⁸ G. Cowan,⁷⁷ B. E. Cox,⁸⁴ K. Cranmer,¹¹⁰ G. Cree,²⁹ S. Crépe-Renaudin,⁵⁵ F. Crescioli,⁸⁰ W. A. Cribbs,^{146a,146b} M. Crispin Ortuzar,¹²⁰ M. Cristinziani,²¹ V. Croft,¹⁰⁶

G. Crosetti,^{37a,37b} T. Cuhadar Donszelmann,¹³⁹ J. Cummings,¹⁷⁶ M. Curatolo,⁴⁷ C. Cuthbert,¹⁵⁰ H. Czirr,¹⁴¹ P. Czodrowski,³ S. D'Auria,⁵³ M. D'Onofrio,⁷⁴ M. J. Da Cunha Sargedas De Sousa,^{126a,126b} C. Da Via,⁸⁴ W. Dabrowski,^{38a} A. Dafinca,¹²⁰ T. Dai,⁸⁹ O. Dale,¹⁴ F. Dallaire,⁹⁵ C. Dallapiccola,⁸⁶ M. Dam,³⁶ J. R. Dandoy,³¹ N. P. Dang,⁴⁸ A. C. Daniells,¹⁸ M. Danninger,¹⁶⁸ M. Dano Hoffmann,¹³⁶ V. Dao,⁴⁸ G. Darbo,^{50a} S. Darmora,⁸ J. Dassoulas,³ A. Dattagupta,⁶¹ W. Davey,²¹ C. David,¹⁶⁹ T. Davidek,¹²⁹ E. Davies,^{120,m} M. Davies,¹⁵³ P. Davison,⁷⁸ Y. Davygora,^{58a} E. Dawe,⁸⁸ I. Dawson,¹³⁹ R. K. Daya-Ishmukhametova,⁸⁶ K. De,⁸ R. de Asmundis,^{104a} A. De Benedetti,¹¹³ S. De Castro,^{20a,20b} S. De Cecco,⁸⁰ N. De Groot,¹⁰⁶ P. de Jong,¹⁰⁷ H. De la Torre,⁸² F. De Lorenzi,⁶⁴ D. De Pedis,^{132a} A. De Salvo,^{132a} U. De Sanctis,¹⁴⁹ A. De Santo,¹⁴⁹ J. B. De Vivie De Regie,¹¹⁷ W. J. Dearnaley,⁷² R. Debbe,²⁵ C. Debenedetti,¹³⁷ D. V. Dedovich,⁶⁵ I. Deigaard,¹⁰⁷ J. Del Peso,⁸² T. Del Prete,^{124a,124b} D. Delgove,¹¹⁷ F. Deliot,¹³⁶ C. M. Delitzsch,⁴⁹ M. Deliyergiyev,⁷⁵ A. Dell'Acqua,³⁰ L. Dell'Asta,²² M. Dell'Orso,^{124a,124b} M. Della Pietra,^{104a,k} D. della Volpe,⁴⁹ M. Delmastro,⁵ P. A. Delsart,⁵⁵ C. Deluca,¹⁰⁷ D. A. DeMarco,¹⁵⁸ S. Demers,¹⁷⁶ M. Demichev,⁶⁵ A. Demilly,⁸⁰ S. P. Denisov,¹³⁰ D. Derendarz,³⁹ J. E. Derkaoui,^{135d} F. Derue,⁸⁰ P. Dervan,⁷⁴ K. Desch,²¹ C. Deterre,⁴² P. O. Deviveiros,³⁰ A. Dewhurst,¹³¹ S. Dhaliwal,²³ A. Di Ciaccio,^{133a,133b} L. Di Ciaccio,⁵ A. Di Domenico,^{132a,132b} C. Di Donato,^{104a,104b} A. Di Girolamo,³⁰ B. Di Girolamo,³⁰ A. Di Mattia,¹⁵² B. Di Micco,^{134a,134b} R. Di Nardo,⁴⁷ A. Di Simone,⁴⁸ R. Di Sipio,¹⁵⁸ D. Di Valentino,²⁹ C. Diaconu,⁸⁵ M. Diamond,¹⁵⁸ F. A. Dias,⁴⁶ M. A. Diaz,^{32a} E. B. Diehl,⁸⁹ J. Dietrich,¹⁶ S. Diglio,⁸⁵ A. Dimitrievska,¹³ J. Dingfelder,²¹ P. Dita,^{26a} S. Dita,^{26a} F. Dittus,³⁰ F. Djama,⁸⁵ T. Djobava,^{51b} J. I. Djuvsland,^{58a} M. A. B. do Vale,^{24c} D. Dobos,³⁰ M. Dobre,^{26a} C. Doglioni,⁸¹ T. Dohmae,¹⁵⁵ J. Dolejsi,¹²⁹ Z. Dolezal,¹²⁹ B. A. Dolgoshein,^{98a} M. Donadelli,^{24d} S. Donati,^{124a,124b} P. Dondero,^{121a,121b} J. Donini,³⁴ J. Dopke,¹³¹ A. Doria,^{104a} M. T. Dova,⁷¹ A. T. Doyle,⁵³ E. Drechsler,⁵⁴ M. Dris,¹⁰ E. Dubreuil,³⁴ E. Duchovni,¹⁷² G. Duckeck,¹⁰⁰ O. A. Ducu,^{26a,85} D. Duda,¹⁰⁷ A. Dudarev,³⁰ L. Duflot,¹¹⁷ L. Duguid,⁷⁷ M. Dührssen,³⁰ M. Dunford,^{58a} H. Duran Yildiz,^{4a} M. Düren,⁵² A. Durglishvili,^{51b} D. Duschinger,⁴⁴ M. Dyndal,^{38a} C. Eckardt,⁴² K. M. Ecker,¹⁰¹ R. C. Edgar,⁸⁹ W. Edson,² N. C. Edwards,⁴⁶ W. Ehrenfeld,²¹ T. Eifert,³⁰ G. Eigen,¹⁴ K. Einsweiler,¹⁵ T. Ekelof,¹⁶⁶ M. El Kacimi,^{135c} M. Ellert,¹⁶⁶ S. Elles,⁵ F. Ellinghaus,¹⁷⁵ A. A. Elliot,¹⁶⁹ N. Ellis,³⁰ J. Elmsheuser,¹⁰⁰ M. Elsing,³⁰ D. Emeliyanov,¹³¹ Y. Enari,¹⁵⁵ O. C. Endner,⁸³ M. Endo,¹¹⁸ J. Erdmann,⁴³ A. Ereditato,¹⁷ G. Ernis,¹⁷⁵ J. Ernst,² M. Ernst,²⁵ S. Errede,¹⁶⁵ E. Ertel,⁸³ M. Escalier,¹¹⁷ H. Esch,⁴³ C. Escobar,¹²⁵ B. Esposito,⁴⁷ A. I. Etienne,¹³⁶ E. Etzion,¹⁵³ H. Evans,⁶¹ A. Ezhilov,¹²³ L. Fabbri,^{20a,20b} G. Facini,³¹ R. M. Fakhruddinov,¹³⁰ S. Falciano,^{132a} R. J. Falla,⁷⁸ J. Faltova,¹²⁹ Y. Fang,^{33a} M. Fantì,^{91a,91b} A. Farbin,⁸ A. Farilla,^{134a} T. Farooque,¹² S. Farrell,¹⁵ S. M. Farrington,¹⁷⁰ P. Farthouat,³⁰ F. Fassi,^{135e} P. Fassnacht,³⁰ D. Fassouliotis,⁹ M. Fauci Giannelli,⁷⁷ A. Favareto,^{50a,50b} L. Fayard,¹¹⁷ P. Federic,^{144a} O. L. Fedin,^{123,n} W. Fedorko,¹⁶⁸ S. Feigl,³⁰ L. Feligioni,⁸⁵ C. Feng,^{33d} E. J. Feng,⁶ H. Feng,⁸⁹ A. B. Fenyuk,¹³⁰ L. Feremenga,⁸ P. Fernandez Martinez,¹⁶⁷ S. Fernandez Perez,³⁰ J. Ferrando,⁵³ A. Ferrari,¹⁶⁶ P. Ferrari,¹⁰⁷ R. Ferrari,^{121a} D. E. Ferreira de Lima,⁵³ A. Ferrer,¹⁶⁷ D. Ferrere,⁴⁹ C. Ferretti,⁸⁹ A. Ferretto Parodi,^{50a,50b} M. Fiascaris,³¹ F. Fiedler,⁸³ A. Filipčič,⁷⁵ M. Filipuzzi,⁴² F. Filthaut,¹⁰⁶ M. Fincke-Keeler,¹⁶⁹ K. D. Finelli,¹⁵⁰ M. C. N. Fiolhais,^{126a,126c} L. Fiorini,¹⁶⁷ A. Firan,⁴⁰ A. Fischer,² C. Fischer,¹² J. Fischer,¹⁷⁵ W. C. Fisher,⁹⁰ E. A. Fitzgerald,²³ N. Flaschel,⁴² I. Fleck,¹⁴¹ P. Fleischmann,⁸⁹ S. Fleischmann,¹⁷⁵ G. T. Fletcher,¹³⁹ G. Fletcher,⁷⁶ R. R. M. Fletcher,¹²² T. Flick,¹⁷⁵ A. Floderus,⁸¹ L. R. Flores Castillo,^{60a} M. J. Flowerdew,¹⁰¹ A. Formica,¹³⁶ A. Forti,⁸⁴ D. Fournier,¹¹⁷ H. Fox,⁷² S. Fracchia,¹² P. Francavilla,⁸⁰ M. Franchini,^{20a,20b} D. Francis,³⁰ L. Franconi,¹¹⁹ M. Franklin,⁵⁷ M. Frate,¹⁶³ M. Fraternali,^{121a,121b} D. Freeborn,⁷⁸ S. T. French,²⁸ F. Friedrich,⁴⁴ D. Froidevaux,³⁰ J. A. Frost,¹²⁰ C. Fukunaga,¹⁵⁶ E. Fullana Torregrosa,⁸³ B. G. Fulson,¹⁴³ T. Fusayas,¹⁰² J. Fuster,¹⁶⁷ C. Gabaldon,⁵⁵ O. Gabizon,¹⁷⁵ A. Gabrielli,^{20a,20b} A. Gabrielli,^{132a,132b} G. P. Gach,^{38a} S. Gadatsch,³⁰ S. Gadomski,⁴⁹ G. Gagliardi,^{50a,50b} P. Gagnon,⁶¹ C. Galea,¹⁰⁶ B. Galhardo,^{126a,126c} E. J. Gallas,¹²⁰ B. J. Gallop,¹³¹ P. Gallus,¹²⁸ G. Galster,³⁶ K. K. Gan,¹¹¹ J. Gao,^{33b,85} Y. Gao,⁴⁶ Y. S. Gao,^{143,f} F. M. Garay Walls,⁴⁶ F. Garbersson,¹⁷⁶ C. García,¹⁶⁷ J. E. García Navarro,¹⁶⁷ M. Garcia-Sciveres,¹⁵ R. W. Gardner,³¹ N. Garelli,¹⁴³ V. Garonne,¹¹⁹ C. Gatti,⁴⁷ A. Gaudiello,^{50a,50b} G. Gaudio,^{121a} B. Gaur,¹⁴¹ L. Gauthier,⁹⁵ P. Gauzzi,^{132a,132b} I. L. Gavrilenko,⁹⁶ C. Gay,¹⁶⁸ G. Gaycken,²¹ E. N. Gazis,¹⁰ P. Ge,^{33d} Z. Gecse,¹⁶⁸ C. N. P. Gee,¹³¹ Ch. Geich-Gimbel,²¹ M. P. Geisler,^{58a} C. Gemme,^{50a} M. H. Genest,⁵⁵ S. Gentile,^{132a,132b} M. George,⁵⁴ S. George,⁷⁷ D. Gerbaudo,¹⁶³ A. Gershon,¹⁵³ S. Ghasemi,¹⁴¹ H. Ghazlane,^{135b} B. Giacobbe,^{20a} S. Giagu,^{132a,132b} V. Giangiobbe,¹² P. Giannetti,^{124a,124b} B. Gibbard,²⁵ S. M. Gibson,⁷⁷ M. Gilchriese,¹⁵ T. P. S. Gillam,²⁸ D. Gillberg,³⁰ G. Gilles,³⁴ D. M. Gingrich,^{3,e} N. Giokaris,⁹ M. P. Giordani,^{164a,164c} F. M. Giorgi,^{20a} F. M. Giorgi,¹⁶ P. F. Giraud,¹³⁶ P. Giromini,⁴⁷ D. Giugni,^{91a} C. Giuliani,⁴⁸ M. Giulini,^{58b} B. K. Gjelsten,¹¹⁹ S. Gkaitatzis,¹⁵⁴ I. Gkialas,¹⁵⁴ E. L. Gkoukousis,¹¹⁷ L. K. Gladilin,⁹⁹ C. Glasman,⁸² J. Glatzer,³⁰ P. C. F. Glaysheer,⁴⁶ A. Glazov,⁴² M. Goblirsch-Kolb,¹⁰¹ J. R. Goddard,⁷⁶ J. Godlewski,³⁹ S. Goldfarb,⁸⁹ T. Golling,⁴⁹ D. Golubkov,¹³⁰ A. Gomes,^{126a,126b,126d} R. Gonçalves,^{126a} J. Goncalves Pinto Firmino Da Costa,¹³⁶ L. Gonella,²¹

S. González de la Hoz,¹⁶⁷ G. Gonzalez Parra,¹² S. Gonzalez-Sevilla,⁴⁹ L. Goossens,³⁰ P. A. Gorbounov,⁹⁷ H. A. Gordon,²⁵ I. Gorelov,¹⁰⁵ B. Gorini,³⁰ E. Gorini,^{73a,73b} A. Gorišek,⁷⁵ E. Gornicki,³⁹ A. T. Goshaw,⁴⁵ C. Gössling,⁴³ M. I. Gostkin,⁶⁵ D. Goujdami,^{135c} A. G. Goussiou,¹³⁸ N. Govender,^{145b} E. Gozani,¹⁵² H. M. X. Grabas,¹³⁷ L. Graber,⁵⁴ I. Grabowska-Bold,^{38a} P. O. J. Gradin,¹⁶⁶ P. Grafström,^{20a,20b} K.-J. Grahn,⁴² J. Gramling,⁴⁹ E. Gramstad,¹¹⁹ S. Grancagnolo,¹⁶ V. Gratchev,¹²³ H. M. Gray,³⁰ E. Graziani,^{134a} Z. D. Greenwood,^{79,o} K. Gregersen,⁷⁸ I. M. Gregor,⁴² P. Grenier,¹⁴³ J. Griffiths,⁸ A. A. Grillo,¹³⁷ K. Grimm,⁷² S. Grinstein,^{12,p} Ph. Gris,³⁴ J.-F. Grivaz,¹¹⁷ J. P. Grohs,⁴⁴ A. Grohsjean,⁴² E. Gross,¹⁷² J. Grosse-Knetter,⁵⁴ G. C. Grossi,⁷⁹ Z. J. Grout,¹⁴⁹ L. Guan,⁸⁹ J. Guenther,¹²⁸ F. Guescini,⁴⁹ D. Guest,¹⁷⁶ O. Gueta,¹⁵³ E. Guido,^{50a,50b} T. Guillemain,¹¹⁷ S. Guindon,² U. Gul,⁵³ C. Gumpert,⁴⁴ J. Guo,^{33e} Y. Guo,^{33b} S. Gupta,¹²⁰ G. Gustavino,^{132a,132b} P. Gutierrez,¹¹³ N. G. Gutierrez Ortiz,⁷⁸ C. Gutsche,⁴⁴ C. Guyot,¹³⁶ C. Gwenlan,¹²⁰ C. B. Gwilliam,⁷⁴ A. Haas,¹¹⁰ C. Haber,¹⁵ H. K. Hadavand,⁸ N. Haddad,^{135e} P. Haefner,²¹ S. Hageböck,²¹ Z. Hajduk,³⁹ H. Hakobyan,¹⁷⁷ M. Haleem,⁴² J. Haley,¹¹⁴ D. Hall,¹²⁰ G. Halladjian,⁹⁰ G. D. Hallewell,⁸⁵ K. Hamacher,¹⁷⁵ P. Hamal,¹¹⁵ K. Hamano,¹⁶⁹ A. Hamilton,^{145a} G. N. Hamity,¹³⁹ P. G. Hamnett,⁴² L. Han,^{33b} K. Hanagaki,^{66,q} K. Hanawa,¹⁵⁵ M. Hance,¹⁵ P. Hanke,^{58a} R. Hanna,¹³⁶ J. B. Hansen,³⁶ J. D. Hansen,³⁶ M. C. Hansen,²¹ P. H. Hansen,³⁶ K. Hara,¹⁶⁰ A. S. Hard,¹⁷³ T. Harenberg,¹⁷⁵ F. Hariri,¹¹⁷ S. Harkusha,⁹² R. D. Harrington,⁴⁶ P. F. Harrison,¹⁷⁰ F. Hartjes,¹⁰⁷ M. Hasegawa,⁶⁷ Y. Hasegawa,¹⁴⁰ A. Hasib,¹¹³ S. Hassani,¹³⁶ S. Haug,¹⁷ R. Hauser,⁹⁰ L. Hauswald,⁴⁴ M. Havranek,¹²⁷ C. M. Hawkes,¹⁸ R. J. Hawkings,³⁰ A. D. Hawkins,⁸¹ T. Hayashi,¹⁶⁰ D. Hayden,⁹⁰ C. P. Hays,¹²⁰ J. M. Hays,⁷⁶ H. S. Hayward,⁷⁴ S. J. Haywood,¹³¹ S. J. Head,¹⁸ T. Heck,⁸³ V. Hedberg,⁸¹ L. Heelan,⁸ S. Heim,¹²² T. Heim,¹⁷⁵ B. Heinemann,¹⁵ L. Heinrich,¹¹⁰ J. Hejbal,¹²⁷ L. Helary,²² S. Hellman,^{146a,146b} D. Hellmich,²¹ C. Hensens,¹² J. Henderson,¹²⁰ R. C. W. Henderson,⁷² Y. Heng,¹⁷³ C. Hengler,⁴² S. Henkelmann,¹⁶⁸ A. Henrichs,¹⁷⁶ A. M. Henriques Correia,³⁰ S. Henrot-Versille,¹¹⁷ G. H. Herbert,¹⁶ Y. Hernández Jiménez,¹⁶⁷ R. Herrberg-Schubert,¹⁶ G. Herten,⁴⁸ R. Hertenberger,¹⁰⁰ L. Hervas,³⁰ G. G. Hesketh,⁷⁸ N. P. Hessey,¹⁰⁷ J. W. Hetherly,⁴⁰ R. Hickling,⁷⁶ E. Higón-Rodríguez,¹⁶⁷ E. Hill,¹⁶⁹ J. C. Hill,²⁸ K. H. Hiller,⁴² S. J. Hillier,¹⁸ I. Hinchliffe,¹⁵ E. Hines,¹²² R. R. Hinman,¹⁵ M. Hirose,¹⁵⁷ D. Hirschbuehl,¹⁷⁵ J. Hobbs,¹⁴⁸ N. Hod,¹⁰⁷ M. C. Hodgkinson,¹³⁹ P. Hodgson,¹³⁹ A. Hoecker,³⁰ M. R. Hoferkamp,¹⁰⁵ F. Hoenig,¹⁰⁰ M. Hohlfeld,⁸³ D. Hohn,²¹ T. R. Holmes,¹⁵ M. Homann,⁴³ T. M. Hong,¹²⁵ L. Hooft van Huysduynen,¹¹⁰ W. H. Hopkins,¹¹⁶ Y. Horii,¹⁰³ A. J. Horton,¹⁴² J.-Y. Hostachy,⁵⁵ S. Hou,¹⁵¹ A. Hoummada,^{135a} J. Howard,¹²⁰ J. Howarth,⁴² M. Hrabovsky,¹¹⁵ I. Hristova,¹⁶ J. Hrivnac,¹¹⁷ T. Hryn'ova,⁵ A. Hrynevich,⁹³ C. Hsu,^{145c} P. J. Hsu,^{151,r} S.-C. Hsu,¹³⁸ D. Hu,³⁵ Q. Hu,^{33b} X. Hu,⁸⁹ Y. Huang,⁴² Z. Hubacek,¹²⁸ F. Hubaut,⁸⁵ F. Huegging,²¹ T. B. Huffman,¹²⁰ E. W. Hughes,³⁵ G. Hughes,⁷² M. Huhtinen,³⁰ T. A. Hülsing,⁸³ N. Huseynov,^{65,c} J. Huston,⁹⁰ J. Huth,⁵⁷ G. Iacobucci,⁴⁹ G. Iakovidis,²⁵ I. Ibragimov,¹⁴¹ L. Iconomidou-Fayard,¹¹⁷ E. Ideal,¹⁷⁶ Z. Idrissi,^{135e} P. Iengo,³⁰ O. Igonkina,¹⁰⁷ T. Iizawa,¹⁷¹ Y. Ikegami,⁶⁶ K. Ikematsu,¹⁴¹ M. Ikeno,⁶⁶ Y. Ilchenko,^{31,s} D. Iliadis,¹⁵⁴ N. Ilic,¹⁴³ T. Ince,¹⁰¹ G. Introzzi,^{121a,121b} P. Ioannou,⁹ M. Iodice,^{134a} K. Iordanidou,³⁵ V. Ippolito,⁵⁷ A. Irls Quiles,¹⁶⁷ C. Isaksson,¹⁶⁶ M. Ishino,⁶⁸ M. Ishitsuka,¹⁵⁷ R. Ishmukhametov,¹¹¹ C. Issever,¹²⁰ S. Istin,^{19a} J. M. Iturbe Ponce,⁸⁴ R. Iuppa,^{133a,133b} J. Ivarsson,⁸¹ W. Iwanski,³⁹ H. Iwasaki,⁶⁶ J. M. Izen,⁴¹ V. Izzo,^{104a} S. Jabbar,³ B. Jackson,¹²² M. Jackson,⁷⁴ P. Jackson,¹ M. R. Jaekel,³⁰ V. Jain,² K. Jakobs,⁴⁸ S. Jakobsen,³⁰ T. Jakoubek,¹²⁷ J. Jakubek,¹²⁸ D. O. Jamin,¹¹⁴ D. K. Jana,⁷⁹ E. Jansen,⁷⁸ R. Jansky,⁶² J. Janssen,²¹ M. Janus,⁵⁴ G. Jarlskog,⁸¹ N. Javadov,^{65,c} T. Javůrek,⁴⁸ L. Jeanty,¹⁵ J. Jejelava,^{51a,t} G.-Y. Jeng,¹⁵⁰ D. Jennens,⁸⁸ P. Jenni,^{48,u} J. Jentzsch,⁴³ C. Jeske,¹⁷⁰ S. Jézéquel,⁵ H. Ji,¹⁷³ J. Jia,¹⁴⁸ Y. Jiang,^{33b} S. Jiggins,⁷⁸ J. Jimenez Pena,¹⁶⁷ S. Jin,^{33a} A. Jinaru,^{26a} O. Jinnouchi,¹⁵⁷ M. D. Joergensen,³⁶ P. Johansson,¹³⁹ K. A. Johns,⁷ K. Jon-And,^{146a,146b} G. Jones,¹⁷⁰ R. W. L. Jones,⁷² T. J. Jones,⁷⁴ J. Jongmanns,^{58a} P. M. Jorge,^{126a,126b} K. D. Joshi,⁸⁴ J. Jovicevic,^{159a} X. Ju,¹⁷³ C. A. Jung,⁴³ P. Jussel,⁶² A. Juste Rozas,^{12,p} M. Kaci,¹⁶⁷ A. Kaczmarska,³⁹ M. Kado,¹¹⁷ H. Kagan,¹¹¹ M. Kagan,¹⁴³ S. J. Kahn,⁸⁵ E. Kajomovitz,⁴⁵ C. W. Kalderon,¹²⁰ S. Kama,⁴⁰ A. Kamenshchikov,¹³⁰ N. Kanaya,¹⁵⁵ S. Kaneti,²⁸ V. A. Kantserov,⁹⁸ J. Kanzaki,⁶⁶ B. Kaplan,¹¹⁰ L. S. Kaplan,¹⁷³ A. Kapliy,³¹ D. Kar,^{145c} K. Karakostas,¹⁰ A. Karamaoun,³ N. Karastathis,^{10,107} M. J. Kareem,⁵⁴ E. Karentzos,¹⁰ M. Karnevskiy,⁸³ S. N. Karpov,⁶⁵ Z. M. Karpova,⁶⁵ K. Karthik,¹¹⁰ V. Kartvelishvili,⁷² A. N. Karyukhin,¹³⁰ L. Kashif,¹⁷³ R. D. Kass,¹¹¹ A. Kastanas,¹⁴ Y. Kataoka,¹⁵⁵ C. Kato,¹⁵⁵ A. Katre,⁴⁹ J. Katzy,⁴² K. Kawagoe,⁷⁰ T. Kawamoto,¹⁵⁵ G. Kawamura,⁵⁴ S. Kazama,¹⁵⁵ V. F. Kazanin,^{109,d} R. Keeler,¹⁶⁹ R. Kehoe,⁴⁰ J. S. Keller,⁴² J. J. Kempster,⁷⁷ H. Keoshkerian,⁸⁴ O. Kepka,¹²⁷ B. P. Kerševan,⁷⁵ S. Kersten,¹⁷⁵ R. A. Keyes,⁸⁷ F. Khalil-zada,¹¹ H. Khandanyan,^{146a,146b} A. Khanov,¹¹⁴ A. G. Kharlamov,^{109,d} T. J. Khoo,²⁸ V. Khovanskij,⁹⁷ E. Khramov,⁶⁵ J. Khubua,^{51b,v} S. Kido,⁶⁷ H. Y. Kim,⁸ S. H. Kim,¹⁶⁰ Y. K. Kim,³¹ N. Kimura,¹⁵⁴ O. M. Kind,¹⁶ B. T. King,⁷⁴ M. King,¹⁶⁷ S. B. King,¹⁶⁸ J. Kirk,¹³¹ A. E. Kiryunin,¹⁰¹ T. Kishimoto,⁶⁷ D. Kisielewska,^{38a} F. Kiss,⁴⁸ K. Kiuchi,¹⁶⁰ O. Kivernyk,¹³⁶ E. Kladiva,^{144b} M. H. Klein,³⁵ M. Klein,⁷⁴ U. Klein,⁷⁴ K. Kleinknecht,⁸³ P. Klimek,^{146a,146b} A. Klimentov,²⁵ R. Klingenberg,⁴³ J. A. Klinger,¹³⁹ T. Klioutchnikova,³⁰ E.-E. Kluge,^{58a} P. Kluit,¹⁰⁷ S. Kluth,¹⁰¹ J. Knapik,³⁹ E. Kneringer,⁶²

E. B. F. G. Knoop, ⁸⁵ A. Knue, ⁵³ A. Kobayashi, ¹⁵⁵ D. Kobayashi, ¹⁵⁷ T. Kobayashi, ¹⁵⁵ M. Kobel, ⁴⁴ M. Kocian, ¹⁴³
P. Kodys, ¹²⁹ T. Koffas, ²⁹ E. Koffeman, ¹⁰⁷ L. A. Kogan, ¹²⁰ S. Kohlmann, ¹⁷⁵ Z. Kohout, ¹²⁸ T. Kohriki, ⁶⁶ T. Koi, ¹⁴³
H. Kolanoski, ¹⁶ I. Koletsou, ⁵ A. A. Komar, ^{96a} Y. Komori, ¹⁵⁵ T. Kondo, ⁶⁶ N. Kondrashova, ⁴² K. Köneke, ⁴⁸ A. C. König, ¹⁰⁶
T. Kono, ⁶⁶ R. Konoplich, ^{110,w} N. Konstantinidis, ⁷⁸ R. Kopeliansky, ¹⁵² S. Koperny, ^{38a} L. Köpke, ⁸³ A. K. Kopp, ⁴⁸ K. Korcyl, ³⁹
K. Kordas, ¹⁵⁴ A. Korn, ⁷⁸ A. A. Korol, ^{109,d} I. Korolkov, ¹² E. V. Korolkova, ¹³⁹ O. Kortner, ¹⁰¹ S. Kortner, ¹⁰¹ T. Kosek, ¹²⁹
V. V. Kostyukhin, ²¹ V. M. Kotov, ⁶⁵ A. Kotwal, ⁴⁵ A. Kourkoumeli-Charalampidi, ¹⁵⁴ C. Kourkoumelis, ⁹ V. Kouskoura, ²⁵
A. Koutsman, ^{159a} R. Kowalewski, ¹⁶⁹ T. Z. Kowalski, ^{38a} W. Kozanecki, ¹³⁶ A. S. Kozhin, ¹³⁰ V. A. Kramarenko, ⁹⁹
G. Kramberger, ⁷⁵ D. Krasnopevtsev, ⁹⁸ M. W. Krasny, ⁸⁰ A. Krasznahorkay, ³⁰ J. K. Kraus, ²¹ A. Kravchenko, ²⁵ S. Kreiss, ¹¹⁰
M. Kretz, ^{58c} J. Kretzschmar, ⁷⁴ K. Kreuzfeldt, ⁵² P. Krieger, ¹⁵⁸ K. Krizka, ³¹ K. Kroeninger, ⁴³ H. Kroha, ¹⁰¹ J. Kroll, ¹²²
J. Kroseberg, ²¹ J. Krstic, ¹³ U. Kruchonak, ⁶⁵ H. Krüger, ²¹ N. Krumnack, ⁶⁴ A. Kruse, ¹⁷³ M. C. Kruse, ⁴⁵ M. Kruskal, ²²
T. Kubota, ⁸⁸ H. Kucuk, ⁷⁸ S. Kuday, ^{4b} S. Kuehn, ⁴⁸ A. Kugel, ^{58c} F. Kuger, ¹⁷⁴ A. Kuhl, ¹³⁷ T. Kuhl, ⁴² V. Kukhtin, ⁶⁵
Y. Kulchitsky, ⁹² S. Kuleshov, ^{32b} M. Kuna, ^{132a,132b} T. Kunigo, ⁶⁸ A. Kupco, ¹²⁷ H. Kurashige, ⁶⁷ Y. A. Kurochkin, ⁹² V. Kus, ¹²⁷
E. S. Kuwertz, ¹⁶⁹ M. Kuze, ¹⁵⁷ J. Kvita, ¹¹⁵ T. Kwan, ¹⁶⁹ D. Kyriazopoulos, ¹³⁹ A. La Rosa, ¹³⁷ J. L. La Rosa Navarro, ^{24d}
L. La Rotonda, ^{37a,37b} C. Lacasta, ¹⁶⁷ F. Lacava, ^{132a,132b} J. Lacey, ²⁹ H. Lacker, ¹⁶ D. Lacour, ⁸⁰ V. R. Lacuesta, ¹⁶⁷ E. Ladygin, ⁶⁵
R. Lafaye, ⁵ B. Laforge, ⁸⁰ T. Lagouri, ¹⁷⁶ S. Lai, ⁵⁴ L. Lambourne, ⁷⁸ S. Lammers, ⁶¹ C. L. Lampen, ⁷ W. Lampl, ⁷ E. Lançon, ¹³⁶
U. Landgraf, ⁴⁸ M. P. J. Landon, ⁷⁶ V. S. Lang, ^{58a} J. C. Lange, ¹² A. J. Lankford, ¹⁶³ F. Lanni, ²⁵ K. Lantzsch, ²¹ A. Lanza, ^{121a}
S. Laplace, ⁸⁰ C. Lapoire, ³⁰ J. F. Laporte, ¹³⁶ T. Lari, ^{91a} F. Lasagni Manghi, ^{20a,20b} M. Lassnig, ³⁰ P. Laurelli, ⁴⁷ W. Lavrijsen, ¹⁵
A. T. Law, ¹³⁷ P. Laycock, ⁷⁴ T. Lazovich, ⁵⁷ O. Le Dortz, ⁸⁰ E. Le Guirriec, ⁸⁵ E. Le Menedeu, ¹² M. LeBlanc, ¹⁶⁹ T. LeCompte, ⁶
F. Ledroit-Guillon, ⁵⁵ C. A. Lee, ^{145b} S. C. Lee, ¹⁵¹ L. Lee, ¹ G. Lefebvre, ⁸⁰ M. Lefebvre, ¹⁶⁹ F. Legger, ¹⁰⁰ C. Leggett, ¹⁵
A. Lehan, ⁷⁴ G. Lehmann Miotto, ³⁰ X. Lei, ⁷ W. A. Leight, ²⁹ A. Leisos, ^{154,x} A. G. Leister, ¹⁷⁶ M. A. L. Leite, ^{24d} R. Leitner, ¹²⁹
D. Lellouch, ¹⁷² B. Lemmer, ⁵⁴ K. J. C. Leney, ⁷⁸ T. Lenz, ²¹ B. Lenzi, ³⁰ R. Leone, ⁷ S. Leone, ^{124a,124b} C. Leonidopoulos, ⁴⁶
S. Leontsinis, ¹⁰ C. Leroy, ⁹⁵ C. G. Lester, ²⁸ M. Levchenko, ¹²³ J. Levêque, ⁵ D. Levin, ⁸⁹ L. J. Levinson, ¹⁷² M. Levy, ¹⁸
A. Lewis, ¹²⁰ A. M. Leyko, ²¹ M. Leyton, ⁴¹ B. Li, ^{33b,y} H. Li, ¹⁴⁸ H. L. Li, ³¹ L. Li, ⁴⁵ L. Li, ^{33e} S. Li, ⁴⁵ X. Li, ⁸⁴ Y. Li, ^{33c,z}
Z. Liang, ¹³⁷ H. Liao, ³⁴ B. Liberti, ^{133a} A. Liblong, ¹⁵⁸ P. Lichard, ³⁰ K. Lie, ¹⁶⁵ J. Liebal, ²¹ W. Liebig, ¹⁴ C. Limbach, ²¹
A. Limosani, ¹⁵⁰ S. C. Lin, ^{151,aa} T. H. Lin, ⁸³ F. Linde, ¹⁰⁷ B. E. Lindquist, ¹⁴⁸ J. T. Linnemann, ⁹⁰ E. Lipeles, ¹²² A. Lipniacka, ¹⁴
M. Lisovyi, ^{58b} T. M. Liss, ¹⁶⁵ D. Lissauer, ²⁵ A. Lister, ¹⁶⁸ A. M. Litke, ¹³⁷ B. Liu, ^{151,bb} D. Liu, ¹⁵¹ H. Liu, ⁸⁹ J. Liu, ⁸⁵ J. B. Liu, ^{33b}
K. Liu, ⁸⁵ L. Liu, ¹⁶⁵ M. Liu, ⁴⁵ M. Liu, ^{33b} Y. Liu, ^{33b} M. Livan, ^{121a,121b} A. Lleres, ⁵⁵ J. Llorente Merino, ⁸² S. L. Lloyd, ⁷⁶
F. Lo Sterzo, ¹⁵¹ E. Lobodzinska, ⁴² P. Loch, ⁷ W. S. Lockman, ¹³⁷ F. K. Loebinger, ⁸⁴ A. E. Loevschall-Jensen, ³⁶ A. Loginov, ¹⁷⁶
T. Lohse, ¹⁶ K. Lohwasser, ⁴² M. Lokajicek, ¹²⁷ B. A. Long, ²² J. D. Long, ⁸⁹ R. E. Long, ⁷² K. A. Looper, ¹¹¹ L. Lopes, ^{126a}
D. Lopez Mateos, ⁵⁷ B. Lopez Paredes, ¹³⁹ I. Lopez Paz, ¹² J. Lorenz, ¹⁰⁰ N. Lorenzo Martinez, ⁶¹ M. Losada, ¹⁶² P. Loscutoff, ¹⁵
P. J. Lösel, ¹⁰⁰ X. Lou, ^{33a} A. Lounis, ¹¹⁷ J. Love, ⁶ P. A. Love, ⁷² N. Lu, ⁸⁹ H. J. Lubatti, ¹³⁸ C. Luci, ^{132a,132b} A. Lucotte, ⁵⁵
F. Luehring, ⁶¹ W. Lukas, ⁶² L. Luminari, ^{132a} O. Lundberg, ^{146a,146b} B. Lund-Jensen, ¹⁴⁷ D. Lynn, ²⁵ R. Lysak, ¹²⁷ E. Lytken, ⁸¹
H. Ma, ²⁵ L. L. Ma, ^{33d} G. Maccarrone, ⁴⁷ A. Macchiolo, ¹⁰¹ C. M. Macdonald, ¹³⁹ B. Maček, ⁷⁵ J. Machado Miguens, ^{122,126b}
D. Macina, ³⁰ D. Madaffari, ⁸⁵ R. Madar, ³⁴ H. J. Maddocks, ⁷² W. F. Mader, ⁴⁴ A. Madsen, ¹⁶⁶ J. Maeda, ⁶⁷ S. Maeland, ¹⁴
T. Maeno, ²⁵ A. Maevskiy, ⁹⁹ E. Magradze, ⁵⁴ K. Mahboubi, ⁴⁸ J. Mahlstedt, ¹⁰⁷ C. Maiani, ¹³⁶ C. Maidantchik, ^{24a}
A. A. Maier, ¹⁰¹ T. Maier, ¹⁰⁰ A. Maio, ^{126a,126b,126d} S. Majewski, ¹¹⁶ Y. Makida, ⁶⁶ N. Makovec, ¹¹⁷ B. Malaescu, ⁸⁰ Pa. Malecki, ³⁹
V. P. Maleev, ¹²³ F. Malek, ⁵⁵ U. Mallik, ⁶³ D. Malon, ⁶ C. Malone, ¹⁴³ S. Maltezos, ¹⁰ V. M. Malyshev, ¹⁰⁹ S. Malyukov, ³⁰
J. Mamuzic, ⁴² G. Mancini, ⁴⁷ B. Mandelli, ³⁰ L. Mandelli, ^{91a} I. Mandić, ⁷⁵ R. Mandrysch, ⁶³ J. Maneira, ^{126a,126b}
A. Manfredini, ¹⁰¹ L. Manhaes de Andrade Filho, ^{24b} J. Manjarres Ramos, ^{159b} A. Mann, ¹⁰⁰ A. Manousakis-Katsikakis, ⁹
B. Mansoulie, ¹³⁶ R. Mantifel, ⁸⁷ M. Mantoani, ⁵⁴ L. Mapelli, ³⁰ L. March, ^{145c} G. Marchiori, ⁸⁰ M. Marcisovsky, ¹²⁷
C. P. Marino, ¹⁶⁹ M. Marjanovic, ¹³ D. E. Marley, ⁸⁹ F. Marroquim, ^{24a} S. P. Marsden, ⁸⁴ Z. Marshall, ¹⁵ L. F. Marti, ¹⁷
S. Marti-Garcia, ¹⁶⁷ B. Martin, ⁹⁰ T. A. Martin, ¹⁷⁰ V. J. Martin, ⁴⁶ B. Martin dit Latour, ¹⁴ M. Martinez, ^{12,p} S. Martin-Haugh, ¹³¹
V. S. Martoiu, ^{26a} A. C. Martyniuk, ⁷⁸ M. Marx, ¹³⁸ F. Marzano, ^{132a} A. Marzin, ³⁰ L. Masetti, ⁸³ T. Mashimo, ¹⁵⁵
R. Mashinistov, ⁹⁶ J. Masik, ⁸⁴ A. L. Maslennikov, ^{109,d} I. Massa, ^{20a,20b} L. Massa, ^{20a,20b} N. Massol, ⁵ P. Mastrandrea, ¹⁴⁸
A. Mastroberardino, ^{37a,37b} T. Masubuchi, ¹⁵⁵ P. Mättig, ¹⁷⁵ J. Mattmann, ⁸³ J. Maurer, ^{26a} S. J. Maxfield, ⁷⁴ D. A. Maximov, ^{109,d}
R. Mazini, ¹⁵¹ S. M. Mazza, ^{91a,91b} L. Mazzaferro, ^{133a,133b} G. Mc Goldrick, ¹⁵⁸ S. P. Mc Kee, ⁸⁹ A. McCam, ⁸⁹
R. L. McCarthy, ¹⁴⁸ T. G. McCarthy, ²⁹ N. A. McCubbin, ¹³¹ K. W. McFarlane, ^{56,a} J. A. Mcfayden, ⁷⁸ G. Mchedlidze, ⁵⁴
S. J. McMahon, ¹³¹ R. A. McPherson, ^{169,1} M. Medinnis, ⁴² S. Meehan, ^{145a} S. Mehlhase, ¹⁰⁰ A. Mehta, ⁷⁴ K. Meier, ^{58a}
C. Meineck, ¹⁰⁰ B. Meirose, ⁴¹ B. R. Mellado Garcia, ^{145c} F. Meloni, ¹⁷ A. Mengarelli, ^{20a,20b} S. Menke, ¹⁰¹ E. Meoni, ¹⁶¹

K. M. Mercurio,⁵⁷ S. Mergelmeyer,²¹ P. Mermoud,⁴⁹ L. Merola,^{104a,104b} C. Meroni,^{91a} F. S. Merritt,³¹ A. Messina,^{132a,132b}
 J. Metcalfe,²⁵ A. S. Mete,¹⁶³ C. Meyer,⁸³ C. Meyer,¹²² J.-P. Meyer,¹³⁶ J. Meyer,¹⁰⁷ H. Meyer Zu Theenhausen,^{58a}
 R. P. Middleton,¹³¹ S. Miglioranzi,^{164a,164c} L. Mijović,²¹ G. Mikenberg,¹⁷² M. Mikestikova,¹²⁷ M. Mikuž,⁷⁵ M. Milesi,⁸⁸
 A. Milic,³⁰ D. W. Miller,³¹ C. Mills,⁴⁶ A. Milov,¹⁷² D. A. Milstead,^{146a,146b} A. A. Minaenko,¹³⁰ Y. Minami,¹⁵⁵
 I. A. Minashvili,⁶⁵ A. I. Mincer,¹¹⁰ B. Mindur,^{38a} M. Mineev,⁶⁵ Y. Ming,¹⁷³ L. M. Mir,¹² T. Mitani,¹⁷¹ J. Mitrevski,¹⁰⁰
 V. A. Mitsou,¹⁶⁷ A. Miucci,⁴⁹ P. S. Miyagawa,¹³⁹ J. U. Mjörnmark,⁸¹ T. Moa,^{146a,146b} K. Mochizuki,⁸⁵ S. Mohapatra,³⁵
 W. Mohr,⁴⁸ S. Molander,^{146a,146b} R. Moles-Valls,²¹ K. Mönig,⁴² C. Monini,⁵⁵ J. Monk,³⁶ E. Monnier,⁸⁵
 J. Montejo Berlingen,¹² F. Monticelli,⁷¹ S. Monzani,^{132a,132b} R. W. Moore,³ N. Morange,¹¹⁷ D. Moreno,¹⁶²
 M. Moreno Llácer,⁵⁴ P. Morettini,^{50a} D. Mori,¹⁴² M. Morii,⁵⁷ M. Morinaga,¹⁵⁵ V. Morisbak,¹¹⁹ S. Moritz,⁸³ A. K. Morley,¹⁵⁰
 G. Mornacchi,³⁰ J. D. Morris,⁷⁶ S. S. Mortensen,³⁶ A. Morton,⁵³ L. Morvaj,¹⁰³ M. Mosidze,^{51b} J. Moss,¹¹¹ K. Motohashi,¹⁵⁷
 R. Mount,¹⁴³ E. Mountricha,²⁵ S. V. Mouraviev,^{96,a} E. J. W. Moyses,⁸⁶ S. Muanza,⁸⁵ R. D. Mudd,¹⁸ F. Mueller,¹⁰¹
 J. Mueller,¹²⁵ R. S. P. Mueller,¹⁰⁰ T. Mueller,²⁸ D. Muenstermann,⁴⁹ P. Mullen,⁵³ G. A. Mullier,¹⁷ J. A. Murillo Quijada,¹⁸
 W. J. Murray,^{170,131} H. Musheghyan,⁵⁴ E. Musto,¹⁵² A. G. Myagkov,^{130,cc} M. Myska,¹²⁸ B. P. Nachman,¹⁴³ O. Nackenhorst,⁵⁴
 J. Nadal,⁵⁴ K. Nagai,¹²⁰ R. Nagai,¹⁵⁷ Y. Nagai,⁸⁵ K. Nagano,⁶⁶ A. Nagarkar,¹¹¹ Y. Nagasaka,⁵⁹ K. Nagata,¹⁶⁰ M. Nagel,¹⁰¹
 E. Nagy,⁸⁵ A. M. Nairz,³⁰ Y. Nakahama,³⁰ K. Nakamura,⁶⁶ T. Nakamura,¹⁵⁵ I. Nakano,¹¹² H. Namasivayam,⁴¹
 R. F. Naranjo Garcia,⁴² R. Narayan,³¹ D. I. Narrias Villar,^{58a} T. Naumann,⁴² G. Navarro,¹⁶² R. Nayyar,⁷ H. A. Neal,⁸⁹
 P. Yu. Nechaeva,⁹⁶ T. J. Neep,⁸⁴ P. D. Nef,¹⁴³ A. Negri,^{121a,121b} M. Negrini,^{20a} S. Nektarijevic,¹⁰⁶ C. Nellist,¹¹⁷ A. Nelson,¹⁶³
 S. Nemecek,¹²⁷ P. Nemethy,¹¹⁰ A. A. Nepomuceno,^{24a} M. Nessi,^{30,dd} M. S. Neubauer,¹⁶⁵ M. Neumann,¹⁷⁵ R. M. Neves,¹¹⁰
 P. Nevski,²⁵ P. R. Newman,¹⁸ D. H. Nguyen,⁶ R. B. Nickerson,¹²⁰ R. Nicolaidou,¹³⁶ B. Nicquevert,³⁰ J. Nielsen,¹³⁷
 N. Nikiforou,³⁵ A. Nikiforov,¹⁶ V. Nikolaenko,^{130,cc} I. Nikolic-Audit,⁸⁰ K. Nikolopoulos,¹⁸ J. K. Nilsen,¹¹⁹ P. Nilsson,²⁵
 Y. Ninomiya,¹⁵⁵ A. Nisati,^{132a} R. Nisius,¹⁰¹ T. Nobe,¹⁵⁵ M. Nomachi,¹¹⁸ I. Nomidis,²⁹ T. Nooney,⁷⁶ S. Norberg,¹¹³
 M. Nordberg,³⁰ O. Novgorodova,⁴⁴ S. Nowak,¹⁰¹ M. Nozaki,⁶⁶ L. Nozka,¹¹⁵ K. Ntekas,¹⁰ G. Nunes Hanninger,⁸⁸
 T. Nunnemann,¹⁰⁰ E. Nurse,⁷⁸ F. Nuti,⁸⁸ B. J. O'Brien,⁴⁶ F. O'grady,⁷ D. C. O'Neil,¹⁴² V. O'Shea,⁵³ F. G. Oakham,^{29,e}
 H. Oberlack,¹⁰¹ T. Obermann,²¹ J. Ocariz,⁸⁰ A. Ochi,⁶⁷ I. Ochoa,⁷⁸ J. P. Ochoa-Ricoux,^{32a} S. Oda,⁷⁰ S. Odaka,⁶⁶ H. Ogren,⁶¹
 A. Oh,⁸⁴ S. H. Oh,⁴⁵ C. C. Ohm,¹⁵ H. Ohman,¹⁶⁶ H. Oide,³⁰ W. Okamura,¹¹⁸ H. Okawa,¹⁶⁰ Y. Okumura,³¹ T. Okuyama,⁶⁶
 A. Olariu,^{26a} S. A. Olivares Pino,⁴⁶ D. Oliveira Damazio,²⁵ E. Oliver Garcia,¹⁶⁷ A. Olszewski,³⁹ J. Olszowska,³⁹
 A. Onofre,^{126a,126e} P. U. E. Onyisi,^{31,s} C. J. Oram,^{159a} M. J. Oreglia,³¹ Y. Oren,¹⁵³ D. Orestano,^{134a,134b} N. Orlando,¹⁵⁴
 C. Oropeza Barrera,⁵³ R. S. Orr,¹⁵⁸ B. Osculati,^{50a,50b} R. Ospanov,⁸⁴ G. Otero y Garzon,²⁷ H. Otono,⁷⁰ M. Ouchrif,^{135d}
 F. Ould-Saada,¹¹⁹ A. Ouraou,¹³⁶ K. P. Oussoren,¹⁰⁷ Q. Ouyang,^{33a} A. Ovcharova,¹⁵ M. Owen,⁵³ R. E. Owen,¹⁸
 V. E. Ozcan,^{19a} N. Ozturk,⁸ K. Pachal,¹⁴² A. Pacheco Pages,¹² C. Padilla Aranda,¹² M. Pačáková,⁴⁸ S. Pagan Griso,¹⁵
 E. Paganis,¹³⁹ F. Paige,²⁵ P. Pais,⁸⁶ K. Pajchel,¹¹⁹ G. Palacino,^{159b} S. Palestini,³⁰ M. Palka,^{38b} D. Pallin,³⁴ A. Palma,^{126a,126b}
 Y. B. Pan,¹⁷³ E. Panagiotopoulou,¹⁰ C. E. Pandini,⁸⁰ J. G. Panduro Vazquez,⁷⁷ P. Pani,^{146a,146b} S. Panitkin,²⁵ D. Pantea,^{26a}
 L. Paolozzi,⁴⁹ Th. D. Papadopoulou,¹⁰ K. Papageorgiou,¹⁵⁴ A. Paramonov,⁶ D. Paredes Hernandez,¹⁵⁴ M. A. Parker,²⁸
 K. A. Parker,¹³⁹ F. Parodi,^{50a,50b} J. A. Parsons,³⁵ U. Parzefall,⁴⁸ E. Pasqualucci,^{132a} S. Passaggio,^{50a} F. Pastore,^{134a,134b,a}
 Fr. Pastore,⁷⁷ G. Pásztor,²⁹ S. Patariaia,¹⁷⁵ N. D. Patel,¹⁵⁰ J. R. Pater,⁸⁴ T. Pauly,³⁰ J. Pearce,¹⁶⁹ B. Pearson,¹¹³ L. E. Pedersen,³⁶
 M. Pedersen,¹¹⁹ S. Pedraza Lopez,¹⁶⁷ R. Pedro,^{126a,126b} S. V. Peleganchuk,^{109,d} D. Pelikan,¹⁶⁶ O. Penc,¹²⁷ C. Peng,^{33a}
 H. Peng,^{33b} B. Penning,³¹ J. Penwell,⁶¹ D. V. Perepelitsa,²⁵ E. Perez Codina,^{159a} M. T. Pérez García-Estañá,¹⁶⁷ L. Perini,^{91a,91b}
 H. Pernegger,³⁰ S. Perrella,^{104a,104b} R. Peschke,⁴² V. D. Peshekhonov,⁶⁵ K. Peters,³⁰ R. F. Y. Peters,⁸⁴ B. A. Petersen,³⁰
 T. C. Petersen,³⁶ E. Petit,⁴² A. Petridis,¹ C. Petridou,¹⁵⁴ P. Petroff,¹¹⁷ E. Petrolo,^{132a} F. Petrucci,^{134a,134b} N. E. Pettersson,¹⁵⁷
 R. Pezoa,^{32b} P. W. Phillips,¹³¹ G. Piacquadio,¹⁴³ E. Pianori,¹⁷⁰ A. Picazio,⁴⁹ E. Piccaro,⁷⁶ M. Piccinini,^{20a,20b}
 M. A. Pickering,¹²⁰ R. Piegai,²⁷ D. T. Pignotti,¹¹¹ J. E. Pilcher,³¹ A. D. Pilkington,⁸⁴ J. Pina,^{126a,126b,126d}
 M. Pinamonti,^{164a,164c,ee} J. L. Pinfold,³ A. Pingel,³⁶ S. Pires,⁸⁰ H. Pirumov,⁴² M. Pitt,¹⁷² C. Pizio,^{91a,91b} L. Plazak,^{144a}
 M.-A. Pleier,²⁵ V. Pleskot,¹²⁹ E. Plotnikova,⁶⁵ P. Plucinski,^{146a,146b} D. Pluth,⁶⁴ R. Poettgen,^{146a,146b} L. Poggioli,¹¹⁷ D. Pohl,²¹
 G. Polesello,^{121a} A. Poley,⁴² A. Policicchio,^{37a,37b} R. Polifka,¹⁵⁸ A. Polini,^{20a} C. S. Pollard,⁵³ V. Polychronakos,²⁵
 K. Pommès,³⁰ L. Pontecorvo,^{132a} B. G. Pope,⁹⁰ G. A. Popeneciu,^{26b} D. S. Popovic,¹³ A. Poppleton,³⁰ S. Pospisil,¹²⁸
 K. Potamianos,¹⁵ I. N. Potrap,⁶⁵ C. J. Potter,¹⁴⁹ C. T. Potter,¹¹⁶ G. Poulard,³⁰ J. Poveda,³⁰ V. Pozdnyakov,⁶⁵ P. Pralavorio,⁸⁵
 A. Pranko,¹⁵ S. Prasad,³⁰ S. Prell,⁶⁴ D. Price,⁸⁴ L. E. Price,⁶ M. Primavera,^{73a} S. Prince,⁸⁷ M. Proissl,⁴⁶ K. Prokofiev,^{60c}
 F. Prokoshin,^{32b} E. Protopapadaki,¹³⁶ S. Protopopescu,²⁵ J. Proudfoot,⁶ M. Przybycien,^{38a} E. Ptacek,¹¹⁶ D. Puddu,^{134a,134b}
 E. Pueschel,⁸⁶ D. Puldon,¹⁴⁸ M. Purohit,^{25,ff} P. Puzo,¹¹⁷ J. Qian,⁸⁹ G. Qin,⁵³ Y. Qin,⁸⁴ A. Quadt,⁵⁴ D. R. Quarrie,¹⁵

W. B. Quayle,^{164a,164b} M. Queitsch-Maitland,⁸⁴ D. Quilty,⁵³ S. Raddum,¹¹⁹ V. Radeka,²⁵ V. Radescu,⁴²
 S. K. Radhakrishnan,¹⁴⁸ P. Radloff,¹¹⁶ P. Rados,⁸⁸ F. Ragusa,^{91a,91b} G. Rahal,¹⁷⁸ S. Rajagopalan,²⁵ M. Rammensee,³⁰
 C. Rangel-Smith,¹⁶⁶ F. Rauscher,¹⁰⁰ S. Rave,⁸³ T. Ravenscroft,⁵³ M. Raymond,³⁰ A. L. Read,¹¹⁹ N. P. Readioff,⁷⁴
 D. M. Rebuffi,^{121a,121b} A. Redelbach,¹⁷⁴ G. Redlinger,²⁵ R. Reece,¹³⁷ K. Reeves,⁴¹ L. Rehnisch,¹⁶ J. Reichert,¹²² H. Reisin,²⁷
 M. Relich,¹⁶³ C. Rembser,³⁰ H. Ren,^{33a} A. Renaud,¹¹⁷ M. Rescigno,^{132a} S. Resconi,^{91a} O. L. Rezanova,^{109,d} P. Reznicek,¹²⁹
 R. Rezvani,⁹⁵ R. Richter,¹⁰¹ S. Richter,⁷⁸ E. Richter-Was,^{38b} O. Ricken,²¹ M. Ridel,⁸⁰ P. Rieck,¹⁶ C. J. Riegel,¹⁷⁵ J. Rieger,⁵⁴
 M. Rijssenbeek,¹⁴⁸ A. Rimoldi,^{121a,121b} L. Rinaldi,^{20a} B. Ristić,⁴⁹ E. Ritsch,³⁰ I. Riu,¹² F. Rizatdinova,¹¹⁴ E. Rizvi,⁷⁶
 S. H. Robertson,^{87,1} A. Robichaud-Veronneau,⁸⁷ D. Robinson,²⁸ J. E. M. Robinson,⁴² A. Robson,⁵³ C. Roda,^{124a,124b}
 S. Roe,³⁰ O. Røhne,¹¹⁹ S. Rolli,¹⁶¹ A. Romaniouk,⁹⁸ M. Romano,^{20a,20b} S. M. Romano Saez,³⁴ E. Romero Adam,¹⁶⁷
 N. Rompotis,¹³⁸ M. Ronzani,⁴⁸ L. Roos,⁸⁰ E. Ros,¹⁶⁷ S. Rosati,^{132a} K. Rosbach,⁴⁸ P. Rose,¹³⁷ P. L. Rosendahl,¹⁴
 O. Rosenthal,¹⁴¹ V. Rossetti,^{146a,146b} E. Rossi,^{104a,104b} L. P. Rossi,^{50a} J. H. N. Rosten,²⁸ R. Rosten,¹³⁸ M. Rotaru,^{26a} I. Roth,¹⁷²
 J. Rothberg,¹³⁸ D. Rousseau,¹¹⁷ C. R. Royon,¹³⁶ A. Rozanov,⁸⁵ Y. Rozen,¹⁵² X. Ruan,^{145c} F. Rubbo,¹⁴³ I. Rubinskiy,⁴²
 V. I. Rud,⁹⁹ C. Rudolph,⁴⁴ M. S. Rudolph,¹⁵⁸ F. Rühr,⁴⁸ A. Ruiz-Martinez,³⁰ Z. Rurikova,⁴⁸ N. A. Rusakovich,⁶⁵
 A. Ruschke,¹⁰⁰ H. L. Russell,¹³⁸ J. P. Rutherford,⁷ N. Ruthmann,⁴⁸ Y. F. Ryabov,¹²³ M. Rybar,¹⁶⁵ G. Rybkin,¹¹⁷
 N. C. Ryder,¹²⁰ A. F. Saavedra,¹⁵⁰ G. Sabato,¹⁰⁷ S. Sacerdoti,²⁷ A. Saddique,³ H. F. W. Sadrozinski,¹³⁷ R. Sadykov,⁶⁵
 F. Safai Tehrani,^{132a} M. Sahinsoy,^{58a} M. Saimpert,¹³⁶ T. Saito,¹⁵⁵ H. Sakamoto,¹⁵⁵ Y. Sakurai,¹⁷¹ G. Salamanna,^{134a,134b}
 A. Salamon,^{133a} J. E. Salazar Loyola,^{32b} M. Saleem,¹¹³ D. Salek,¹⁰⁷ P. H. Sales De Bruin,¹³⁸ D. Salihagic,¹⁰¹ A. Salmikov,¹⁴³
 J. Salt,¹⁶⁷ D. Salvatore,^{37a,37b} F. Salvatore,¹⁴⁹ A. Salvucci,^{60a} A. Salzburger,³⁰ D. Sammel,⁴⁸ D. Sampsonidis,¹⁵⁴
 A. Sanchez,^{104a,104b} J. Sánchez,¹⁶⁷ V. Sanchez Martinez,¹⁶⁷ H. Sandaker,¹¹⁹ R. L. Sandbach,⁷⁶ H. G. Sander,⁸³
 M. P. Sanders,¹⁰⁰ M. Sandhoff,¹⁷⁵ C. Sandoval,¹⁶² R. Sandstroem,¹⁰¹ D. P. C. Sankey,¹³¹ M. Sannino,^{50a,50b} A. Sansoni,⁴⁷
 C. Santoni,³⁴ R. Santonico,^{133a,133b} H. Santos,^{126a} I. Santoyo Castillo,¹⁴⁹ K. Sapp,¹²⁵ A. Sapronov,⁶⁵ J. G. Saraiva,^{126a,126d}
 B. Sarrazin,²¹ O. Sasaki,⁶⁶ Y. Sasaki,¹⁵⁵ K. Sato,¹⁶⁰ G. Sauvage,^{5,a} E. Sauvan,⁵ G. Savage,⁷⁷ P. Savard,^{158,e} C. Sawyer,¹³¹
 L. Sawyer,^{79,o} J. Saxon,³¹ C. Sbarra,^{20a} A. Sbrizzi,^{20a,20b} T. Scanlon,⁷⁸ D. A. Scannicchio,¹⁶³ M. Scarcella,¹⁵⁰
 V. Scarfone,^{37a,37b} J. Schaarschmidt,¹⁷² P. Schacht,¹⁰¹ D. Schaefer,³⁰ R. Schaefer,⁴² J. Schaeffer,⁸³ S. Schaepe,²¹
 S. Schaezel,^{58b} U. Schäfer,⁸³ A. C. Schaffer,¹¹⁷ D. Schaile,¹⁰⁰ R. D. Schamberger,¹⁴⁸ V. Scharf,^{58a} V. A. Schegelsky,¹²³
 D. Scheirich,¹²⁹ M. Schernau,¹⁶³ C. Schiavi,^{50a,50b} C. Schillo,⁴⁸ M. Schioppa,^{37a,37b} S. Schlenker,³⁰ K. Schmieden,³⁰
 C. Schmitt,⁸³ S. Schmitt,^{58b} S. Schmitt,⁴² B. Schneider,^{159a} Y. J. Schnellbach,⁷⁴ U. Schnoor,⁴⁴ L. Schoeffel,¹³⁶
 A. Schoening,^{58b} B. D. Schoenrock,⁹⁰ E. Schopf,²¹ A. L. S. Schorlemmer,⁵⁴ M. Schott,⁸³ D. Schouten,^{159a} J. Schovancova,⁸
 S. Schramm,⁴⁹ M. Schreyer,¹⁷⁴ C. Schroeder,⁸³ N. Schuh,⁸³ M. J. Schultens,²¹ H.-C. Schultz-Coulon,^{58a} H. Schulz,¹⁶
 M. Schumacher,⁴⁸ B. A. Schumm,¹³⁷ Ph. Schune,¹³⁶ C. Schwanenberger,⁸⁴ A. Schwartzman,¹⁴³ T. A. Schwarz,⁸⁹
 Ph. Schwegler,¹⁰¹ H. Schweiger,⁸⁴ Ph. Schwemling,¹³⁶ R. Schwienhorst,⁹⁰ J. Schwindling,¹³⁶ T. Schwindt,²¹ F. G. Sciacca,¹⁷
 E. Scifo,¹¹⁷ G. Sciolla,²³ F. Scuri,^{124a,124b} F. Scutti,²¹ J. Searcy,⁸⁹ G. Sedov,⁴² E. Sedykh,¹²³ P. Seema,²¹ S. C. Seidel,¹⁰⁵
 A. Seiden,¹³⁷ F. Seifert,¹²⁸ J. M. Seixas,^{24a} G. Sekhniaidze,^{104a} K. Sekhon,⁸⁹ S. J. Sekula,⁴⁰ D. M. Seliverstov,^{123,a}
 N. Semprini-Cesari,^{20a,20b} C. Serfon,³⁰ L. Serin,¹¹⁷ L. Serkin,^{164a,164b} T. Serre,⁸⁵ M. Sessa,^{134a,134b} R. Seuster,^{159a}
 H. Severini,¹¹³ T. Sfiligoi,⁷⁵ F. Sforza,³⁰ A. Sfyrla,³⁰ E. Shabalina,⁵⁴ M. Shamim,¹¹⁶ L. Y. Shan,^{33a} R. Shang,¹⁶⁵ J. T. Shank,²²
 M. Shapiro,¹⁵ P. B. Shatalov,⁹⁷ K. Shaw,^{164a,164b} S. M. Shaw,⁸⁴ A. Shcherbakova,^{146a,146b} C. Y. Shehu,¹⁴⁹ P. Sherwood,⁷⁸
 L. Shi,^{151,gg} S. Shimizu,⁶⁷ C. O. Shimmin,¹⁶³ M. Shimojima,¹⁰² M. Shiyakova,⁶⁵ A. Shmeleva,⁹⁶ D. Shoaleh Saadi,⁹⁵
 M. J. Shochet,³¹ S. Shojaii,^{91a,91b} S. Shrestha,¹¹¹ E. Shulga,⁹⁸ M. A. Shupe,⁷ S. Shushkevich,⁴² P. Sicho,¹²⁷ P. E. Sidebo,¹⁴⁷
 O. Sidiropoulou,¹⁷⁴ D. Sidorov,¹¹⁴ A. Sidoti,^{20a,20b} F. Siegert,⁴⁴ Dj. Sijacki,¹³ J. Silva,^{126a,126d} Y. Silver,¹⁵³
 S. B. Silverstein,^{146a} V. Simak,¹²⁸ O. Simard,⁵ Lj. Simic,¹³ S. Simion,¹¹⁷ E. Simioni,⁸³ B. Simmons,⁷⁸ D. Simon,³⁴
 R. Simoniello,^{91a,91b} P. Sinervo,¹⁵⁸ N. B. Sinev,¹¹⁶ M. Sioli,^{20a,20b} G. Siragusa,¹⁷⁴ A. N. Sisakyan,^{65,a} S. Yu. Sivoklokov,⁹⁹
 J. Sjölin,^{146a,146b} T. B. Sjursen,¹⁴ M. B. Skinner,⁷² H. P. Skottowe,⁵⁷ P. Skubic,¹¹³ M. Slater,¹⁸ T. Slavicek,¹²⁸
 M. Slawinska,¹⁰⁷ K. Sliwa,¹⁶¹ V. Smakhtin,¹⁷² B. H. Smart,⁴⁶ L. Smestad,¹⁴ S. Yu. Smirnov,⁹⁸ Y. Smirnov,⁹⁸
 L. N. Smirnova,^{99,hh} O. Smirnova,⁸¹ M. N. K. Smith,³⁵ R. W. Smith,³⁵ M. Smizanska,⁷² K. Smolek,¹²⁸ A. A. Snesarev,⁹⁶
 G. Snidero,⁷⁶ S. Snyder,²⁵ R. Sobie,^{169,l} F. Socher,⁴⁴ A. Soffer,¹⁵³ D. A. Soh,^{151,gg} G. Sokhrannyi,⁷⁵ C. A. Solans,³⁰
 M. Solar,¹²⁸ J. Solc,¹²⁸ E. Yu. Soldatov,⁹⁸ U. Soldevila,¹⁶⁷ A. A. Solodkov,¹³⁰ A. Soloshenko,⁶⁵ O. V. Solovyanov,¹³⁰
 V. Solovyev,¹²³ P. Sommer,⁴⁸ H. Y. Song,^{33b} N. Soni,¹ A. Sood,¹⁵ A. Sopczak,¹²⁸ B. Sopko,¹²⁸ V. Sopko,¹²⁸ V. Sorin,¹²
 D. Sosa,^{58b} M. Sosebee,⁸ C. L. Sotiropoulou,^{124a,124b} R. Soualah,^{164a,164c} A. M. Soukharev,^{109,d} D. South,⁴² B. C. Sowden,⁷⁷
 S. Spagnolo,^{73a,73b} M. Spalla,^{124a,124b} M. Spangenberg,¹⁷⁰ F. Spanò,⁷⁷ W. R. Spearman,⁵⁷ D. Sperlich,¹⁶ F. Spettel,¹⁰¹

R. Spighi,^{20a} G. Spigo,³⁰ L. A. Spiller,⁸⁸ M. Spousta,¹²⁹ T. Spreitzer,¹⁵⁸ R. D. St. Denis,^{53,a} S. Staerz,⁴⁴ J. Stahlman,¹²² R. Stamen,^{58a} S. Stamm,¹⁶ E. Stanecka,³⁹ C. Stancu,^{134a} M. Stancu-Bellu,⁴² M. M. Stanitzki,⁴² S. Stapnes,¹¹⁹ E. A. Starchenko,¹³⁰ J. Stark,⁵⁵ P. Staroba,¹²⁷ P. Starovoitov,^{58a} R. Staszewski,³⁹ P. Stavina,^{144a,a} P. Steinberg,²⁵ B. Stelzer,¹⁴² H. J. Stelzer,³⁰ O. Stelzer-Chilton,^{159a} H. Stenzel,⁵² G. A. Stewart,⁵³ J. A. Stillings,²¹ M. C. Stockton,⁸⁷ M. Stoebe,⁸⁷ G. Stoicea,^{26a} P. Stolte,⁵⁴ S. Stonjek,¹⁰¹ A. R. Stradling,⁸ A. Straessner,⁴⁴ M. E. Stramaglia,¹⁷ J. Strandberg,¹⁴⁷ S. Strandberg,^{146a,146b} A. Strandlie,¹¹⁹ E. Strauss,¹⁴³ M. Strauss,¹¹³ P. Strizenec,^{144b} R. Ströhmer,¹⁷⁴ D. M. Strom,¹¹⁶ R. Stroynowski,⁴⁰ A. Strubig,¹⁰⁶ S. A. Stucci,¹⁷ B. Stugu,¹⁴ N. A. Styles,⁴² D. Su,¹⁴³ J. Su,¹²⁵ R. Subramaniam,⁷⁹ A. Succurro,¹² Y. Sugaya,¹¹⁸ C. Suhr,¹⁰⁸ M. Suk,¹²⁸ V. V. Sulin,⁹⁶ S. Sultansoy,^{4c} T. Sumida,⁶⁸ S. Sun,⁵⁷ X. Sun,^{33a} J. E. Sundermann,⁴⁸ K. Suruliz,¹⁴⁹ G. Susinno,^{37a,37b} M. R. Sutton,¹⁴⁹ S. Suzuki,⁶⁶ M. Svatos,¹²⁷ M. Swiatlowski,¹⁴³ I. Sykora,^{144a} T. Sykora,¹²⁹ D. Ta,⁹⁰ C. Taccini,^{134a,134b} K. Tackmann,⁴² J. Taenzer,¹⁵⁸ A. Taffard,¹⁶³ R. Tafirout,^{159a} N. Taiblum,¹⁵³ H. Takai,²⁵ R. Takashima,⁶⁹ H. Takeda,⁶⁷ T. Takeshita,¹⁴⁰ Y. Takubo,⁶⁶ M. Talby,⁸⁵ A. A. Talyshv,^{109,d} J. Y. C. Tam,¹⁷⁴ K. G. Tan,⁸⁸ J. Tanaka,¹⁵⁵ R. Tanaka,¹¹⁷ S. Tanaka,⁶⁶ B. B. Tannenwald,¹¹¹ N. Tannoury,²¹ S. Tapprogge,⁸³ S. Tarem,¹⁵² F. Tarrade,²⁹ G. F. Tartarelli,^{91a} P. Tas,¹²⁹ M. Tasevsky,¹²⁷ T. Tashiro,⁶⁸ E. Tassi,^{37a,37b} A. Tavares Delgado,^{126a,126b} Y. Tayalati,^{135d} F. E. Taylor,⁹⁴ G. N. Taylor,⁸⁸ W. Taylor,^{159b} F. A. Teischinger,³⁰ M. Teixeira Dias Castanheira,⁷⁶ P. Teixeira-Dias,⁷⁷ K. K. Temming,⁴⁸ D. Temple,¹⁴² H. Ten Kate,³⁰ P. K. Teng,¹⁵¹ J. J. Teoh,¹¹⁸ F. Tepel,¹⁷⁵ S. Terada,⁶⁶ K. Terashi,¹⁵⁵ J. Terron,⁸² S. Terzo,¹⁰¹ M. Testa,⁴⁷ R. J. Teuscher,^{158,l} T. Thevenaux-Pelzer,³⁴ J. P. Thomas,¹⁸ J. Thomas-Wilsker,⁷⁷ E. N. Thompson,³⁵ P. D. Thompson,¹⁸ R. J. Thompson,⁸⁴ A. S. Thompson,⁵³ L. A. Thomsen,¹⁷⁶ E. Thomson,¹²² M. Thomson,²⁸ R. P. Thun,^{89,a} M. J. Tibbetts,¹⁵ R. E. Tiede Torres,⁸⁵ V. O. Tikhomirov,^{96,ii} Yu. A. Tikhonov,^{109,d} S. Timoshenko,⁹⁸ E. Tiouchichine,⁸⁵ P. Tipton,¹⁷⁶ S. Tisserant,⁸⁵ K. Todome,¹⁵⁷ T. Todorov,⁵ S. Todorova-Nova,¹²⁹ J. Tojo,⁷⁰ S. Tokár,^{144a} K. Tokushuku,⁶⁶ K. Tollefson,⁹⁰ E. Tolley,⁵⁷ L. Tomlinson,⁸⁴ M. Tomoto,¹⁰³ L. Tompkins,^{143,ij} K. Toms,¹⁰⁵ E. Torrence,¹¹⁶ H. Torres,¹⁴² E. Torró Pastor,¹³⁸ J. Toth,^{85,kk} F. Touchard,⁸⁵ D. R. Tovey,¹³⁹ T. Trefzger,¹⁷⁴ L. Tremblet,³⁰ A. Tricoli,³⁰ I. M. Trigger,^{159a} S. Trincaz-Duvoid,⁸⁰ M. F. Tripania,¹² W. Trischuk,¹⁵⁸ B. Trocmé,⁵⁵ C. Troncon,^{91a} M. Trotter-McDonald,¹⁵ M. Trovatelli,¹⁶⁹ P. True,⁹⁰ L. Truong,^{164a,164c} M. Trzebinski,³⁹ A. Trzupek,³⁹ C. Tsarouchas,³⁰ J. C-L. Tseng,¹²⁰ P. V. Tsiarehka,⁹² D. Tsonou,¹⁵⁴ G. Tsipolitis,¹⁰ N. Tsirintanis,⁹ S. Tsiskaridze,¹² V. Tsiskaridze,⁴⁸ E. G. Tskhadadze,^{51a} I. I. Tsukerman,⁹⁷ V. Tsulaia,¹⁵ S. Tsuno,⁶⁶ D. Tsybychev,¹⁴⁸ A. Tudorache,^{26a} V. Tudorache,^{26a} A. N. Tuna,⁵⁷ S. A. Tuppuri,^{20a,20b} S. Turchikhin,^{99,hh} D. Turecek,¹²⁸ R. Turra,^{91a,91b} A. J. Turvey,⁴⁰ P. M. Tuts,³⁵ A. Tykhonov,⁴⁹ M. Tylmad,^{146a,146b} M. Tyndel,¹³¹ I. Ueda,¹⁵⁵ R. Ueno,²⁹ M. Ughetto,^{146a,146b} M. Ugland,¹⁴ F. Ukegawa,¹⁶⁰ G. Unal,³⁰ A. Undrus,²⁵ G. Unel,¹⁶³ F. C. Ungaro,⁴⁸ Y. Unno,⁶⁶ C. Unverdorben,¹⁰⁰ J. Urban,^{144b} P. Urquijo,⁸⁸ P. Urrejola,⁸³ G. Usai,⁸ A. Usanova,⁶² L. Vacavant,⁸⁵ V. Vacek,¹²⁸ B. Vachon,⁸⁷ C. Valderanis,⁸³ N. Valencic,¹⁰⁷ S. Valentinetti,^{20a,20b} A. Valero,¹⁶⁷ L. Valery,¹² S. Valkar,¹²⁹ E. Valladolid Gallego,¹⁶⁷ S. Vallecorsa,⁴⁹ J. A. Valls Ferrer,¹⁶⁷ W. Van Den Wollenberg,¹⁰⁷ P. C. Van Der Deijl,¹⁰⁷ R. van der Geer,¹⁰⁷ H. van der Graaf,¹⁰⁷ N. van Eldik,¹⁵² P. van Gemmeren,⁶ J. Van Nieuwkoop,¹⁴² I. van Vulpen,¹⁰⁷ M. C. van Woerden,³⁰ M. Vanadia,^{132a,132b} W. Vandelli,³⁰ R. Vanguri,¹²² A. Vaniachine,⁶ F. Vannucci,⁸⁰ G. Vardanyan,¹⁷⁷ R. Vari,^{132a} E. W. Varnes,⁷ T. Varol,⁴⁰ D. Varouchas,⁸⁰ A. Vartapetian,⁸ K. E. Varvell,¹⁵⁰ F. Vazeille,³⁴ T. Vazquez Schroeder,⁸⁷ J. Veatch,⁷ L. M. Veloce,¹⁵⁸ F. Veloso,^{126a,126c} T. Velz,²¹ S. Veneziano,^{132a} A. Ventura,^{73a,73b} D. Ventura,⁸⁶ M. Venturi,¹⁶⁹ N. Venturi,¹⁵⁸ A. Venturini,²³ V. Vercesi,^{121a} M. Verducci,^{132a,132b} W. Verkerke,¹⁰⁷ J. C. Vermeulen,¹⁰⁷ A. Vest,⁴⁴ M. C. Vetterli,^{142,e} O. Viazlo,⁸¹ I. Vichou,¹⁶⁵ T. Vickey,¹³⁹ O. E. Vickey Boeriu,¹³⁹ G. H. A. Viehhauser,¹²⁰ S. Viel,¹⁵ R. Vigne,⁶² M. Villa,^{20a,20b} M. Villaplana Perez,^{91a,91b} E. Vilucchi,⁴⁷ M. G. Vinciter,²⁹ V. B. Vinogradov,⁶⁵ I. Vivarelli,¹⁴⁹ F. Vives Vaque,³ S. Vlachos,¹⁰ D. Vladoiu,¹⁰⁰ M. Vlasak,¹²⁸ M. Vogel,^{32a} P. Vokac,¹²⁸ G. Volpi,^{124a,124b} M. Volpi,⁸⁸ H. von der Schmitt,¹⁰¹ H. von Radziewski,⁴⁸ E. von Toerne,²¹ V. Vorobel,¹²⁹ K. Vorobev,⁹⁸ M. Vos,¹⁶⁷ R. Voss,³⁰ J. H. Vosseveld,⁷⁴ N. Vranjes,¹³ M. Vranjes Milosavljevic,¹³ V. Vrba,¹²⁷ M. Vreeswijk,¹⁰⁷ R. Vuillermet,³⁰ I. Vukotic,³¹ Z. Vykydal,¹²⁸ P. Wagner,²¹ W. Wagner,¹⁷⁵ H. Wahlberg,⁷¹ S. Wahrmund,⁴⁴ J. Wakabayashi,¹⁰³ J. Walder,⁷² R. Walker,¹⁰⁰ W. Walkowiak,¹⁴¹ C. Wang,¹⁵¹ F. Wang,¹⁷³ H. Wang,¹⁵ H. Wang,⁴⁰ J. Wang,⁴² J. Wang,^{33a} K. Wang,⁸⁷ R. Wang,⁶ S. M. Wang,¹⁵¹ T. Wang,²¹ T. Wang,³⁵ X. Wang,¹⁷⁶ C. Wanotayaroj,¹¹⁶ A. Warburton,⁸⁷ C. P. Ward,²⁸ D. R. Wardrope,⁷⁸ A. Washbrook,⁴⁶ C. Wasicki,⁴² P. M. Watkins,¹⁸ A. T. Watson,¹⁸ I. J. Watson,¹⁵⁰ M. F. Watson,¹⁸ G. Watts,¹³⁸ S. Watts,⁸⁴ B. M. Waugh,⁷⁸ S. Webb,⁸⁴ M. S. Weber,¹⁷ S. W. Weber,¹⁷⁴ J. S. Webster,³¹ A. R. Weidberg,¹²⁰ B. Weinert,⁶¹ J. Weingarten,⁵⁴ C. Weiser,⁴⁸ H. Weits,¹⁰⁷ P. S. Wells,³⁰ T. Wenaus,²⁵ T. Wengler,³⁰ S. Wenig,³⁰ N. Wermes,²¹ M. Werner,⁴⁸ P. Werner,³⁰ M. Wessels,^{58a} J. Wetter,¹⁶¹ K. Whalen,¹¹⁶ A. M. Wharton,⁷² A. White,⁸ M. J. White,¹ R. White,^{32b} S. White,^{124a,124b} D. Whiteson,¹⁶³ F. J. Wickens,¹³¹ W. Wiedenmann,¹⁷³ M. Wielers,¹³¹ P. Wienemann,²¹ C. Wiglesworth,³⁶

L. A. M. Wiik-Fuchs,²¹ A. Wildauer,¹⁰¹ H. G. Wilkens,³⁰ H. H. Williams,¹²² S. Williams,¹⁰⁷ C. Willis,⁹⁰ S. Willocq,⁸⁶ A. Wilson,⁸⁹ J. A. Wilson,¹⁸ I. Wingerter-Seez,⁵ F. Winklmeier,¹¹⁶ B. T. Winter,²¹ M. Wittgen,¹⁴³ J. Wittkowski,¹⁰⁰ S. J. Wollstadt,⁸³ M. W. Wolter,³⁹ H. Wolters,^{126a,126c} B. K. Wosiek,³⁹ J. Wotschack,³⁰ M. J. Woudstra,⁸⁴ K. W. Wozniak,³⁹ M. Wu,⁵⁵ M. Wu,³¹ S. L. Wu,¹⁷³ X. Wu,⁴⁹ Y. Wu,⁸⁹ T. R. Wyatt,⁸⁴ B. M. Wynne,⁴⁶ S. Xella,³⁶ D. Xu,^{33a} L. Xu,²⁵ B. Yabsley,¹⁵⁰ S. Yacoob,^{145a} R. Yakabe,⁶⁷ M. Yamada,⁶⁶ D. Yamaguchi,¹⁵⁷ Y. Yamaguchi,¹¹⁸ A. Yamamoto,⁶⁶ S. Yamamoto,¹⁵⁵ T. Yamanaka,¹⁵⁵ K. Yamauchi,¹⁰³ Y. Yamazaki,⁶⁷ Z. Yan,²² H. Yang,^{33e} H. Yang,¹⁷³ Y. Yang,¹⁵¹ W.-M. Yao,¹⁵ Y. Yasu,⁶⁶ E. Yatsenko,⁵ K. H. Yau Wong,²¹ J. Ye,⁴⁰ S. Ye,²⁵ I. Yeletsikh,⁶⁵ A. L. Yen,⁵⁷ E. Yildirim,⁴² K. Yorita,¹⁷¹ R. Yoshida,⁶ K. Yoshihara,¹²² C. Young,¹⁴³ C. J. S. Young,³⁰ S. Youssef,²² D. R. Yu,¹⁵ J. Yu,⁸ J. M. Yu,⁸⁹ J. Yu,¹¹⁴ L. Yuan,⁶⁷ S. P. Y. Yuen,²¹ A. Yurkewicz,¹⁰⁸ I. Yusuff,^{28,11} B. Zabinski,³⁹ R. Zaidan,⁶³ A. M. Zaitsev,^{130,cc} J. Zalieckas,¹⁴ A. Zaman,¹⁴⁸ S. Zambito,⁵⁷ L. Zanello,^{132a,132b} D. Zanzi,⁸⁸ C. Zeitnitz,¹⁷⁵ M. Zeman,¹²⁸ A. Zemla,^{38a} Q. Zeng,¹⁴³ K. Zengel,²³ O. Zenin,¹³⁰ T. Ženiš,^{144a} D. Zerwas,¹¹⁷ D. Zhang,⁸⁹ F. Zhang,¹⁷³ H. Zhang,^{33c} J. Zhang,⁶ L. Zhang,⁴⁸ R. Zhang,^{33b} X. Zhang,^{33d} Z. Zhang,¹¹⁷ X. Zhao,⁴⁰ Y. Zhao,^{33d,117} Z. Zhao,^{33b} A. Zhemchugov,⁶⁵ J. Zhong,¹²⁰ B. Zhou,⁸⁹ C. Zhou,⁴⁵ L. Zhou,³⁵ L. Zhou,⁴⁰ N. Zhou,^{33f} C. G. Zhu,^{33d} H. Zhu,^{33a} J. Zhu,⁸⁹ Y. Zhu,^{33b} X. Zhuang,^{33a} K. Zhukov,⁹⁶ A. Zibell,¹⁷⁴ D. Zieminska,⁶¹ N. I. Zimine,⁶⁵ C. Zimmermann,⁸³ S. Zimmermann,⁴⁸ Z. Zinonos,⁵⁴ M. Zinser,⁸³ M. Ziolkowski,¹⁴¹ L. Živković,¹³ G. Zobernig,¹⁷³ A. Zoccoli,^{20a,20b} M. zur Nedden,¹⁶ G. Zurzolo,^{104a,104b} and L. Zwalinski³⁰

(ATLAS Collaboration)

¹*Department of Physics, University of Adelaide, Adelaide, Australia*

²*Physics Department, SUNY Albany, Albany, New York, USA*

³*Department of Physics, University of Alberta, Edmonton AB, Canada*

^{4a}*Department of Physics, Ankara University, Ankara, Turkey*

^{4b}*Istanbul Aydin University, Istanbul, Turkey*

^{4c}*Division of Physics, TOBB University of Economics and Technology, Ankara, Turkey*

⁵*LAPP, CNRS/IN2P3 and Université Savoie Mont Blanc, Annecy-le-Vieux, France*

⁶*High Energy Physics Division, Argonne National Laboratory, Argonne, Illinois, USA*

⁷*Department of Physics, University of Arizona, Tucson, Arizona, USA*

⁸*Department of Physics, The University of Texas at Arlington, Arlington, Texas, USA*

⁹*Physics Department, University of Athens, Athens, Greece*

¹⁰*Physics Department, National Technical University of Athens, Zografou, Greece*

¹¹*Institute of Physics, Azerbaijan Academy of Sciences, Baku, Azerbaijan*

¹²*Institut de Física d'Altes Energies and Departament de Física de la Universitat Autònoma de Barcelona, Barcelona, Spain*

¹³*Institute of Physics, University of Belgrade, Belgrade, Serbia*

¹⁴*Department for Physics and Technology, University of Bergen, Bergen, Norway*

¹⁵*Physics Division, Lawrence Berkeley National Laboratory and University of California, Berkeley, California, USA*

¹⁶*Department of Physics, Humboldt University, Berlin, Germany*

¹⁷*Albert Einstein Center for Fundamental Physics and Laboratory for High Energy Physics, University of Bern, Bern, Switzerland*

¹⁸*School of Physics and Astronomy, University of Birmingham, Birmingham, United Kingdom*

^{19a}*Department of Physics, Bogazici University, Istanbul, Turkey*

^{19b}*Department of Physics Engineering, Gaziantep University, Gaziantep, Turkey*

^{19c}*Department of Physics, Dogus University, Istanbul, Turkey*

^{20a}*INFN Sezione di Bologna, Italy*

^{20b}*Dipartimento di Fisica e Astronomia, Università di Bologna, Bologna, Italy*

²¹*Physikalisches Institut, University of Bonn, Bonn, Germany*

²²*Department of Physics, Boston University, Boston, Massachusetts, USA*

²³*Department of Physics, Brandeis University, Waltham, Massachusetts, USA*

^{24a}*Universidade Federal do Rio De Janeiro COPPE/EE/IF, Rio de Janeiro, Brazil*

^{24b}*Electrical Circuits Department, Federal University of Juiz de Fora (UFJF), Juiz de Fora, Brazil*

^{24c}*Federal University of Sao Joao del Rei (UFSJ), Sao Joao del Rei, Brazil*

^{24d}*Instituto de Física, Universidade de Sao Paulo, Sao Paulo, Brazil*

²⁵*Physics Department, Brookhaven National Laboratory, Upton, New York, USA*

²⁶*National Institute of Physics and Nuclear Engineering, Bucharest, Romania*

- ^{26b}*National Institute for Research and Development of Isotopic and Molecular Technologies, Physics Department, Cluj Napoca, Romania*
- ^{26c}*University Politehnica Bucharest, Bucharest, Romania*
- ^{26d}*West University in Timisoara, Timisoara, Romania*
- ²⁷*Departamento de Física, Universidad de Buenos Aires, Buenos Aires, Argentina*
- ²⁸*Cavendish Laboratory, University of Cambridge, Cambridge, United Kingdom*
- ²⁹*Department of Physics, Carleton University, Ottawa, ON, Canada*
- ³⁰*CERN, Geneva, Switzerland*
- ³¹*Enrico Fermi Institute, University of Chicago, Chicago, Illinois, USA*
- ^{32a}*Departamento de Física, Pontificia Universidad Católica de Chile, Santiago, Chile*
- ^{32b}*Departamento de Física, Universidad Técnica Federico Santa María, Valparaíso, Chile*
- ^{33a}*Institute of High Energy Physics, Chinese Academy of Sciences, Beijing, China*
- ^{33b}*Department of Modern Physics, University of Science and Technology of China, Anhui, China*
- ^{33c}*Department of Physics, Nanjing University, Jiangsu, China*
- ^{33d}*School of Physics, Shandong University, Shandong, China*
- ^{33e}*Department of Physics and Astronomy, Shanghai Key Laboratory for Particle Physics and Cosmology, Shanghai Jiao Tong University, Shanghai, China*
- ^{33f}*Physics Department, Tsinghua University, Beijing 100084, China*
- ³⁴*Laboratoire de Physique Corpusculaire, Clermont Université and Université Blaise Pascal and CNRS/IN2P3, Clermont-Ferrand, France*
- ³⁵*Nevis Laboratory, Columbia University, Irvington, New York, USA*
- ³⁶*Niels Bohr Institute, University of Copenhagen, Kobenhavn, Denmark*
- ^{37a}*INFN Gruppo Collegato di Cosenza, Laboratori Nazionali di Frascati, Italy*
- ^{37b}*Dipartimento di Fisica, Università della Calabria, Rende, Italy*
- ^{38a}*AGH University of Science and Technology, Faculty of Physics and Applied Computer Science, Krakow, Poland*
- ^{38b}*Marian Smoluchowski Institute of Physics, Jagiellonian University, Krakow, Poland*
- ³⁹*Institute of Nuclear Physics Polish Academy of Sciences, Krakow, Poland*
- ⁴⁰*Physics Department, Southern Methodist University, Dallas, Texas, USA*
- ⁴¹*Physics Department, University of Texas at Dallas, Richardson, Texas, USA*
- ⁴²*DESY, Hamburg and Zeuthen, Germany*
- ⁴³*Institut für Experimentelle Physik IV, Technische Universität Dortmund, Dortmund, Germany*
- ⁴⁴*Institut für Kern- und Teilchenphysik, Technische Universität Dresden, Dresden, Germany*
- ⁴⁵*Department of Physics, Duke University, Durham, North Carolina, USA*
- ⁴⁶*SUPA - School of Physics and Astronomy, University of Edinburgh, Edinburgh, United Kingdom*
- ⁴⁷*INFN Laboratori Nazionali di Frascati, Frascati, Italy*
- ⁴⁸*Fakultät für Mathematik und Physik, Albert-Ludwigs-Universität, Freiburg, Germany*
- ⁴⁹*Section de Physique, Université de Genève, Geneva, Switzerland*
- ^{50a}*INFN Sezione di Genova, Italy*
- ^{50b}*Dipartimento di Fisica, Università di Genova, Genova, Italy*
- ^{51a}*E. Andronikashvili Institute of Physics, Iv. Javakhishvili Tbilisi State University, Tbilisi, Georgia*
- ^{51b}*High Energy Physics Institute, Tbilisi State University, Tbilisi, Georgia*
- ⁵²*II Physikalisches Institut, Justus-Liebig-Universität Giessen, Giessen, Germany*
- ⁵³*SUPA - School of Physics and Astronomy, University of Glasgow, Glasgow, United Kingdom*
- ⁵⁴*II Physikalisches Institut, Georg-August-Universität, Göttingen, Germany*
- ⁵⁵*Laboratoire de Physique Subatomique et de Cosmologie, Université Grenoble-Alpes, CNRS/IN2P3, Grenoble, France*
- ⁵⁶*Department of Physics, Hampton University, Hampton, Virginia, USA*
- ⁵⁷*Laboratory for Particle Physics and Cosmology, Harvard University, Cambridge, Massachusetts, USA*
- ^{58a}*Kirchhoff-Institut für Physik, Ruprecht-Karls-Universität Heidelberg, Heidelberg, Germany*
- ^{58b}*Physikalisches Institut, Ruprecht-Karls-Universität Heidelberg, Heidelberg, Germany*
- ^{58c}*ZITI Institut für technische Informatik, Ruprecht-Karls-Universität Heidelberg, Mannheim, Germany*
- ⁵⁹*Faculty of Applied Information Science, Hiroshima Institute of Technology, Hiroshima, Japan*
- ^{60a}*Department of Physics, The Chinese University of Hong Kong, Shatin, N.T., Hong Kong, China*
- ^{60b}*Department of Physics, The University of Hong Kong, Hong Kong, China*
- ^{60c}*Department of Physics, The Hong Kong University of Science and Technology, Clear Water Bay, Kowloon, Hong Kong, China*
- ⁶¹*Department of Physics, Indiana University, Bloomington, Indiana, USA*
- ⁶²*Institut für Astro- und Teilchenphysik, Leopold-Franzens-Universität, Innsbruck, Austria*

- ⁶³*University of Iowa, Iowa City, Iowa, USA*
- ⁶⁴*Department of Physics and Astronomy, Iowa State University, Ames, Iowa, USA*
- ⁶⁵*Joint Institute for Nuclear Research, JINR Dubna, Dubna, Russia*
- ⁶⁶*KEK, High Energy Accelerator Research Organization, Tsukuba, Japan*
- ⁶⁷*Graduate School of Science, Kobe University, Kobe, Japan*
- ⁶⁸*Faculty of Science, Kyoto University, Kyoto, Japan*
- ⁶⁹*Kyoto University of Education, Kyoto, Japan*
- ⁷⁰*Department of Physics, Kyushu University, Fukuoka, Japan*
- ⁷¹*Instituto de Física La Plata, Universidad Nacional de La Plata and CONICET, La Plata, Argentina*
- ⁷²*Physics Department, Lancaster University, Lancaster, United Kingdom*
- ^{73a}*INFN Sezione di Lecce, Italy*
- ^{73b}*Dipartimento di Matematica e Fisica, Università del Salento, Lecce, Italy*
- ⁷⁴*Oliver Lodge Laboratory, University of Liverpool, Liverpool, United Kingdom*
- ⁷⁵*Department of Physics, Jožef Stefan Institute and University of Ljubljana, Ljubljana, Slovenia*
- ⁷⁶*School of Physics and Astronomy, Queen Mary University of London, London, United Kingdom*
- ⁷⁷*Department of Physics, Royal Holloway University of London, Surrey, United Kingdom*
- ⁷⁸*Department of Physics and Astronomy, University College London, London, United Kingdom*
- ⁷⁹*Louisiana Tech University, Ruston, Louisiana, USA*
- ⁸⁰*Laboratoire de Physique Nucléaire et de Hautes Energies, UPMC and Université Paris-Diderot and CNRS/IN2P3, Paris, France*
- ⁸¹*Fysiska institutionen, Lunds universitet, Lund, Sweden*
- ⁸²*Departamento de Física Teórica C-15, Universidad Autónoma de Madrid, Madrid, Spain*
- ⁸³*Institut für Physik, Universität Mainz, Mainz, Germany*
- ⁸⁴*School of Physics and Astronomy, University of Manchester, Manchester, United Kingdom*
- ⁸⁵*CPPM, Aix-Marseille Université and CNRS/IN2P3, Marseille, France*
- ⁸⁶*Department of Physics, University of Massachusetts, Amherst, Massachusetts, USA*
- ⁸⁷*Department of Physics, McGill University, Montreal, QC, Canada*
- ⁸⁸*School of Physics, University of Melbourne, Victoria, Australia*
- ⁸⁹*Department of Physics, The University of Michigan, Ann Arbor, Michigan, USA*
- ⁹⁰*Department of Physics and Astronomy, Michigan State University, East Lansing, Michigan, USA*
- ^{91a}*INFN Sezione di Milano, Italy*
- ^{91b}*Dipartimento di Fisica, Università di Milano, Milano, Italy*
- ⁹²*B.I. Stepanov Institute of Physics, National Academy of Sciences of Belarus, Minsk, Republic of Belarus*
- ⁹³*National Scientific and Educational Centre for Particle and High Energy Physics, Minsk, Republic of Belarus*
- ⁹⁴*Department of Physics, Massachusetts Institute of Technology, Cambridge, Massachusetts, USA*
- ⁹⁵*Group of Particle Physics, University of Montreal, Montreal, QC, Canada*
- ⁹⁶*P.N. Lebedev Institute of Physics, Academy of Sciences, Moscow, Russia*
- ⁹⁷*Institute for Theoretical and Experimental Physics (ITEP), Moscow, Russia*
- ⁹⁸*National Research Nuclear University MEPhI, Moscow, Russia*
- ⁹⁹*D.V. Skobel'syn Institute of Nuclear Physics, M.V. Lomonosov Moscow State University, Moscow, Russia*
- ¹⁰⁰*Fakultät für Physik, Ludwig-Maximilians-Universität München, München, Germany*
- ¹⁰¹*Max-Planck-Institut für Physik (Werner-Heisenberg-Institut), München, Germany*
- ¹⁰²*Nagasaki Institute of Applied Science, Nagasaki, Japan*
- ¹⁰³*Graduate School of Science and Kobayashi-Maskawa Institute, Nagoya University, Nagoya, Japan*
- ^{104a}*INFN Sezione di Napoli, Italy*
- ^{104b}*Dipartimento di Fisica, Università di Napoli, Napoli, Italy*
- ¹⁰⁵*Department of Physics and Astronomy, University of New Mexico, Albuquerque, North Mexico, USA*
- ¹⁰⁶*Institute for Mathematics, Astrophysics and Particle Physics, Radboud University Nijmegen/Nikhef, Nijmegen, Netherlands*
- ¹⁰⁷*Nikhef National Institute for Subatomic Physics and University of Amsterdam, Amsterdam, Netherlands*
- ¹⁰⁸*Department of Physics, Northern Illinois University, DeKalb, Illinois, USA*
- ¹⁰⁹*Budker Institute of Nuclear Physics, SB RAS, Novosibirsk, Russia*
- ¹¹⁰*Department of Physics, New York University, New York, New York, USA*
- ¹¹¹*Ohio State University, Columbus, Ohio, USA*
- ¹¹²*Faculty of Science, Okayama University, Okayama, Japan*
- ¹¹³*Homer L. Dodge Department of Physics and Astronomy, University of Oklahoma, Norman, Oklahoma, USA*
- ¹¹⁴*Department of Physics, Oklahoma State University, Stillwater, Oklahoma, USA*
- ¹¹⁵*Palacký University, RCPTM, Olomouc, Czech Republic*

- ¹¹⁶*Center for High Energy Physics, University of Oregon, Eugene, Oregon, USA*
- ¹¹⁷*LAL, Université Paris-Sud and CNRS/IN2P3, Orsay, France*
- ¹¹⁸*Graduate School of Science, Osaka University, Osaka, Japan*
- ¹¹⁹*Department of Physics, University of Oslo, Oslo, Norway*
- ¹²⁰*Department of Physics, Oxford University, Oxford, United Kingdom*
- ^{121a}*INFN Sezione di Pavia, Italy*
- ^{121b}*Dipartimento di Fisica, Università di Pavia, Pavia, Italy*
- ¹²²*Department of Physics, University of Pennsylvania, Philadelphia, Pennsylvania, USA*
- ¹²³*National Research Centre "Kurchatov Institute" B.P.Konstantinov Petersburg Nuclear Physics Institute, St. Petersburg, Russia*
- ^{124a}*INFN Sezione di Pisa, Italy*
- ^{124b}*Dipartimento di Fisica E. Fermi, Università di Pisa, Pisa, Italy*
- ¹²⁵*Department of Physics and Astronomy, University of Pittsburgh, Pittsburgh, Pennsylvania, USA*
- ^{126a}*Laboratório de Instrumentação e Física Experimental de Partículas - LIP, Lisboa, Portugal*
- ^{126b}*Faculdade de Ciências, Universidade de Lisboa, Lisboa, Portugal*
- ^{126c}*Department of Physics, University of Coimbra, Coimbra, Portugal*
- ^{126d}*Centro de Física Nuclear da Universidade de Lisboa, Lisboa, Portugal*
- ^{126e}*Departamento de Física, Universidade do Minho, Braga, Portugal*
- ^{126f}*Departamento de Física Teórica y del Cosmos and CAFPE, Universidad de Granada, Granada (Spain), Portugal*
- ^{126g}*Dep Física and CEFITEC of Faculdade de Ciências e Tecnologia, Universidade Nova de Lisboa, Caparica, Portugal*
- ¹²⁷*Institute of Physics, Academy of Sciences of the Czech Republic, Praha, Czech Republic*
- ¹²⁸*Czech Technical University in Prague, Praha, Czech Republic*
- ¹²⁹*Faculty of Mathematics and Physics, Charles University in Prague, Praha, Czech Republic*
- ¹³⁰*State Research Center Institute for High Energy Physics, Protvino, Russia*
- ¹³¹*Particle Physics Department, Rutherford Appleton Laboratory, Didcot, United Kingdom*
- ^{132a}*INFN Sezione di Roma, Italy*
- ^{132b}*Dipartimento di Fisica, Sapienza Università di Roma, Roma, Italy*
- ^{133a}*INFN Sezione di Roma Tor Vergata, Italy*
- ^{133b}*Dipartimento di Fisica, Università di Roma Tor Vergata, Roma, Italy*
- ^{134a}*INFN Sezione di Roma Tre, Italy*
- ^{134b}*Dipartimento di Matematica e Fisica, Università Roma Tre, Roma, Italy*
- ^{135a}*Faculté des Sciences Ain Chock, Réseau Universitaire de Physique des Hautes Energies - Université Hassan II, Casablanca, Morocco*
- ^{135b}*Centre National de l'Energie des Sciences Techniques Nucleaires, Rabat, Morocco*
- ^{135c}*Faculté des Sciences Semlalia, Université Cadi Ayyad, LPHEA-Marrakech, Morocco*
- ^{135d}*Faculté des Sciences, Université Mohamed Premier and LPTPM, Oujda, Morocco*
- ^{135e}*Faculté des sciences, Université Mohammed V-Agdal, Rabat, Morocco*
- ¹³⁶*DSM/MIRFU (Institut de Recherches sur les Lois Fondamentales de l'Univers), CEA Saclay (Commissariat à l'Energie Atomique et aux Energies Alternatives), Gif-sur-Yvette, France*
- ¹³⁷*Santa Cruz Institute for Particle Physics, University of California Santa Cruz, Santa Cruz, California, USA*
- ¹³⁸*Department of Physics, University of Washington, Seattle, Washington, USA*
- ¹³⁹*Department of Physics and Astronomy, University of Sheffield, Sheffield, United Kingdom*
- ¹⁴⁰*Department of Physics, Shinshu University, Nagano, Japan*
- ¹⁴¹*Fachbereich Physik, Universität Siegen, Siegen, Germany*
- ¹⁴²*Department of Physics, Simon Fraser University, Burnaby, BC, Canada*
- ¹⁴³*SLAC National Accelerator Laboratory, Stanford, California, USA*
- ^{144a}*Faculty of Mathematics, Physics & Informatics, Comenius University, Bratislava, Slovak Republic*
- ^{144b}*Department of Subnuclear Physics, Institute of Experimental Physics of the Slovak Academy of Sciences, Kosice, Slovak Republic*
- ^{145a}*Department of Physics, University of Cape Town, Cape Town, South Africa*
- ^{145b}*Department of Physics, University of Johannesburg, Johannesburg, South Africa*
- ^{145c}*School of Physics, University of the Witwatersrand, Johannesburg, South Africa*
- ^{146a}*Department of Physics, Stockholm University, Sweden*
- ^{146b}*The Oskar Klein Centre, Stockholm, Sweden*
- ¹⁴⁷*Physics Department, Royal Institute of Technology, Stockholm, Sweden*
- ¹⁴⁸*Departments of Physics & Astronomy and Chemistry, Stony Brook University, Stony Brook, New York, USA*

- ¹⁴⁹*Department of Physics and Astronomy, University of Sussex, Brighton, United Kingdom*
- ¹⁵⁰*School of Physics, University of Sydney, Sydney, Australia*
- ¹⁵¹*Institute of Physics, Academia Sinica, Taipei, Taiwan*
- ¹⁵²*Department of Physics, Technion: Israel Institute of Technology, Haifa, Israel*
- ¹⁵³*Raymond and Beverly Sackler School of Physics and Astronomy, Tel Aviv University, Tel Aviv, Israel*
- ¹⁵⁴*Department of Physics, Aristotle University of Thessaloniki, Thessaloniki, Greece*
- ¹⁵⁵*International Center for Elementary Particle Physics and Department of Physics, The University of Tokyo, Tokyo, Japan*
- ¹⁵⁶*Graduate School of Science and Technology, Tokyo Metropolitan University, Tokyo, Japan*
- ¹⁵⁷*Department of Physics, Tokyo Institute of Technology, Tokyo, Japan*
- ¹⁵⁸*Department of Physics, University of Toronto, Toronto, ON, Canada*
- ^{159a}*TRIUMF, Vancouver, BC, Canada*
- ^{159b}*Department of Physics and Astronomy, York University, Toronto, ON, Canada*
- ¹⁶⁰*Faculty of Pure and Applied Sciences, University of Tsukuba, Tsukuba, Japan*
- ¹⁶¹*Department of Physics and Astronomy, Tufts University, Medford, Massachusetts, USA*
- ¹⁶²*Centro de Investigaciones, Universidad Antonio Narino, Bogota, Colombia*
- ¹⁶³*Department of Physics and Astronomy, University of California Irvine, Irvine, California, USA*
- ^{164a}*INFN Gruppo Collegato di Udine, Sezione di Trieste, Udine, Italy*
- ^{164b}*ICTP, Trieste, Italy*
- ^{164c}*Dipartimento di Chimica, Fisica e Ambiente, Università di Udine, Udine, Italy*
- ¹⁶⁵*Department of Physics, University of Illinois, Urbana, Illinois, USA*
- ¹⁶⁶*Department of Physics and Astronomy, University of Uppsala, Uppsala, Sweden*
- ¹⁶⁷*Instituto de Física Corpuscular (IFIC) and Departamento de Física Atómica, Molecular y Nuclear and Departamento de Ingeniería Electrónica and Instituto de Microelectrónica de Barcelona (IMB-CNM), University of Valencia and CSIC, Valencia, Spain*
- ¹⁶⁸*Department of Physics, University of British Columbia, Vancouver, BC, Canada*
- ¹⁶⁹*Department of Physics and Astronomy, University of Victoria, Victoria, BC, Canada*
- ¹⁷⁰*Department of Physics, University of Warwick, Coventry, United Kingdom*
- ¹⁷¹*Waseda University, Tokyo, Japan*
- ¹⁷²*Department of Particle Physics, The Weizmann Institute of Science, Rehovot, Israel*
- ¹⁷³*Department of Physics, University of Wisconsin, Madison, Wisconsin, USA*
- ¹⁷⁴*Fakultät für Physik und Astronomie, Julius-Maximilians-Universität, Würzburg, Germany*
- ¹⁷⁵*Fachbereich C Physik, Bergische Universität Wuppertal, Wuppertal, Germany*
- ¹⁷⁶*Department of Physics, Yale University, New Haven, Connecticut, USA*
- ¹⁷⁷*Yerevan Physics Institute, Yerevan, Armenia*
- ¹⁷⁸*Centre de Calcul de l'Institut National de Physique Nucléaire et de Physique des Particules (IN2P3), Villeurbanne, France*

^aDeceased.

^bAlso at Department of Physics, King's College London, London, United Kingdom.

^cAlso at Institute of Physics, Azerbaijan Academy of Sciences, Baku, Azerbaijan.

^dAlso at Novosibirsk State University, Novosibirsk, Russia.

^eAlso at TRIUMF, Vancouver BC, Canada.

^fAlso at Department of Physics, California State University, Fresno CA, United States of America.

^gAlso at Department of Physics, University of Fribourg, Fribourg, Switzerland.

^hAlso at Departamento de Física e Astronomia, Faculdade de Ciências, Universidade do Porto, Portugal.

ⁱAlso at Tomsk State University, Tomsk, Russia.

^jAlso at CPPM, Aix-Marseille Université and CNRS/IN2P3, Marseille, France.

^kAlso at Università di Napoli Parthenope, Napoli, Italy.

^lAlso at Institute of Particle Physics (IPP), Canada.

^mAlso at Particle Physics Department, Rutherford Appleton Laboratory, Didcot, United Kingdom.

ⁿAlso at Department of Physics, St. Petersburg State Polytechnical University, St. Petersburg, Russia.

^oAlso at Louisiana Tech University, Ruston LA, United States of America.

^pAlso at Institutio Catalana de Recerca i Estudis Avancats, ICREA, Barcelona, Spain.

^qAlso at Graduate School of Science, Osaka University, Osaka, Japan.

^rAlso at Department of Physics, National Tsing Hua University, Taiwan.

^sAlso at Department of Physics, The University of Texas at Austin, Austin TX, United States of America.

^tAlso at Institute of Theoretical Physics, Ilia State University, Tbilisi, Georgia.

^uAlso at CERN, Geneva, Switzerland.

^vAlso at Georgian Technical University (GTU), Tbilisi, Georgia.

^wAlso at Manhattan College, New York NY, United States of America.

^xAlso at Hellenic Open University, Patras, Greece.

^yAlso at Institute of Physics, Academia Sinica, Taipei, Taiwan.

^zAlso at LAL, Université Paris-Sud and CNRS/IN2P3, Orsay, France.

^{aa}Also at Academia Sinica Grid Computing, Institute of Physics, Academia Sinica, Taipei, Taiwan.

^{bb}Also at School of Physics, Shandong University, Shandong, China.

^{cc}Also at Moscow Institute of Physics and Technology State University, Dolgoprudny, Russia.

^{dd}Also at Section de Physique, Université de Genève, Geneva, Switzerland.

^{ec}Also at International School for Advanced Studies (SISSA), Trieste, Italy.

^{ff}Also at Department of Physics and Astronomy, University of South Carolina, Columbia SC, United States of America.

^{gg}Also at School of Physics and Engineering, Sun Yat-sen University, Guangzhou, China.

^{hh}Also at Faculty of Physics, M.V.Lomonosov Moscow State University, Moscow, Russia.

ⁱⁱAlso at National Research Nuclear University MEPhI, Moscow, Russia.

^{jj}Also at Department of Physics, Stanford University, Stanford CA, United States of America.

^{kk}Also at Institute for Particle and Nuclear Physics, Wigner Research Centre for Physics, Budapest, Hungary.

^{ll}Also at University of Malaya, Department of Physics, Kuala Lumpur, Malaysia.